2009-01-01

Quantitative analyses of dispersion, doping and electronic separation of single wall HiPco carbon nanotubes

Priya Baskar Rao

Recommended Citation

Rao, Priya Baskar. 92009). *Enhanced absorption metal oxides for photocatalytic applications*. Technological University Dublin. doi:10.21427/D76W2S

Quantitative Analyses of Dispersion, Doping and Electronic Separation of Single Wall HiPco Carbon Nanotubes

By

Priya Baskar Rao

A thesis submitted to Dublin Institute of Technology
for the degree of Doctor of Philosophy (Ph.D.)

School of Physics, Dublin Institute of Technology,
Kevin Street, Dublin 8.

Prof. Hugh J. Byrne

June 2009

Abstract

As prepared SWNTs are obtained in bundles with a mixture of both metallic and semi conducting tubes. For many specific applications, electronically separated single individual tubes are required and in order to reach these application criteria, the tubes should be processed. This thesis reports on a systematic exploration of methods to routinely process, electronically separate and characterise commercially available single walled carbon nanotubes (SWNTs).

Commercially available HiPco SWNTs were dispersed in water with the assistance of 1 % by weight sodium dodecyl benzene sulphate (SDBS). The tubes were dispersed in the water surfactant system through the aid of sonication and centrifugation. The concentration dependent properties were studied in order to establish the aggregation state of the sample. The starting concentration was 5 mg/ml and this was sequentially diluted by a factor of two down to 1.2×10^{-3} mg/ml. UV/Vis/NIR absorption, Raman spectroscopy and atomic force microscopy (AFM) were performed. Using the Lambert Beer law the critical debundling point (CDP) was found to be 0.07±0.03 mg/ml and the extinction coefficient at 600 nm was found to be 215 mL mg^{-1} m^{-1} for low concentrations (individual tubes) and 99.5 mL mg^{-1} m^{-1} for higher concentrations (bundles). Once establishing the CDP, chiral indices of the tubes were determined by curve fitting the UV/Vis/NIR absorption spectrum and the Radial Breathing Modes (RBM) of the Raman spectrum. Though the chiral indices of the tubes were obtained from two different methods, the values converged enabling UV/Vis/NIR and Raman spectroscopy to be used for routine characterisation.

A quantitative analysis of doping of individual tubes at the CDP was conducted by varying the pH from 1 to 13 and monitoring the Raman spectrum. A drastic change in RBM of the Raman spectrum was observed. Mixed Gaussian and Lorentzian line shapes were fitted, and the doping behaviour was modelled using a simple protonation model. The protonation rate was found to relate to the optical band gap and the number of protons acting per SWNT was also calculated. It was concluded that metallic tubes can be more readily protonated than their semi conducting counter parts.

Functionalization of the pristine tubes (both HiPco and arc discharge) was carried out in an attempt to separate the nanotubes according to electronic character. This functionalization method resulted in significant damage to the SWNT and the separation process was deemed not suitable for routine processing. One of the most straight forward techniques and an alternative to functionalization method is based on microwave treatment, whereby exposing the tubes to radiation preferentially destroys the metallic SWNT due to their high dielectric constant, leaving behind the semi conducting tubes. Microwave treated SWNT were dispersed in water surfactant solution and were studied using Raman spectroscopy both at 514 nm and 633 nm excitation wavelength. The ratio of the G-/G+ mode and the RBM ratios were plotted against the exposure time. Curve fitting was performed to obtain the rates of the reaction and the optimum irradiation conditions were established. A batch of SWNTs treated under these conditions was produced and solutions in water surfactant were prepared and concentration dependent studies were conducted enabling enriched semi conducting tubes to be dispersed at a certain concentration. These studies thus enabled a

clear characterisation of the Raman and UV/Vis/NIR absorption characteristics of semi conducting bundles and the isolated tubes as well as the debundling process.

DECLARATION

I certify that this thesis which I now submit for examination for the award of doctor of philosophy, is entirely my own work and has not been taken from the work of others, save and to the extent that such work has been cited and acknowledged within the text of my work.

This thesis was prepared according to the regulations for postgraduate study by research of the Dublin Institute of Technology and has not been submitted in whole or part for an award in any other Institute or University.

The work reported on in this thesis conforms to the principles and requirements of the Institute's guidelines for ethics in research.

The institute has permission to keep, or lend or to copy this thesis in whole or in part, on condition that any such use of the material or the thesis be duly acknowledged.

Signature___________________________________ Date___/___/___
Candidate

To my mother

ACKNOWLEDGEMENTS

First of all I would like to thank my supervisor Prof. Hugh Byrne for giving me an opportunity to do my PhD. Thank you so much for your patience (when correcting my manuscripts and thesis), answering and also bearing with all my silly questions and also thanks for all your prompt emails right from the first which I got in the midnight!!! . I would like to thank Intel Ireland for their funding and also holding yearly conference which I felt an excellent plat form for encouraging students. I would like to thank Paolo Rapposelli and Bernie Capraro from Intel for their cooperation, suggestions and meetings that were held through the course. I would like to thank all the technicians Theresa, Anne, Luke and Paddy for all the help during my experiments and Andrew for the help with the Labspec software!!! I would like to thank Dr. Valeria Nicolosi for her help with the AFM measurements. Special thanks to Theresa for proof reading my thesis by which the externals were delighted. I would also like to thank all the administrators Louisa, Sabrina, Rosa and Damien for their help. Peter Knief – Thank you so much for all the help with the computer stuff. Thank you to all with whom I shared the office and the labs. I had a nice time with Qiaohuan and Sourabhi - thank you girls. I have to thank George who has a been a part of Focas. I would like to thank the “small” Indian gang for making me laugh and feel the days shorter in foreign country. Thank you every one in FOCAS and DIT Kevin street.

Niraj – thank you so much for supporting me during all my ups and downs. I always thank Nimmi aunty who has been a great support for me. I would like to thank “Amma and Revathy” though last but not least, the pains that you have undertaken that I am writing this acknowledgement today. Hats off to you…..

ABBREVATIONS

AFM	**Atomic Force Microscopy**
STM	**Scanning Tunnelling Microscopy**
SWNT	**Single Walled carbon Nanotubes**
MWNT	**Multi Walled carbon Nanotubes**
C=C	**Carbon to carbon double bond**
C-C	**Carbon to carbon single bond**
HiPco	**High Pressure carbon monoxide disproportionation**
FTIR	**Fourier Transform Infra Red**
RBM	**Radial Breathing Mode**
G-Mode	**Graphitic Mode**
TEM	**Transmission Electron Microscopy**
HNO_3	**Nitric acid**
H_2SO_4	**Sulphuric acid**
-COOH	**Carboxylic acid group**
NO_2	**Nitrogen Dioxide**
CH_4	**Methane**
O_2	**Oxygen**
NH_3	**Ammonia**
UV/Vis/NIR	**Ultra Violet/Visible/Near Infra Red**
UV	**Ultra Violet**
DNA	**Deoxyribo Nucleic Acid**
CNT	**Carbon Nano Tube**

CMOS	**Complimentary Metal Oxide Semiconductor**
1D	**One Dimensional**
vHS	**van Hove Singularities**
BWF	**Breit -Wigner- Fano**
DOS	**Density of States**
SDBS	**Sodium Dodecyl Benzene Sulphonate**
SDS	**Sodium Dodecyl Sulphonate**
THF	**Tetra Hydro Furan**
NMP	**N-methylpyrrolidone**
ATR	**Attenuated Total Reflectance**
CDP	**Critical Debundling Point**
DMF	**Dimethylfomamamide**
DMA	**Dimethylacetamide**
DEA	**Diethylactemide**
DMP	**Dimethylpropanamide**
FWHM	**Full Width Half Maximum**
NaCl	**Sodium Chloride**
NaOH	**Sodium Hydroxide**
HCl	**Hydrochloric acid**
ODA	**Octa Decyl Amine**
SiO_2	**Silicon Dioxide**

TABLE OF CONTENTS

Chapter - 1 Introduction 10

1.1 Nanoscience and Nanotechnology 10

1.2 Naturally Existing Nanostructures 11

1.3 Nano structured materials – Properties 12

1.4 Fabrication Routes 13

1.5 Tools and techniques 14

1.6 Applications of Nanostructured materials – “Carbon Nanotubes” 15

1.7 Nanoelectronics- Motivation and Research Objectives 18

1.8 Research – Overview 20

  1.8.1. Characterisation 22

1.9 Thesis Outline 24

References 26

Chapter 2 - Single Walled Carbon Nanotubes 32

2.1 Physical Structure of Carbon Nanotubes 32

2.2 Electronic Structure of Carbon Nanotubes 36

2.3 Spectroscopic characterisation of Carbon Nanotubes 40

  2.3.1. Absorption Spectroscopy 40

  2.3.2. Raman spectroscopy 43

2.4 Carbon Nanotube Dispersions 48

2.5 Summary 52

References 53

Chapter 3 - Experimental Techniques 58

3.1 Electronic Spectroscopy 58

3.1.1. Basic Principle 58

3.1.2. Absorbance and Scattering 60

3.1.3. Schematic set up of UV/Vis/NIR Absorbance Spectrometer 63

3.1.4. Integrating Sphere 64

3.2. Vibrational Spectroscopy 66

3.2.1. Basic Principles 66

3.2.2. Fourier Transform Infra Red Spectroscopy- Basic Principle 67

3.2.3. Instrument Set up 68

3.2.4. Raman Spectroscopy - Raman Scattering 70

3.2.5. Raman- Instrument Set Up 75

3.2.6. Raman and FTIR spectroscopy – Comparison and selection Rules 76

3.3 Microscopy Techniques 77

3.3.1. Atomic Force Microscope - Working Principles and Instrument set up 77

3.4 Summary 82

References 83

Chapter 4 - SWNTs Dispersions 84

4.1 Introduction 84

4.2 Experimental 86

4.3 Results and Discussion 89

4.4 Summary 107

References 108

Chapter 5 - Spectroscopic Assignment of Nanotubes 111

5.1 Introduction 111

5.2 Experimental 112

5.3 Results and Discussion 113

5.3.1 Absorption spectroscopy 113

5.3.2 Raman Spectroscopy 117

5.4 Summary 123

References 124

Chapter 6 - Doping of SWNTS 127

6.1 Introduction 127

6.2 Experimental Procedures 128

6.3 Results and Discussion 129

6.4 Summary 136

References 137

Chapter 7 - Separation based on Electronic properties- Chemical Functionalization 138

7.1 Introduction 138

7.2 Experimental 140

7.3 Results and Discussion 141

7.4Summary 150

References 151

Chapter 8 - Separation and Dispersion– Semiconducting Tubes 153

8.1 Introduction 153

8.2 Experimental 154

8.3 Results and Discussion 155

8.4 Summary 169

References 170

Chapter 9 – Conclusions 171

9.1Summary 171

9.2 Future work 174

Publications and Presentations 176

TABLE OF ILLUSTRATIONS

Figure 1.1 a **Butterfly's nanostructured wing scale** **11**

Figure 1.1 b **Nano fibres found in the edelweiss plant** **11**

Figure 1.2 **Graphical representation of Moore's law** **18**

Figure 1.3a **As prepared Carbon nanotubes** **21**

Figure 1.3b **Bundles of SWNT as observed by TEM** **21**

Figure 2.1 **Schematic representation of SWNT and MWNT** **32**

Figure 2.2 **Schematic representation of a graphene sheet** **34**

Figure 2.3 a **Schematic representation of Armchair SWNT** **35**

Figure 2.3 b **Schematic representation of Zigzag SWNT** **35**

Figure 2.3 c **Schematic representation of chiral tube** **35**

Figure 2.4 **One dimensional energy dispersion of SWNT** **37**

Figure 2.5 **Overall representation of chirality of SWNT** **38**

Figure 2.6 **Schematic representation of the DOS of SWNT** **39**

Figure 2.7 **Absorption spectrum of HiPco SWNTs in aqueous SDBS** **41**

Figure 2.8 **Kataura plot** **42**

Figure 2.9 **Schematic representations of different kinds of vibration in SWNT** **44**

Figure 2.10 **Typical Raman spectrum of SWNT in aqueous SDBS** **45**

Figure 3.1 **Different electronic and vibration sates in a di-atomic molecule** **59**

Figure 3.2 **Jablonski diagram showing absorption and emission** **60**

Figure 3.3a **Rayleigh scattering** **63**

Figure 3.3b **Formation of forward lobe in Rayleigh scattering** **63**

Figure 3.4 **Schematic set-up of UV/Vis/NIR** **64**

Figure 3.5 **Schematic representation of the integrating sphere** **65**

Figure 3.6 **a) Schematic setup of FTIR imaging System** **69**

b) FTIR - Visual Image /Transmittance **69**

c) FTIR - IR/Transmittance **69**

Figure 3.7 **a) Schematics energy levels in a diatomic molecule** **71**

b) Schematic representation of stokes and anti stokes shift **71**

Figure 3.8 **Instruments S. A. Labram 1B** **76**

Figure 3.9 **Different types of stretches in a carbon dioxide molecule** **77**

Figure 3.10 **Working principle of AFM** **78**

Figure 3.11 **Graph showing contact and non contact mode operation** **79**

Figure 3.12 **Veeco Multimode Nanoscope 3a** **81**

Figure 4.1 **UV/Vis/NIR spectra of light water and heavy water** **87**

Figure 4.2 **TEM image of As prepared nanotube SWNT** **90**

Figure 4.3 **Absorbance spectra of HiPco SWNT after each sonication step** **90**

Figure 4.4 **Absorption spectra of HiPco SWNTs in aqueous SDBS before centrifugation** **92**

Figure 4.5 **Absorption spectra of SWNTs measured in standard chamber and integrating sphere** **93**

Figure 4.6 **Extinction due to scattering of HiPco SWNTs measured before and after centrifugation** **94**

Figure 4.7 **S$_{22}$ region of the absorption spectrum showing red shift due to debundling of tubes** **95**

Figure 4.8 Absorbance of HiPco SWNT as a function of concentration 96

Figure 4.9 (a) AFM image of SWNT at low concentration 98

(b) Section analysis of SWNT shown in figure 4.9 a 98

(c) Histogram -bundle size distribution for low concentration 98

Figure 4.10 (a) AFM image of SWNT at high concentration 100

(b) Section analysis of SWNT shown in figure 4.10 a 100

(c) Histogram - bundle size distribution higher concentration 100

Figure 4.11 (a) Deconvoluted RBM spectra of HiPco SWNT 102

(b) RBM intensity of HiPco SWNT as a function of concentration 102

Figure 4.12 (a) Deconvoluted G-mode spectra of HiPco SWNT 103

(b) BWF intensity of HiPco SWNT as a function of concentration 103

Figure 5.1 Absorption spectra of SWNT in aqueous SDBS 113

Figure 5.2 Kataura plot 115

Figure 5.3 Curve fitted absorption spectrum of HiPco SWNT 116

Figure 5.4 Curve fitted RBM of the HiPco SWNTs - 633nm 118

Figure 5.5 Curve fitted RBM of the HiPco SWNTs - 514nm 118

Figure 5.6 Kataura plot from absorption and Raman spectroscopy 122

Figure 6.1 a) Absorption spectra of HiPco SWNT at varying pH 129

b) Absorption spectra of HiPco SWNT at 6.75 and 1.43 pH 130

Figure 6.2 RBM at different pH 131

Figure 6.3 G-modes at different pH 132

Figure 6.4 a)RBM intensity against pH – metallic SWNT 133

b) RBM Intensity against t pH – semi conducting SWNT 133

Figure 6.5 Plot of –ln K_p as a function of band gap 134

Figure 7.1 a) Schematic representation reaction of the acid treated SWNT with ODA 139

b) FTIR spectrum of pristine HiPco 142

Figure 7.2 FTIR spectrum of HiPco SWNTs acid treated for 24 hours 143

Figure 7.3 FTIR spectrum of pristine ODA 143

Figure 7.4 FTIR spectra of HiPco SWNT acid treated for 2 hours 145

Figure 7.5 a) FTIR spectrum of deposit 146

b) FTIR spectrum of supernatant 146

Figure 7.6 Absorption spectra of deposit and supernatant 146

Figure 7.7 Raman spectra of HiPco SWNTs at 532 nm 147

Figure 7.8 Raman spectra of Arc Discharge SWNTs at 660 nm 147

Figure 7.9 Raman spectra of amorphous carbon films 148

Figure 8.1 Raman Spectrum of HiPco SWNTs in aqueous SDBS 633 nm 156

Figure 8.2 RBMs of microwave treated HiPco SWNTs 158

Figure 8.3 a) Absorption spectra of microwave treated SWNTs 162

b) Background subtracted absorption spectra of HiPco SWNTs 162

Figure 8.4 a) $RBM_{200cm^{-1}} / RBM_{255cm^{-1}}$ plotted against microwave exposure 164

b) G^-/G^+ plotted against microwave exposure 164

Figure 8.5 Absorbance concentration dependence of HiPco SWNTs 168

CHAPTER 1

“Introduction”

1.1 Nanoscience and Nanotechnology

> ***I want to build a billion tiny factories, models of each other, which are manufacturing simultaneously. . . The principles of physics, as far as I can see, do not speak against the possibility of manoeuvring things atom by atom. It is not an attempt to violate any laws; it is something, in principle, that can be done; but in practice, it has not been done because we are too big.***
>
> ***-Richard Feynman***

The above quote explains a very complex science in a very simple way – Nanoscience, is the study of manipulating materials or objects at the “Nano” scale. The word “nano” is Greek meaning “dwarf” but the prefix has been adapted to the scale of 10^{-9}, a nanosecond being 10^{-9} sec, a nanometer being 10^{-9} m, the length scale of small molecules. Nanoscience basically deals with maneuvering individual atoms and molecules to create new materials or novel structures with peculiar properties. Naturally, reducing the dimensions of a system from the macro scale to the nano scale leads to a profound influence on its physical behavior. This phenomenon can be exploited to make devices at the nano scale such as one dimensional transistors[1] and nanostructures like quantum dots and wires leading to the concepts of nanotechnology and nanoscience. There is a fine line between the two and the Royal Society of London[2] has defined ***Nanoscience*** *as “the study of phenomena and* *manipulation of materials at atomic, molecular and macromolecular scales, where properties differ significantly from those at a larger scale"* and ***Nanotechnology*** *as "the design, characterization, production and application of structures, devices and systems by controlling shape and size at nanometer scale".*

1.2 Naturally Existing Nanostructures

Nature has extensively supplied us with nanostructures. Figure 1.1a shows the nano photonic structure found in butterfly wings. Apart from giving the spectacular colouring to the wings[3,4], the nanostructure also protects them from harsh climatic conditions[5]. Gecko lizards have a remarkable ability to cling to any surface and this ability stems from the 200 nm wide keratin hairs that coat the soles of their feet[6]. Moths' eyes have hexagonal nanostructures on their surface and as the sizes of these structures are smaller than the wavelength of the visible light they absorb most of the visible light. This results in an anti reflective layer on the surface of the eye that makes moth's vision much better in dim light and darkness[7]. Edelweiss is an alpine flower which lives at high altitudes, in a strong UV radiation environment. They are covered with nanostructured filaments or fibres (fig 1.1b) on the periphery of the petals which are responsible for protecting the flower.

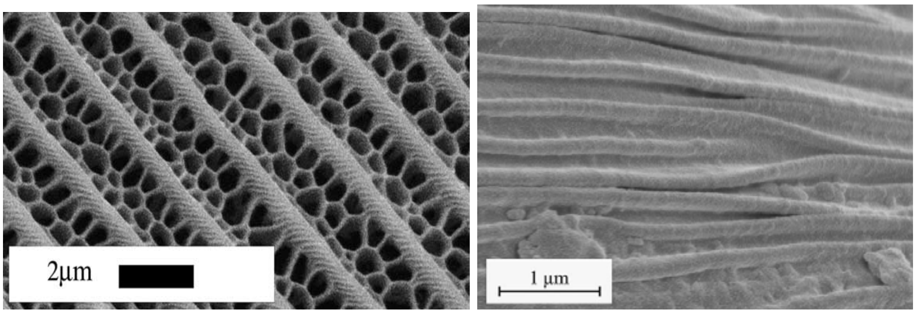

Figure 1.1: SEM image of the a) butterfly's nanostructured wing scale[3,4] b) nano fibers found in the edelweiss plant[8].

The dimension of these nano fibres (act as photonic crystals) is around the same as the wavelength of UV light (Figure 1.1b). Therefore they absorb UV light and reflect the rest of the electromagnetic radiation spectrum. The absorbed UV radiation is coupled in a guided mode along the fiber and then dissipated safely, thus protecting the reproductive parts of the plant from harmful radiation[8].

1.3 Nano structured materials – Properties

The term nanostructured materials cover various types of nano materials and one dimensional structures. Some examples are nano particles (e.g. gold and silver) and quantum dots (e.g. cadmium selenide) which are "zero" dimensional, nano wires (e.g. platinum, 3-5, 2-4 semiconductors, oxides) and nano tubes (e.g. boron nitride, carbon) which are one dimensional and nano films (e.g. Phthalocyanines) and nano arrays (e.g. proteins and DNA) which are two dimensional. Most interestingly, the properties of nanostructured materials significantly differ from the corresponding bulk materials. A good example is that of gold nano particles, whereby, depending upon the size of the particle, the colour changes. Bulk gold which is metallic yellow turns to red, purple, or pink at the nanoscale[9,10,11]. This is due to the localisation of surface plasmons which when aggregates leading to obviously a red shift[9]. Zhu Huai Yong[12] discovered that gold nano particles of different sizes were used to colour the window glasses in medieval churches. In 1857, Faraday recorded the preparation of a colloidal sample of gold nano particles[13].

The following are some other properties of nanostructures which make them of interest for both research and applications; 1) large fractions of surface atoms[14] 2) high surface energy[14] 3) quantum confinement[14] 4) reduced imperfections[14] 5) large surface area to volume ratio 6) high aspect ratio as in carbon nanotubes[15] (CNT) and nanowires[16] 7) ballistic electron transport[16]. Even mechanical and thermal properties are distinct for nanostructured materials. For example, carbon nanotubes have been one of the key materials in research, mainly due to their intriguing properties like high aspect ratio[15] (length to diameter ratio which can be as large as 10^4-10^5), high Young's modulus which is ~1TPa[17] and high thermal conductivity of 6600 W/mK at room temperature[18]. In terms of electronic properties, they can be obtained as either metallic or semiconducting nanotubes[15], depending on their architecture.

1.4 Fabrication Routes

"Top down" and "bottom up" are the two fabrication routes to develop nanostructured materials or devices. Top-down fabrication is a subtractive method whereby a bulk material as the starting entity is processed to produce nano materials or nano devices and bottom-up fabrication is an additive process that starts with precursor atoms or molecules and assembles them to make nano materials or devices.

Moore's law, which states that "the transistor performance and the density on a chip doubles annually[19]", is an often quoted example of a top down approach. Other top down approaches are Ball Milling (nano particles[20]) and Nanolithography (Nano Electromechanical Systems[21]). Of the two fabrication methods, the bottom up approach mimics nature better and therefore K. Eric Drexler defines the term Nanotechnology as "*the projected ability to construct items from the bottom up, using techniques and tools being* *developed today to make complete, high performance products*[22]". Electro[23] spinning (nano fibres[23]), Chemical Vapor Deposition (carbon nanotubes[24,25]) Arc Discharge (carbon nanotubes[26]), Laser Ablation (carbon nanotubes[27,28]), Atomic Layer Deposition (Thin films[29]), Self Assembly (of nano particles for specific application like drug delivery[30]), Electro Deposition (nano films[31]), Sol gel (nano particles[32] and quantum dots[33]) are some common bottom up methods.

1.5 Tools and techniques

Recent technological advances have provided fabrication routes to reproducibly develop nano structures, giving rise to the question of "manipulation" and "characterization" on this scale. Advances in the techniques of Scanning Probe Microscopy have in a way solved many of the handling problems and for the purpose of characterization, spectroscopic methods such as Raman spectroscopy (which for example can give a fingerprint of carbon nanotubes[34]), photoelectron spectroscopy (which can be used to analyze electronic transitions[35]), absorption and emission spectroscopy (used for analyzing nanotubes[36] and nanoparticles[37,38]), have found many applications. In the early 1980's the scanning tunneling microscope was invented by Gerd Binnig and Heinrich Rohrer, at IBM-Zurich in Switzerland, an achievement for which they were awarded the Nobel Prize in Physics in 1986. This was the first instrument that was able to "see" atoms. A few years later, the Atomic Force Microscope was invented, expanding the capabilities and types of materials that could be investigated. Since scanning probe microscopy was born, various similar techniques like scanning gate microscopy, magnetic force microscopy, electrostatic force microscopy etc. have evolved to "see" different properties at the nanometer scale. In addition, “older” techniques such as electron microscopy have continued to evolve, and High Resolution Transmission Electron Microscopy (HRTEM) can now image in the nanometer range[28]. Currently, there are a large number of complementary instruments that help scientists in the nano realm. In addition to the enabling technologies, scientists have realized the future potential of this research.

Nanoscience can be considered as the science of 21st century, bringing about new insights towards the application of science, some of the advantages being low cost of the end products, reduction in size, less power consumption, increased speed etc. Norio Taniguchio popularized the word “nanotechnology” in the 1974s, established that the technology mainly consists of the processing of separation, consolidation, and deformation of materials by one atom or one molecule [66]."

1.6 Applications of Nanostructured materials – “Carbon Nanotubes”

Nanotechnology has a vast array of potential applications from the electronics industry to medicine. Quantum dots are being researched[39,40] for targeted imaging of cancer cells. Chemically functionalized single-walled carbon nanotubes (SWNT) have shown promise in tumour-targeted accumulation in mice and very recently, the ability of CNT to adsorb near-infrared radiation was exploited to kill cancer cells[41]. The tubes have been reported to exhibit biocompatibility and excretion. Zhuang Liu et al. have shown *in vivo* SWNT drug delivery for tumour suppression in mice[42]. Pristine SWNTs were wrapped with polyethylene glycol (PEG) modified with a phospholipids (PL) moiety and folic acid (FA). Because tumour cells are known to over express folate receptors, the PLPEG-FA/SWNT entities were only internalised inside the cancer cells, which were then destroyed by using a laser wavelength of 808 nm. Laser pulses induced local heating and consequently death, only of those tumour cells that had taken up the CNT[41].

Nano structured polymer membranes have been reported to effectively filter dust particles in air and water, essential requirements in the control over airborne and waterborne contaminants, hazards biological agents, allergens and pollutants in food, pharmaceuticals and biotechnology processes[43]. Recently, free-standing films of nano fibrous composite materials have been developed, which could have optical, biological, metallic and magnetic applications[44]. Non covalent functionalization of CNTs has been reported for binding specific proteins and the detection of clinically important bio molecules such as antibodies associated with human anti immune diseases[45]. The ability of the carbon nanotubes to penetrate into the cells opens up potential applications in the area of nano medicine as potential drug delivery agents[46]. Realisation of such potential applications, however, demands a complete understanding of the fundamental properties of the CNT.

Composites of nanotubes can be used as antistatic shielding on airplanes wings[47] and conducting composites have potential applications as transparent conductors[48]. Their high aspect ratio makes them ideal for field emission materials, they can potentially be used as electron guns for the next generation of scanning electron microscopes (SEMs) and transmission electron microscopes (TEMs)[49]. Their large surface area and low resistivity are of great interest in electrochemistry[50] and their potential applications in electronic circuits have been demonstrated[51-53]. IBM reported a charge transfer p-doping scheme for obtaining stable, unipolar carbon nanotube field effect transistors(CNT-FETs) with a self-aligned gate structure[54]. Highly transparent FETS have been fabricated using CNT networks which involved simple spraying of the tubes, dissolved using surfactants, onto a polyester substrate [55]. CNTs also have a strong potential in the area of display devices such as cathode ray tubes and flat panel displays because of their high field emission at low voltages[56]. A team at the Université du Québec à Trois-Rivières in Canada used single-walled carbon nanotubes (SWNTs) as catalysts to quadruple the hydrogen adsorption kinetics of the reversible storage materials[57].

Both single wall and multiwall nanotubes are being investigated for their application in the field of sensors. The high aspect ratio presents a large surface for adsorption of gas molecules leading to either donation or withdrawal of electrons which obviously changes their electronic properties. This factor makes CNTs suitable candidates for sensing gases such as NO_2, NH_3, CH_4, and O_2, organic and inorganic vapours. Recent paper[58] on multi walled carbon nanotube films grown by thermal chemical vapour deposition on a micro machined substrate with a chrome heater and a diaphragm demonstrated their use as sensing materials for nitrogen dioxide (NO_2). The films showed a p-type electrical resistivity with decreasing electrical resistance upon exposure to NO_2[58]. A polymer coated CNT network sensitive to pH was developed by M. Kaempgen *et.al* [59] and they also observed that the device showed a longer response time and a drifting signal at high alkalinity.

1.7 Nanoelectronics- Motivation and Research Objectives

Moore's law (Figure 1.2) indicates that the density and the performance of transistors double every 24 months and this law has been the driving force for electronic industries in recent times. Increasing the number of transistors on the chip concomitantly increases the current leakage and also the power consumption which is a major disadvantage. With this in mind, Intel (in 2007) came up with the new high energy efficiency 45nm Hafnium - Based High - k Metal Gate Transistor (http://www.intel.com/technology/45nm/). As can be seen from Figure 1.2, to keep Moore's law moving in the same fashion for the next few decades, new nano size materials, device architectures and manufacturing methods have to be developed. All these innovations should replace the existing CMOS (Complementary metal-oxide semiconductor) or hybrid technologies to improve the transistors' performance.

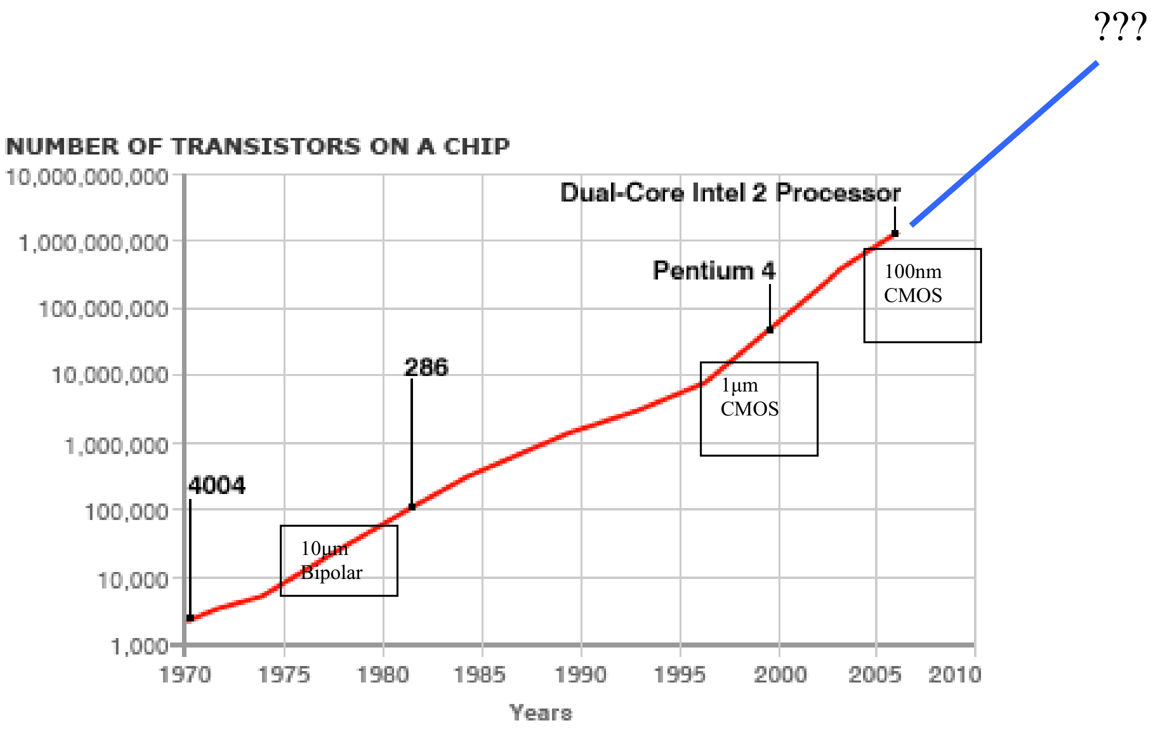

SOURCE: Data quest/Intel

Figure 1.2 Graphical representation of Moore's law

In this regard, carbon nanotubes have been identified as potentially playing a significant role. They have been targeted by industries such as IBM and INTEL because of their potential applications and unique properties as already mentioned. Single walled carbon nanotubes are obtained as both metallic and semiconducting tubes during synthesis. The metallic tubes can be potentially used as interconnects or vias and semiconducting tubes can be used in Field Effect Transistors (FETs). Hybridising carbon nanotubes in chips is expected to be a major breakthrough in the electronics industry from east to west and myriad research groups are working simultaneously on these materials in various aspects.

However, successful application of these materials faces several specific major obstacles;

1) They are grown as bundles and with various levels of impurities.
2) They are produced as mixtures of metallic and semi conducting tubes.
3) They are largely insoluble and so difficult to process and purify.

Furthermore, much of the research to date has been on impure samples of ill defined structure, implying that the fundamental understanding of their intrinsic properties is somewhat obscured. Standard routine and straight forward methods for processing and characterisation of pristine nanotubes and electronically separated tubes are one of the basic requirements to be accomplished before any further industrial application can be realised. This project aims at bringing solutions for such industrial problems.

The main research objectives are

1) Solubalise HiPco SWNTs and demonstrate debundling using optical scattering measurements and establish spectroscopic signatures of debundled nanotubes along with a standard method for sample preparation.

2) Manipulate and establish spectroscopic signatures of electronically mixed samples of carbon nanotubes.

3) Separate semiconducting and metallic nanotubes and therefore establish their spectroscopic signatures

1.8 Research – Overview

Discovered by S. Iijima[60] in 1991, the basic properties of carbon nanotubes are being extensively studied in order to harness them for various applications. They can be of the multi walled (MWNTs) or single walled (SWNTs) variety[61]. For electronic applications, it is the single walled structures which have most potential and therefore this project, sponsored by Intel Ireland, has focussed on their processing and characterisation.

Although there are various methods of growing SWNTs, including laser ablation[28], chemical vapour deposition[24], arc discharge[26] , high pressure carbon monoxide decomposition[62] (HiPco), all methods result in carbon nanotubes in bundled or aggregated form as shown in Figure 1.3a and b. Also the tubes are obtained with a mixture of both metallic and semiconducting species which is a major disadvantage when it comes to industrial applications. Impurities like metallic catalyst particles, amorphous carbon nanoparticles of graphite are also present in the pristine material[63]. The presence of impurities has also been a major problem for the industrial applications of tubes.

Figure 1.3a: As prepared Carbon nanotubes.

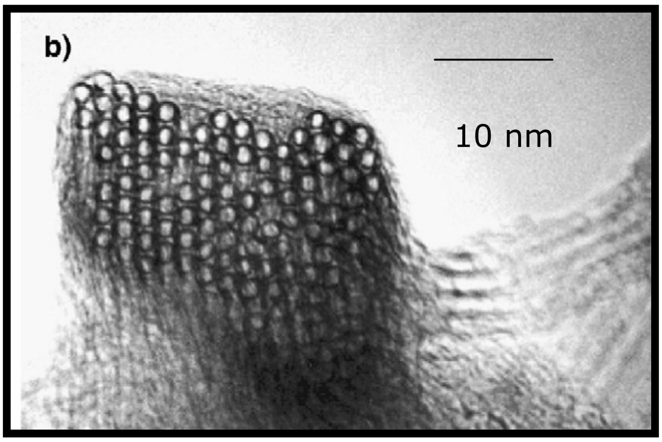

Figure 1.3b: Bundles of SWNT observed by TEM[28].

Aggregation occurs due to the high cohesive energy of the bundles which has been reported to be 4 eV/nm and the van der Waals interaction between individual nanotubes is as strong as 1 eV/nm[64]. The electronic character of a given tube is determined by the way the graphene sheet is rolled along its axis (although this is a simplified model of how they are constructed, a carbon nanotube can be considered as a rolled sheet of graphene) or the so called chirality. Given these two factors, engineers and technologists have found it difficult to integrate single individual carbon nanotubes in intricate components where individual electronically separated tubes are mandatory.

This project is completely dedicated to exploring solutions to the problems of carbon nanotube dispersion and electronic separation. The main objectives of this project have been defined under three sections, namely (1) Dispersion of SWNTs (Solubalise and demonstrate debundling using optical scattering measurements and establish spectroscopic signatures of debundled nanotubes) and a standard protocol including the sample preparation method has been formulated. (2) Doping (Manipulate and establish spectroscopic signatures of electronically mixed samples of carbon nanotubes) and (3) Electronic separation (Separate semiconducting and metallic nanotubes and therefore establish their spectroscopic signatures)

At this point it is also necessary to mention that besides improving applications potential, dispersibility of carbon nanotubes is also important for understanding the fundamental chemical and physical properties of nanotubes since it provides a pathway for characterisation and manipulation. In this sense SWNTs can be considered as a prototype for 1 dimensional “nano systems”.

1.8.1. Characterisation

Dispersion Studies: An ideal solution to the issue of bundling would be to disperse the tubes in organic or inorganic solvents with or without the aid of covalent[65] or non covalent functionalization[36]. In this work, HiPco SWNTs (99% purity according to manufacturer’s specifications) are dispersed in 1% aqueous surfactant solution through the aid of sonication and centrifugation. Light scattering and optical absorption spectroscopy are employed to investigate the dispersion of the SWNTs as a function of concentration. Below a certain concentration called the critical debundling point or dispersion limit, the bundles are largely dispersed, resulting in an enrichment of isolated nanotubes and a homogenous dispersion. As a further support the Raman spectroscopy is employed for monitoring the dispersion process. Once dispersed, the UV/Vis/NIR absorption and Raman spectroscopic features of the mixed SWNT sample can be assigned and the fundamental theories describing their relationship to the nanotube structures can be validated.

Doping of SWNT: Electrical doping of mixed sample of SWNTs was performed to demonstrate the electronic properties and also to establish spectroscopic signatures of the electronic states. SWNTs in water surfactant solution at the CDP was doped in order to analyse the reaction rates of metallic tubes and the semiconducting. Equilibrium constant for semiconducting and metallic tubes were determined by using a simple 1^{st} order regression model.

Separating Metallic and Semi conducting nanotubes: One of the project objective was to separate metallic and semiconducting SWNTs and obtain a sample of a uniform or enriched electronic species using the following methods 1) Ionic (non covalent) functionalization and 2) destruction of one type of nanotube. Spectroscopic studies were performed in order to optimise the processes and to establish a signature of the separated species.

1.9 Thesis Outline

Chapter 2 includes an introduction to Carbon nanotubes, their physical structure, electronic structure, water based suspensions of carbon nanotubes using surfactants and the reasoning behind using spectroscopic techniques employed in this research.

Chapter 3 outlines the basic principles of electronic spectroscopy, vibrational spectroscopy and microscopy techniques of relevance to the work. The instrument set up and working principles of UV/visible/NIR absorption spectroscopy, atomic force microscopy, Raman spectroscopy and Fourier Transform Infra Red spectroscopy are discussed with schematic illustrations.

Chapter 4 gives a detailed analysis of concentration dependent studies of SWNTs in water based surfactant solution using UV/visible/NIR absorption and Raman spectroscopy. Scattering measurements using an integrating sphere, the calculation of the extinction coefficient of the isolated and bundled SWNTs and the determination of the critical debundling point of SWNTs are discussed in detail. Finally the spectroscopic signatures of isolated tubes compared to bundles are demonstrated.

In **Chapter 5,** the chiral indices of carbon nanotubes in a given dispersed sample, is determined by performing curve fitting for the absorption and Raman spectra. In doing so the two characterisation techniques are cross referenced and validated and their relative merits are discussed.

Chapter 6 presents the electronic doping of SWNTs at the critical debundling point which was performed by changing the pH of the solution and measuring the corresponding Raman spectra. Using a simple protonation model, the equilibrium protonation constant k_p of metallic and semiconducting is determined. The study elucidates the electronic signatures of metallic and semiconducting tubes independently.

Chapter 7 discusses the procedure undertaken for the separation of semiconducting tubes from metallic tubes. It was carried out by functionalising the tubes with carboxylic groups and then treating with amines. FTIR spectroscopy was used to analyse the functionalization at each stage. Both Raman and Absorption spectroscopy was used to determine if the electronic separation was successful.

In **Chapter 8,** separation of semiconducting from metallic SWNTs was carried out by exposing the as produced carbon nanotubes to microwave radiation, based on the premise that irradiation preferentially degrades metallic SWNTs. Absorption spectroscopy was used to monitor the changes to the sample content during microwave exposure and it was demonstrated that not all the metallic tubes exhibit the same rate of degradation and that prolonged exposure also degrades the semiconducting nanotubes. A simple model was applied to quantify the process and the optimum exposure time was established.

Chapter 9 is the summary and conclusion of the project.

References

(1) Islam, S. K.; Jain, F. C. *International Journal of Infrared and Millimeter Waves* **1998**, *19*, 1649.

(2) http://www.nanotec.org.uk/finalReport.htm. (20-07-09)

(3) Huang, J. Y.; Wang, X. D.; Wang, Z. L. *Nano Letters* **2006**, *6*, 2325.

(4) Gaillot, D. P., Deparis, Olivier; Welch, Victoria; Wagner, Brent K.; Vigneron, Jean Pol; Summers, Christopher.J; . *Physical Review E - Statistical, Nonlinear, and Soft Matter Physics,* **2008,** *78*.

(5) Z. Ba´ lint, K. J. *Neue Entomologische Nachrichten,* **1997**, *68*

(6) http://www.aip.org/tip/INPHFA/vol-10/iss-4/p16.html. (20-07-09)

(7) Wilson. S. J., Hutley. M. C., *Opt. Acta 29* **1982**, *29*, 993.

(8) K. Kerte´sz , Zs. Ba' lint. l., Z. Ve´rtesy , G.I. Ma´rk , V. Lousse , J.-P. Vigneron , L.P. Biro´ ,. *Current Applied Physics* **2006**, *6*, 252.

(9) Algar, W. R.; Massey, M.; Krull , U. J.; *Trends in Analytical Chemistry*, **2009,** 28, 3.

(10) Brown, K. R.; Walter, D. G.; Natan, M. J. *Chemistry of Materials* **2000**, *12*, 306.

(11) Freeman, R. G.; Hommer, M. B.; Grabar, K. C.; Jackson, M. A.; Natan, M. J. *Journal of Physical Chemistry* **1996**, *100*, 718.

(12) http://www.azom.com/news.asp?newsID=13416. (20-07-09)

(13) Faraday, M. *Philosophical Transactions of the Royal Society* **1857**, *147*, 145.

(14) Cao, G. *Nanostructures and Nanomaterials -Synthesis Properties and Application, Imperial College Press,* **2004**.

(15) Saito, R.; Dresselhaus, G.; Dresselhaus, M. S.; *Physical Properties of Carbon Nanotubes* **1998**.

(16) Dresselhaus, M. S.; Lin, Y. M.; Rabin, O.; Jorio, A.; Souza, A. G.; Pimenta, M. A.; Saito, R.; Samsonidze, G. G.; Dresselhaus, G. *Materials Science & Engineering C-Biomimetic and Supramolecular Systems* **2003**, *23*, 129.

(17) Reich, S.; Thomsen, C.; Maultzsch, J. *Carbon Nanotubes- Basic concepts and physical properties,* **2004,** *Wiley-VCH, Weinheim.* .

(18) Berber, S.; Kwon, Y. K.; Tomanek, D. *Physical Review Letters* **2000**, *84*, 4613.

(19) Moore, G. *IEDM Technical Digest* **1975**, *11.*

(20) Wang, Y.; Li, Y.; Rong, C.; Liu, J, P.; *Nanotechnology* **2007**, *18*, 465701.

(21) Deirdre, L.; Alexander, L.; Bruce, D.; Stefano, S.; Ivo, R., *Proceedings of SPIE, the International Society for Optical Engineering* **2007**, *6462*, 64620J.1.

(22) http://www.crnano.org/whatis.htm. (20-07-09)

(23) Subbiah , T.; Bhat , G. S.; Tock , R. W.; Parameswaran , S.; Ramkumar , S. S. *Journal of Applied Polymer Science*

2005, *96*, 557

(24) Kong, J.; Cassell, A. M.; Dai, H. J. *Chemical Physics Letters* **1998**, *292*, 567.

(25) Nerushev, O. A.; Sveningsson, M.; Falk, L. K. L.; Rohmund, F. *Journal of Materials Chemistry* **2001**, *11*, 1122.

(26) Journet, C.; Maser, W. K.; Bernier, P.; Loiseau, A.; delaChapelle, M. L.; Lefrant, S.; Deniard, P.; Lee, R.; Fischer, J. E. *Nature* **1997**, *388*, 756.

(27) Journet, C.; Bernier, P. *Applied Physics a-Materials Science & Processing* **1998**, *67*, 1.

(28) Thess, A.; Lee, R.; Nikolaev, P.; Dai, H. J.; Petit, P.; Robert, J.; Xu, C. H.; Lee, Y. H.; Kim, S. G.; Rinzler, A. G.; Colbert, D. T.; Scuseria, G. E.; Tomanek, D.; Fischer, J. E.; Smalley, R. E. *Science* **1996**, *273*, 483.

(29) http://en.wikipedia.org/wiki/Atomic_layer_deposition. (20-07-09)

(30) Khaled, A.; Guo, S. C.; Li, F.; Guo, P. X. *Nano Letters* **2005**, *5*, 1797.

(31) Saaminathan V, Murali. K. R. *ICSE Proceeding* **2002,** 92.

(32) Taichi Arakawa, T. K., Tsuyoshi Akiyama, and Sunao Yamada *Jpn. J. Appl. Phys.* **2007**, *46*, 2490.

(33) R. Erce-Montilla, M. Pinero., N. de la Rosa-Fox, A. Santos, L. Esquivias *J. Mater. Res* **2001**, *16* 2572.

(34) Dresselhaus, M. S.; Dresselhaus, G.; Saito, R.; Jorio, A. *Physics Reports-Review Section of Physics Letters* **2005**, *409*, 47.

(35) Felten, A.; Ghijsen. J.; Pireaux, J.; Drube, W.; Johnson, R. L.; Liang, D.; Hecq, M.; Tendeloo, G. V.; Bittencourt, C.; *Micron* **2009**, *40* 74.

(36) O'Connell, M. J.; Bachilo, S. M.; Huffman, C. B.; Moore, V. C.; Strano, M. S.; Haroz, E. H.; Rialon, K. L.; Boul, P. J.; Noon, W. H.; Kittrell, C.; Ma, J. P.; Hauge, R. H.; Weisman, R. B.; Smalley, R. E. *Science* **2002**, *297*, 593.

(37) Virender K. Sharma , Ria. A. Yngard, Yekaterina Lin. *Advances in Colloid and Interface Science* **(2009),** *145*, 83.

(38) Fan Dong; Weirong Zhao; ZhongbiaoWu; Guo, S. *Journal of Hazardous Materials* *162* 763.

(39) Ce´dric Klumppa, K. K., Prato, M.; Alberto Bianco *Biochimica et Biophysica Acta* **2006**, *1758*, 404

(40) Jie Pan; Si Shen Feng. *Biomaterials* **2009**, *30* 1176.

(41) Kam, N. W. S.; O'Connell, M.; Wisdom, J. A.; Dai, H. J. *Proceedings of the National Academy of Sciences of the United States of America* **2005**, *102*, 11600.

(42) Zhuang Liu ; Kai Chen ; Corrine Davis ; Sarah Sherlock ; Qizhen Cao ; Xiaoyuan Chen ; Hongjie Dai. *Cancer Research* **2008.**, *68*, 6652.

(43) Barhate , R. S.; Ramakrishna , S. *J. Membr. Sci* **2007**, *296* 1.

(44) Peng, X.; Jin, J.; Ericsson , E. M.; Ichinose, I.; *J. Am. Chem.Soc.* **2007**, *129* 8625.

(45) Chen, R. J.; Bangsaruntip, S.; Drouvalakis, K. A.; Kam, N. W. S.; Shim, M.; Li, Y. M.; Kim, W.; Utz, P. J.; Dai, H. J. *Proceedings of the National Academy of Sciences of the United States of America* **2003**, *100*, 4984.

(46) Venkatesan, N.; Yoshimitsu, J.; Ito, Y.; Shibata, N.; Takada, K. *Biomaterials* **2005**, *26*, 7154.

(47) Robertson, J. *Materials Today,* **2004**, *7*, 46.

(48) Park, C.; Ounaies, Z.; Watson, K. A.; Crooks, R. E.; Smith, J.; Lowther, S. E.; Connell, J. W.; Siochi, E. J.; Harrison, J. S.; Clair, T. L. S. *Chemical Physics Letters* **2002**, *364*, 303.

(49) de Jonge, N.; Lamy, Y.; Schoots, K.; Oosterkamp, T. H. *Nature* **2002**, *420*, 393.

(50) Niu, C. M.; Sichel, E. K.; Hoch, R.; Moy, D.; Tennent, H. *Applied Physics Letters* **1997**, *70*, 1480.

(51) Tans, S. J.; Devoret, M. H.; Dai, H. J.; Thess, A.; Smalley, R. E.; Geerligs, L. J.; Dekker, C. *Nature* **1997**, *386*, 474.

(52) Bachtold, A.; Hadley, P.; Nakanishi, T.; Dekker, C. *Science* **2001**, *294*, 1317.

(53) Heinze, S.; Tersoff, J.; Martel, R.; Derycke, V.; Appenzeller, J.; Avouris, P. *Physical Review Letters* **2002**, *89*.

(54) Chen, J.; Klinke, C.; Afzali, A.; Avouris, P. *Applied Physics Letters* **2005**, *86*, 1.

(55) Artukovic, E.; Kaempgen, M.; Hecht, D. S.; Roth, S.; GrUner, G. *Nano Letters* **2005**, *5*, 757.

(56) Yoon-Taek Jang, Y.-H. L., Byeong-Kwon Ju, Jin-Ho Ahn, Chang-Ki Go, Gong-Seog Park. *Vacuum* **2003**, *68*, 79.

(57) Dehouche, Z.; Lafi, L.; Grimard, N.; Goyette, J.; Chahine, R. *Nanotechnology* **2005**, *16*, 402.

(58) Cho, W. S.; Moon, S. I.; Paek, K. K.; Lee, Y. H.; Park, J. H.; Ju, B. K. *Sensors and Actuators B-Chemical* **2006**, *119*, 180.

(59) Kaempgen, M.; Roth, S. *Journal of Electroanalytical Chemistry* **2006**, *586*, 72.

(60) Iijima, S. *Nature* **1991**, *354*, 56.

(61) Ajayan, P. M.; Lambert, J. M.; Bernier, P.; Barbedette, L.; Colliex, C.; Planeix, J. M. *Chemical Physics Letters* **1993**, *215*, 509.

(62) Bronikowski, M. J.; Willis, P. A.; Colbert, D. T.; Smith, K. A.; Smalley, R. E. *Journal of Vacuum Science & Technology a-Vacuum Surfaces and Films* **2001**, *19*, 1800.

(63) Lobach, A.S.; Spitsina, N. G.; Terekhov, S. V.; Obraztsova. E. D.; *Physics of the Solid State* **2002**, *44*, 475.

(64) Girifalco, L. A.; Hodak, M.; Lee, R. S. *Physical Review B* **2000**, *62*, 13104.

(65) Maeda, Y.; Kimura, S.; Hirashima, Y.; Kanda, M.; Lian, Y. F.; Wakahara, T.; Akasaka, T.; Hasegawa, T.; Tokumoto, H.; Shimizu, T.; Kataura, H.; Miyauchi, Y.;

Maruyama, S.; Kobayashi, K.; Nagase, S. *Journal of Physical Chemistry B* **2004**, *108*, 18395.

(66) Taniguchi, N.; Proc. Intl. Conf. Prod. Eng. Tokyo, Part II, Japan Society of Precision Engineering, 1974.

CHAPTER 2

“Single Walled Carbon Nanotubes”

2.1 Physical Structure of Carbon Nanotubes

Carbon nanotubes can be thought of as a single layer of graphene rolled up to make a seamless cylinder with a diameter of the order of nano meters and a length of up to tens of microns, each end being capped with half a fullerene molecule. Based on the number of concentric layers, carbon nanotubes can be either single walled carbon nanotubes (SWNTs) or multiwall (MWNTs) as shown in figure 2.1.

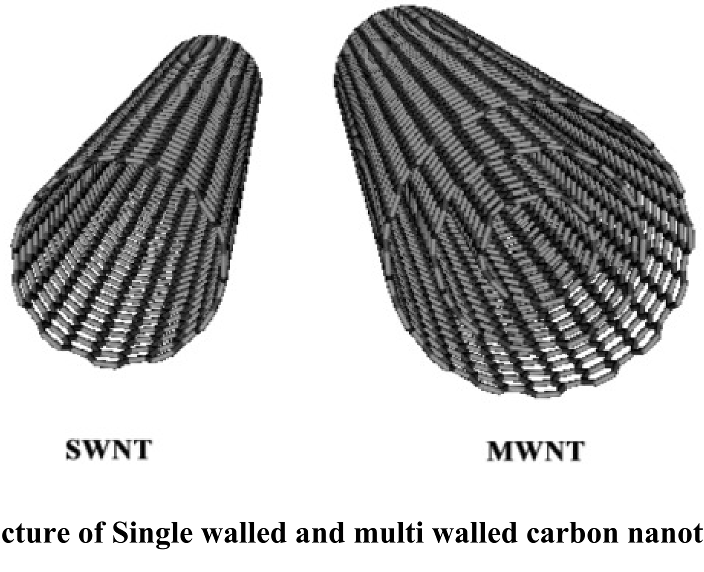

Figure 2.1: Structure of Single walled and multi walled carbon nanotube showing the concentric layers[1].

They have high aspect ratio[2] (length to diameter ratio), which can be as large as 10^4-10^5, high a Young's modulus as high as ~1TPa[3] and high thermal conductivities of 6600 W/mK at room temperature[4]. The carbon atoms are sp^2 hybridised, the hybrid orbitals forming strong σ bonds with neighbouring carbon atoms to make up the hexagonal honeycomb lattice, while the remaining p electron contributes to the large π electron system which provides electron mobility along the tube surface. This electron mobility is largely confined to one direction making them 1D electronic structures.

Depending on their chirality, the 1D electronic structure of SWNTs can be either metallic or semi conducting[2]. The chirality is the direction of the twist of the tube, i.e. the orientation of the hexagonal carbon rings with respect to the tube axis. It is one of the most important factors of the SWNTs that determines many properties such as electrical conductance [5]. Figure 2.2 depicts a single graphene sheet which can form the basis of SWNT. Depending on how the sheet is rolled, the nanotube will have a chirality described by the chiral vector C_h which can be expressed as

$$C_h = na_1 + ma_2 \qquad \text{Equation 2.1}$$

where n and m are integers, a_1 and a_2 are the real space unit vectors of the honey comb graphene layer as shown in figure2.2. If T and T' are the two parallel lines drawn along the nanotube axis, C_h can be obtained in the following manner. On the T and T' lines, mark the carbon atoms O and O' which exactly coincides on the lines and this line connecting OO' is the chiral vector.

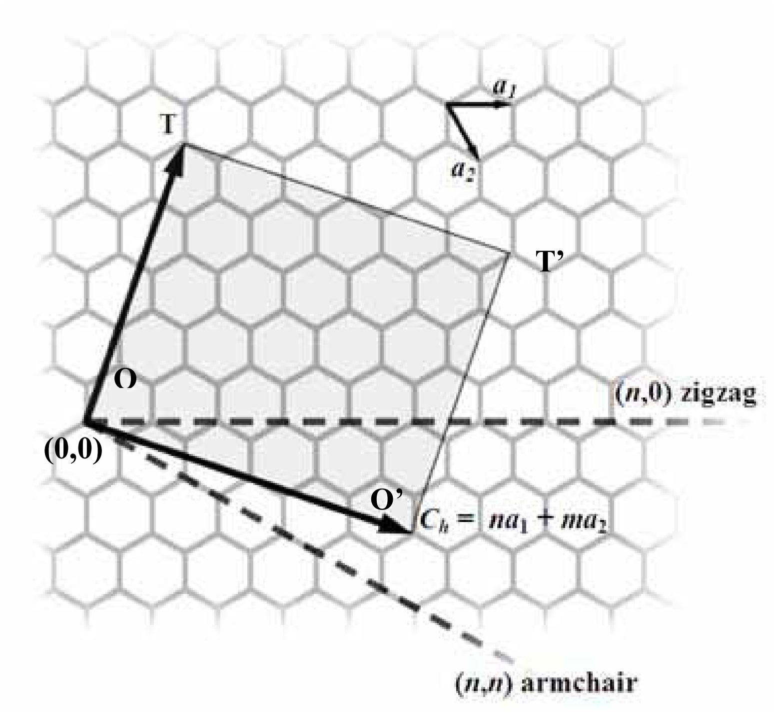

Figure 2.2: Schematic representation of a graphene sheet[6]

The angle between the vector C_h and the unit vector a_1 is the chiral angle θ which can range from $0^\circ \leq \theta \leq 30^\circ$ and can be determined from equation 2.2[7]

$$\theta = \tan^{-1}\left(\frac{\sqrt{3}m}{m+2n}\right) \qquad \text{Equation 2.2}$$

Having determined the chirality, the chiral integers can be directly related to the diameter "d" of the tube, which is given by equation 2.3[8]

$$d = \frac{a_{c-c}\sqrt{3\left(n^2+m^2+nm\right)}}{\pi} \qquad \text{Equation 2.3}$$

where “a_{c-c}” is the lattice constant and is equal to 0.142 nm[7].

SWNTs can be either chiral [(non-symmorphic) (Figure 2.3c)] or achiral (symmorphic) depending on the orientation of the carbon hexagons with respect to the tube axis. A molecule is said to be chiral (from the Greek word *Chiron* – hand) if its mirror image is not super imposable on itself and achiral if it has a super imposable mirror image. Armchair (Figure 2.3a) and Zigzag (Figure 2.3b) carbon nanotubes come under the category of achiral nanotubes. Armchair nanotubes are formed when n = m and the chiral angle θ is 30°. Zigzag nanotubes are formed when either n or m is zero and the chiral angle θ is 0°. These derive their name from the circumferential pattern of the carbon-carbon bonds as shown in the figure 2.3 and 2.2.

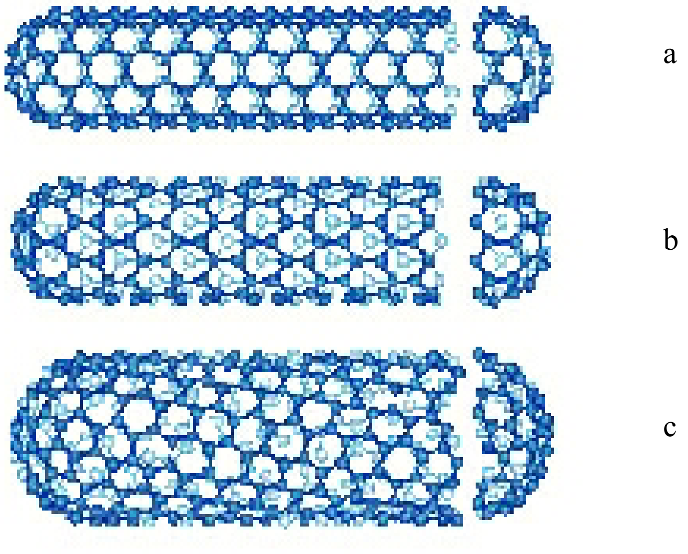

Figure 2.3: a) Armchair, b) Zigzag, c) Chiral tube[9]

2.2 Electronic Structure of Carbon Nanotubes

The differing electronic structures of SWNTs is a result of the chiral structure and has been derived by tight binding calculation for the π electrons of the carbon atoms[2]. The electronic energy gap E_g can be related to the diameter[10] and is given by equation 2.4

$$E_g = t\, a_{c\text{-}c}/d \qquad \text{Equation 2.4}$$

where t is the nearest neighbour carbon to carbon bond tight binding overlap energy.The dispersion relations[11] (Figure 2.4) show how the electronic energy in three types of nanotube varies with wavevector. In the one dimensional energy dispersion relation, the valence and the conduction bands for all the armchair nanotubes cross at the k point and the crossing takes place at the Fermi level[11]. Each curve corresponds to a single quantum sub band. The Fermi level is at $E = 0$, below which energy states (below Fermi level) are fully occupied, while higher energy states (above Fermi level) are completely empty. Figure 2.4 a and 2.4 b show for example the electronic energy dispersion of an armchair (5, 5) nanotube and a zigzag (9, 0) nanotube respectively. In both cases, a small amount of energy is needed to excite an electron into an empty higher state and such nanotubes are termed as metallic. In other words metallic tubes can also be considered as zero band gap semiconductors as some electrons have access to the conduction band without the requirement of external energy. For a zigzag (10, 0) nanotube (Figure 2.4 c), there is a finite band gap between the occupied and empty states, so this nanotube is a semiconductor. A small increase in diameter therefore has a major impact on the conduction properties of carbon nanotubes.

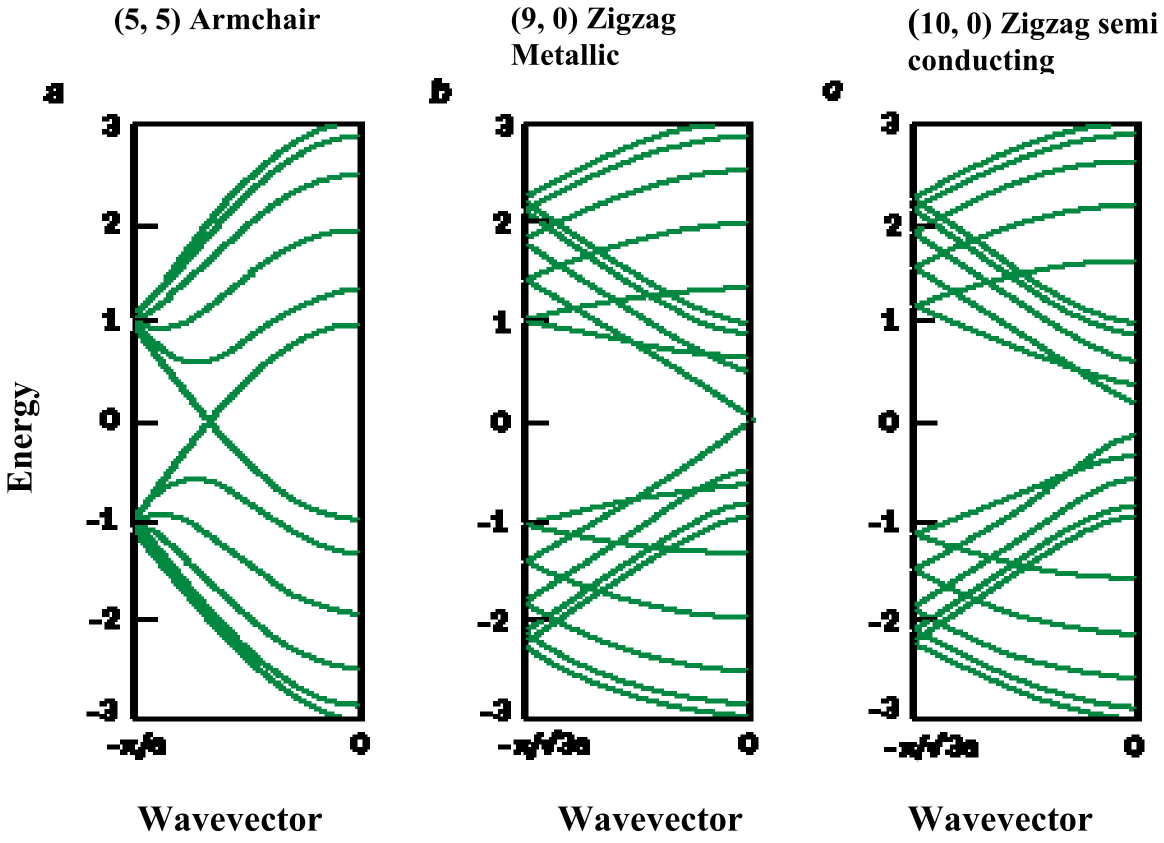

Figure 2.4: One dimensional energy dispersion of (a) (5, 5) Armchair carbon , (b) (9, 0) Zigzag Metallic, (c) (10, 0) Zigzag semi conducting carbon nanotubes[11].

Because of the degeneracy point between the valence band and the conduction band, the armchair nanotube is considered as a zero band gap semi conductor which will exhibit metallic conduction at finite temperatures [12-14]. Therefore armchair tubes are metallic but zigzag nanotubes can be either metallic or semi conducting. For (n, 0), i.e. zigzag tubes, when n is a multiple of 3, the energy gap at k=0 becomes zero (metallic tubes) and when n is not a multiple of 3, an energy gap opens at k=0 (semi conducting tubes). For chiral nanotubes, in general if the difference between n and m is a multiple of 3 the nanotubes are metallic while the others are semi conducting. An overall representation of the range of electronic properties of SWNTs is given in figure 2.5[15] .

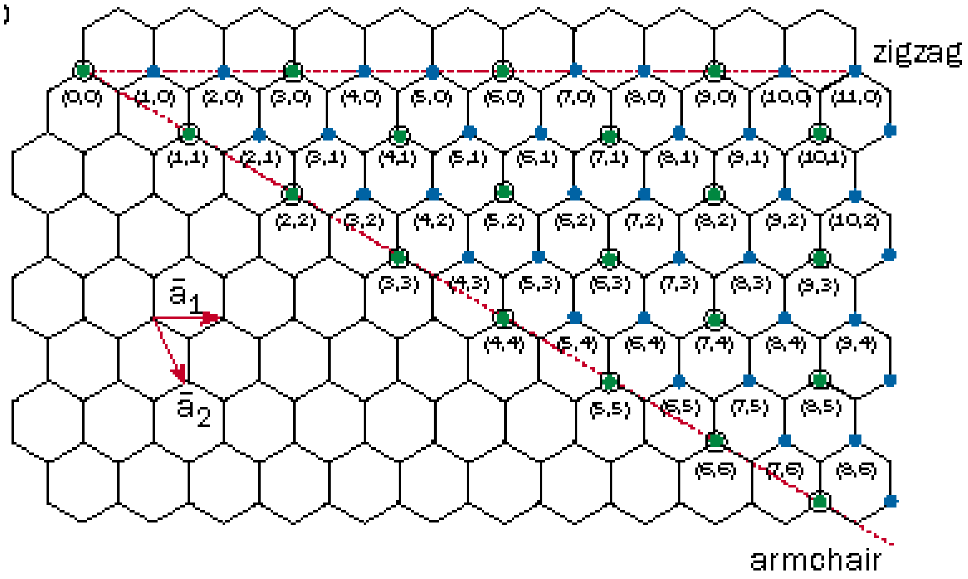

Figure 2.5: Overall representation of chirality of the tubes. The metallic and semi conducting tubes are denoted by green and blue circles respectively[16]

The density of states (DOS) in carbon nanotubes is quantised resulting in sharp peaks known van Hove Singularities[17] (vHSs) as shown in figure 2.6. The value of the DOS at the Fermi level is zero for semi conducting nanotubes as there are no electrons found in the forbidden gap while it is non zero for metallic nanotubes as shown in figure 2.6. An electronic transition can take place between the quantised sub bands - $\mathbf{c}_{n=1,\ 2,\ 3,}$ and $\mathbf{v}_{n=1,2,3}$. $c_{n=1,\ 2,\ 3,}$ and $\mathbf{v}_{n=1,2,3}$ are quantised sub bands in the conduction band and valence band respectively shown for both metallic and semiconducting tubes.

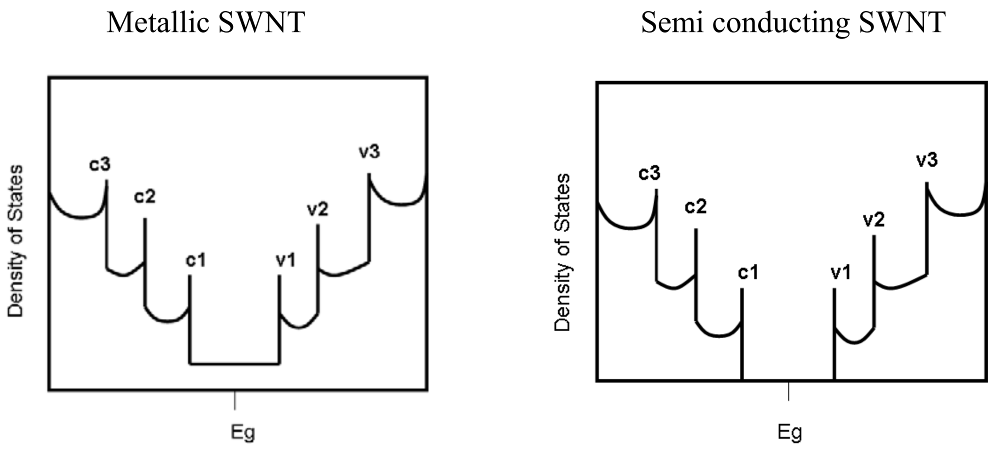

Metallic SWNT

Semi conducting SWNT

Figure 2.6: Schematic representation of the density of states of SWNT[18].

For both the semi conducting and metallic nanotubes, the energy gap depends upon the reciprocal of the nanotube diameter specified by equation 2.4. The term "band gap" in metallic nanotubes is applied to the energy separation of the first pair of singularities in the electronic density of metallic tubes[11].

The electronic structure of atomically resolved individual SWNT using Scanning Tunnelling Microscopy and Spectroscopy was reported by Jeroen *et al* [10]. They confirmed that the electronic properties of the tubes depend on the wrapping angle and also observed the vHSs at the onset of one-dimensional energy bands. This work experimentally proved the proposal that the band gap of the semi conducting tubes was inversely proportional to its diameter.

The transition of electrons from one band to another can take place by absorption of incident radiation of the appropriate energy. The transitions are represented as S_{11} and M_{11} where S and M represent semi conducting and metallic tubes respectively and the numbers represent the respective levels in the density of states as shown in figure 2.6. S_{11} represents the transition of electrons in a semi conducting tube from v1 of the valence band to c1 of the conduction band. This transition can be seen in the Ultra Violet-Visible-Near Infra Red (UV/Vis/NIR) absorption spectrum of SWNT as shown in figure 2.7.

2.3 Spectroscopic characterisation of Carbon Nanotubes

2.3.1. Absorption Spectroscopy

At this juncture it is worthwhile to explain why absorption and Raman spectroscopes have been chosen for characterisation of SWNTs. Single walled carbon nanotubes can be structurally variable resulting in a significant variation of their electronic properties. To obtain information about the structure one should study the unique optical and spectroscopic properties observed in SWNTs which are largely due to the one dimensional confinement of the electron and phonon states in the nanotube density of states (DOS). van Hove Singularities are formed by folding the two dimensional energy bands of the graphene layer into the one dimensional band of the carbon nanotube, by which the density of states of the π bands becomes singular[4]. Whenever the energy of an incident photon matches that of the energy difference between vHSs, an optical transition of the electron from valence band to conduction band can be achieved, leading to resonant enhancement of the corresponding photo physical process[6]. The UV/Vis/NIR absorption spectrum of a SWNT sample (figure 2.7), yields information about the distribution of semi-conducting and metallic tubes within the sample. The boxes represent the approximate boundaries for metallic and semiconducting transitions. M_{11} represents the electronic transitions between valence band 1 to conduction band 1 in the DOS of the metallic tubes. In semiconducting nanotubes, S_{22} and S_{11} are the electronic transitions between the second and the first valence to conduction bands respectively.

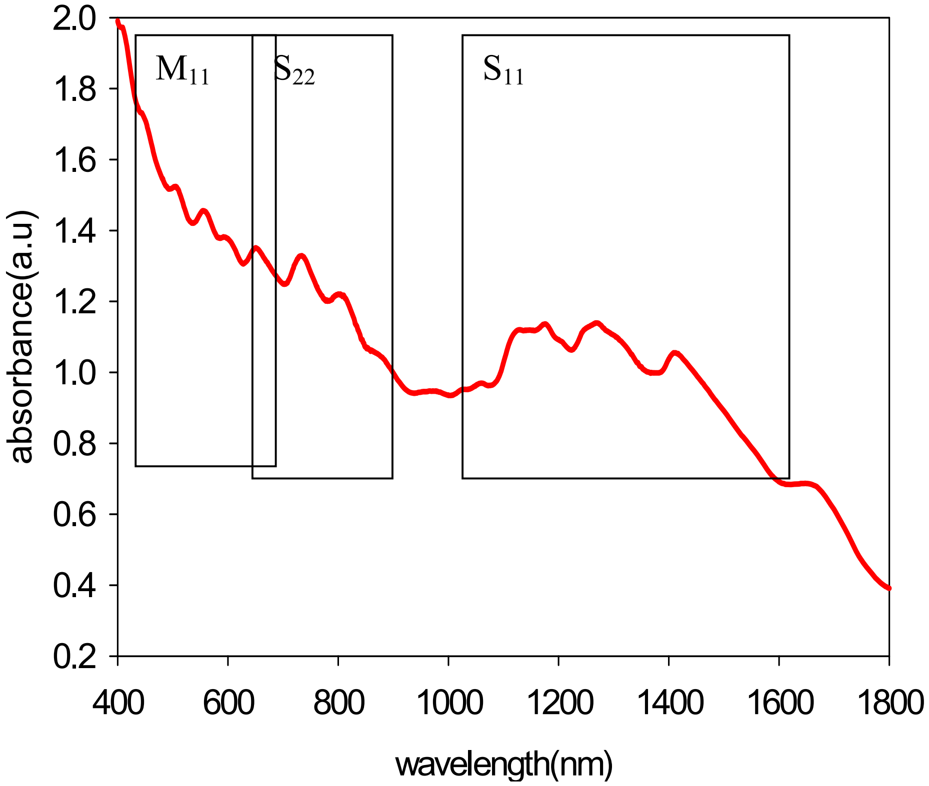

Figure 2.7: Absorption spectrum of HiPco SWNTs in water/SDBS solution showing the electronic transitions of metallic and semiconducting tubes.

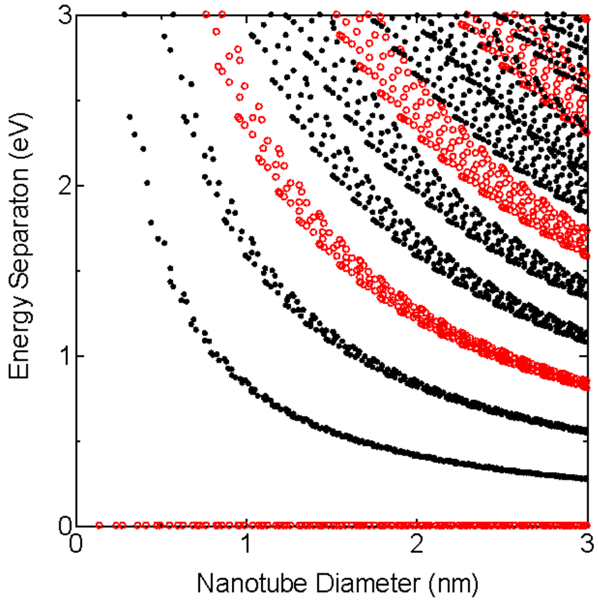

Figure 2.8: The Kataura plot[19] shows the relationship between the energy band gap and the diameter of the tubes. Red circles represent the metallic SWNTs and black circles represent the semiconducting tubes.

As can be seen from the spectrum, transitions between the vHSs of the SWNT occur from the visible region to the near infra red region and Kataura *et al* demonstrated experimentally for the first time, the relationship between the gap energies of the SWNT and their respective diameter[19] as shown in the Figure 2.8. This relationship is given by the following equations

$^{M}E_{11}= 6\gamma\ a_{c\text{-}c}/d$ Equation 2.4 a

$^{S}E_{22}= 4\gamma\ a_{c\text{-}c}/d$ Equation 2.4 b

$^{S}E33= 8\gamma\ a_{c\text{-}c}/d$ Equation 2.4 c

Thus, absorption spectroscopy has been widely used for the optical characterisation of carbon nanotubes, and particularly in dispersion studies , monitoring the separation process[20] and also quantifying it [21-23]. Using the optical absorbance ratio of metallic to semiconducting SWNTs, Houjin Haung[24] showed how metallic and semiconducting SWNTs can be largely affected by the surrounding environment. The red shift of a vHSs can be used as a qualitative measure of agglomeration[25]. Giordani et al[26] reported the observation of large populations of individual nanotubes when SWNTs were solubilised in N-methyl -2- pyrrolidone below the dispersion limit. This dispersion limit was determined by using the Lambert Beer law (absorbance of SWNTs as a function of concentration) to calculate the extinction coefficient of tubes dispersed at higher and lower concentration. In short, absorbance spectroscopy, in addition to its use in studying the electronic structure and composition of a given sample, can be used for many other characterisation purposes. More details of how it is used in this study are given in chapter 4.

2.3.2. Raman spectroscopy

Raman Spectroscopy has also proven to be an excellent probe for examining carbon nanotubes. The strongest Raman modes are the tangential graphitic modes (G mode) and the radial breathing modes (RBM)[27]. Figure 2.9 shows a schematic representation of the vibrations leading to the graphitic and radial breathing modes. A typical Raman spectrum of a HiPco SWNT sample at 633 nm excitation wavelength is shown in figure 2.10. The region at 100 - 400 cm^{-1} is the RBM region, at ~1585 cm^{-1} is the G band, while the D band or the defect mode and G' band (overtone of the D band) occur at ~1350 cm^{-1} and ~2700 cm^{-1} respectively.

The RBM is a bond stretching out of plane phonon mode for which all the carbon atoms move coherently in the radial direction. The RBM frequency can be related to the tube diameter as shown in equation 2.5

$$\omega_{\text{RBM}} = C/d + \Gamma \qquad \text{Equation 2.5}$$

where C is a constant of proportionality and Γ is a damping factor which is introduced in the above expression because of factors such as tube-tube interactions in bundles. From the RBMs (wave number 180 to 340 cm^{-1}) one can tell whether the tubes are metallic or semiconducting by calculating the chiral index from the diameter. For example in figure 2.10 (Raman spectra of HiPco SWNT at 633nm) the RBMs above 240 cm^{-1} derive from semi conducting SWNTs while the RBM peaks below 240 cm^{-1} derive primarily from metallic tubes[19]. C and Γ vary from study to study depending upon the environment of the carbon nanotubes. The value of C is 248 cm^{-1} when the tubes are isolated and on the Silicon substrate[28] and is 223.5 cm^{-1} when dispersed in water with the aid of surfactants[29-31](see in chapter 5).

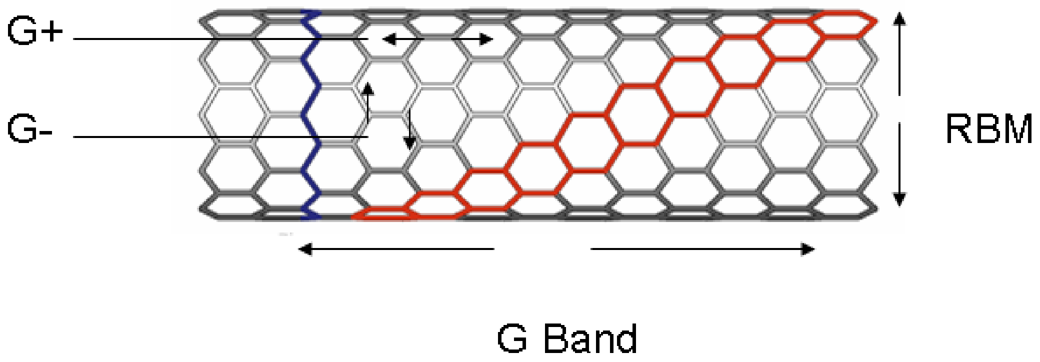

Figure 2.9: Schematic illustration of the different kinds of vibration in a SWNT

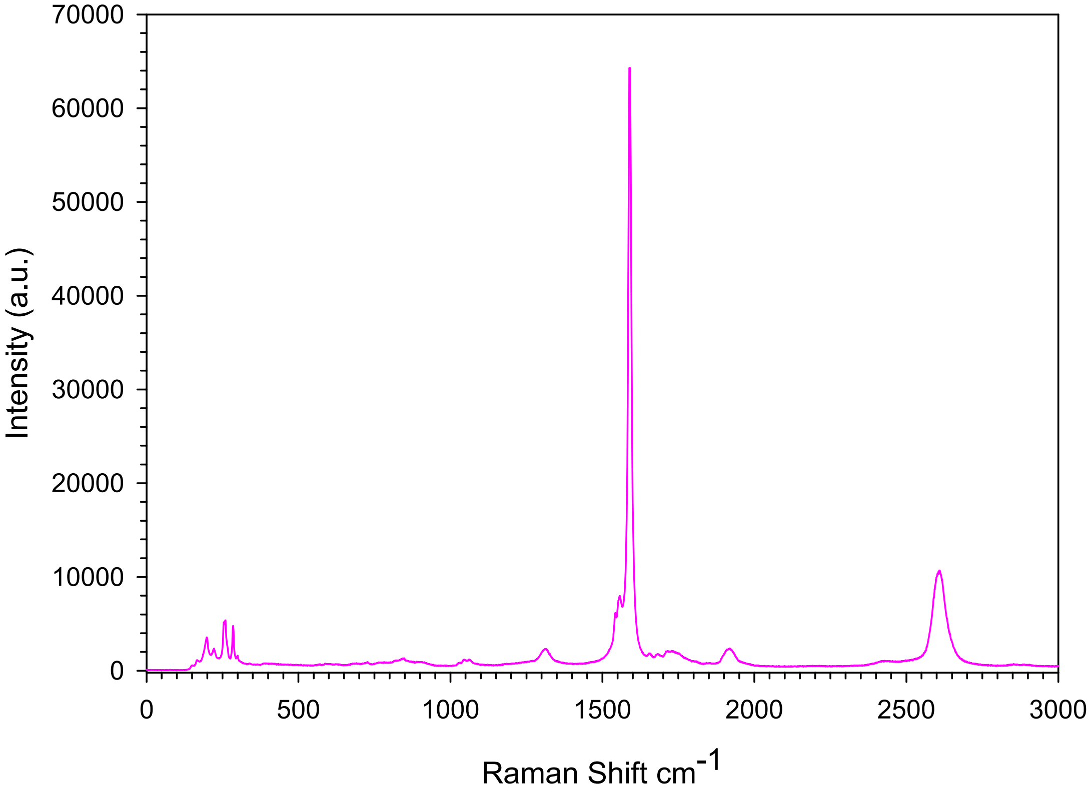

Figure 2.10: A typical Raman Spectra of SWNT in SDBS-water solution. 100-400 cm^{-1} RBM, 1582 cm^{-1} – G mode, D and G' mode occur at 1350 cm^{-1} and 2700 cm^{-1} respectively. Excitation wavelength is 633 nm

The graphitic mode arises due to the tangential vibration of C=C along the nanotube axis and appears at ~1585 cm^{-1}. The G-mode of graphene is split into two main features, the G^+ and the G^- in a carbon nanotube. This split arises due to the curvature of the carbon nanotube. G^+ arises from the vibrations parallel to the back bone of the nanotube and G^- due to the vibrations perpendicular to the tube axis. G^+ has a symmetric Lorentzian line shape and the G^- is sensitive to the electronic properties. If G^- is an asymmetric line shape that is best fitted with a Breit -Wigner- Fano (BWF) line shape, then it is an indication of metallic SWNTs and if G^- is a Lorentzian then it is an indication of semi conducting SWNT[1].

Very recently, M. Paillet *et al.,*[32] observed that the BWF component is an intrinsic feature of metallic SWNT bundles rather than individual nanotubes. They reported that the BWF/G^+ intensity ratio increases with increasing metallic bundling. They also agree with the result obtained by Jiang et al[33] who predicted that the decrease in the BWF/G^+ ratio intensity is due to the interaction between metallic and semi conducting tubes within the same bundle.

The next two important peaks in the Raman Spectra of the SWNTs are the D and G' modes which occur at ~1350 cm^{-1} and ~2700 cm^{-1} respectively. It has been considered that the D mode is a measure of defects in the tubes and the G′ is the second harmonic.

The resonant enhancement of the Raman scattering occurs when the incident excitation energy matches the transition energy between the DOS of the SWNTs. The resonant Raman process increases the signal by a factor of approximately 10^3 compared to the non resonant process. Most importantly, in spectra of SWNT samples, the tubes which dominate at a particular source wavelength are those whose Raman signatures are resonantly enhanced. In the spectrum of figure 2.10, seven RBM peaks can clearly be identified indicating that the sample contains at least seven different nanotubes types with various diameters. However, if the spectrum of the same sample was taken with a different laser source, a rather different spectrum would be obtained. Also, as semiconducting and metallic nanotubes of similar diameters have different transition energies, Raman spectroscopy with several laser energies can be used to characterise the metallic and semiconducting entities in the sample. The Kataura plot (Figure 2.8), can be used to select the laser excitation energy to probe the respective diameter tubes in the metallic and semiconducting region. For example, a 514 nm source predominantly probes metallic tubes and a small range of semiconducting tubes while the situation for 633 nm is the opposite[31]. Thus, it can be important to consider a number of source wavelengths when characterising a sample using Raman spectroscopy.

Like absorption spectroscopy, Raman can be used for dispersion studies of SWNTs[26,34], monitoring the separation process and quantifying it[35,36]. HiPco tubes purified by controlled thermal oxidation in air were studied by Raman spectroscopy at 300 and 5 K[37]. Michael S. Strano used Raman Spectroscopy with a range of excitation wavelengths to compare the observed spectra to an experimentally produced mapping of interband transitions[29]. C. Fantini analysed the DNA assisted SWNT dispersion using Raman spectroscopy and concluded that the sample solution is enriched with semiconducting tubes when the tubes are dispersed with DNA[38].

Therefore optical absorption and Raman spectroscopy are important characterisation methods that have been widely used for the analysis of carbon nanotube samples. SWNTs are ideal materials for Raman Spectroscopy as a simple finger print of the material can be obtained. Small changes in the electronic structure of the tubes can be directly visualised using both spectroscopic methods.

2.4 Carbon Nanotube Dispersions

Many of the properties of SWNTs have been established theoretically and one of the main challenges is to establish processes for routine dispersion, characterisation and also for further application purposes. Also to date there have been no reports of the controlled production of individually separated tubes with one electronically dominating species. One of the post synthesis treatments to obtain individually dispersed SWNTs is to disperse them in organic or inorganic solvents with or without an external dispersing agent. O' Connell *et al*[39] observed fluorescence directly across the band gap of semi conducting nanotubes by preparing aqueous dispersions using Sodium Dodecyl Sulphonate (SDS) surfactant with the aid of sonication and centrifugation. Aqueous dispersion of a high weight fraction of SWNTs was obtained by suspending the tubes with the aid of Sodium Dodecyl Benzene Sulphonate (SDBS) surfactant[40]. Moore *et al.,* reported on the aqueous dispersion of tubes using anionic, cationic, non ionic surfactants and polymers and concluded that SDBS was the optimum surfactant for suspending nanotubes[41]. The presence of the long aliphatic chain and benzene ring were proposed as the main reasons for the high dispersive efficiency of SDBS[40]. Researchers were also interested in studying the interaction and adsorption between the surfactant molecules and the surface of carbon nanotubes[39,42,43]. It was reported by Matarredona[42] *et al.,* that the interaction between surfactant and the nanotube walls is mostly hydrophobic in nature and Islam *et al.*, concluded that electrostatic repulsion of sulphate leads to significant solubilisation in water[40].

SWNTs have also been dispersed in water with the aid of single stranded DNA and electronic separation of SWNTs using ion exchange chromatography was also reported[22].

DNA has furthermore been reported to induce circular dichroism in SWNTs[44]. Huang *et al.,* demonstrated the purification of DNA - wrapped SWNTs and separation into fractions of uniform length using size exclusion chromatography[45].

On the other hand several groups have reported on the dispersion of SWNTs in various organic solvents with and without added dispersing agents. Optical absorption analyses of SWNTs dispersed in N, N - dimethylfomamamide (DMF), N, N - dimethylacetamide (DMA), N, N - diethylactemide (DEA) and N, N - dimethylpropanamide (DMP) have been performed and the dispersion limit /solubility limit of SWNTs for each solvent has been estimated[46]. DMA, with its highly polar π system and optimal geometry was found to be the best solvent for SWNTs with a higher dispersion limit of 6.25 μg /ml than DMF, DEA and DMP and the dispersions also proved to be stable for weeks[46]. First evidence of luminescence from SWNTs dispersed in Tetrahydrofuran (THF) with the aid of octylamine was provided by Yutaka Maeda *et al.*,[47]. They also suggested that the dispersibility of the nanotubes decreases in the order of primary, secondary, and tertiary amines and the reason was due to the fact that the interaction between SWNTs and amines is sensitive to steric hindrance around the nitrogen atom.

Kevin D. Ausman *et al.,* investigated the dispersions of SWNTs in N-methylpyrrolidone (NMP), DMF, hexamethyl phosphoramide, cyclopentanone, tetramethylene sulfoxide and caprolactone (all these solvents have high values of electron pair donicity " β " and negligible values for hydrogen bonding donation parameter " α ") and finally concluded that Lewis basicity without hydrogen donors is a key to good solvation of SWNTs[48]. Also the dispersion limit for the SWNTs dispersed in NMP was determined to be 0.02 mg/mL and the optical extinction coefficient at lower concentration was found to be 3264 mL mg^{-1} m^{-1} [26]. The mass fraction of individual SWNTs increased as the concentration was decreased, approaching 70 % at low concentration (below the dispersion limit)[26]. A systematic study of dispersion of HiPco SWNTs in various organic solvents was carried out by Cheng *et al.*, and they confirmed that the polar interactions and hydrogen bonding play a major role in the in the formation of stable SWNT dispersions[49]. Hedderman *et al.*, studied the interaction of the SWNTs with the dye molecules anthracene and *p*-terphenyl in toluene[50]. They reported that the solubility of the tubes is due to π- π interactions of the dye molecules and the nanotube surface. The results that were obtained also indicated a degree of electronic selectivity suggesting that anthracene preferentially interacted with metallic SWNTs whereas *p*-terphenyl preferentially interacted with semi conducting SWNTs[50].

All theses studies show that dispersion is one of the best, simple and straight forward methods to obtain isolated tubes. Dispersed SWNTs can serve as paradigm for one dimensional structure that can be used for routine spectroscopical and microscopical characterisation.

In this study Sodium Dodecyl Benzene Sulphonate (SDBS -anionic surfactant) is used to disperse HiPco carbon nanotubes in water. This system (water – surfactant) was chosen for the dispersing carbon nanotubes mainly because they can be used for

1) Routine Characterisation - Provide a very simple "solution system" for characterisation using absorption and Raman spectroscopy and for deposition onto substrates for microscopical characterisation.

2) Suspension in a solvent allows for bulk characterisation of the sample without the need for multiple samplings to achieve a sample average as is the case for solid state measurements.

It should also be noted that water has high optical transparency and is a very weak Raman scattering rendering it a minimally invasive matrix.

3) Electronic structure - No change in the electronic structure of carbon nanotubes is induced.

2.5 Summary

In this chapter the physical, electronic and structural properties of single walled carbon nanotubes have been explained and the relationship between them has been demonstrated using absorption spectroscopy and the Raman specroscopy. An overview of the approaches to dispersion of SWNTs in various organic and inorganic solvents of different reseach groups has been given. In the subsequent work, SWNTs will be predominantly studied in water based surfactant solution and the characterisation techniques of UV/Vis/NIR absorption and Raman spectroscopy will predominantly be employed. Various charecterisation techniques, inculding Raman and UV/Vis/NIR absortion spectrocopies, their basic priciples and instrument set up will be discussed in the next chapter.

References

(1) *http://itech.dickinson.edu/chemistry/wp-content/uploads/2008/04/swnt_mwnt.jpg*. (20-07-09)

(2) Saito, R.; Dresselhaus, G.; Dresselhaus, M. S.; *Physical Properties of Carbon Nanotubes* **1998**.

(3) Reich. S., Thomsec. C., Maultzsch, J. *Carbon Nanotubes- Basic concepts and physical properties* **2004**.

(4) Berber, S.; Kwon, Y. K.; Tomanek, D. *Physical Review Letters* **2000**, *84*, 4613.

(5) http://www.pa.msu.edu/cmp/csc/ntproperties/. (20-07-09)

(6) *http://www.ccnano.com/pages/Carbon%20nanotube.htm*. (20-07-09)

(7) Dresselhaus, M. S.; Dresselhaus, G.; Saito, R.; Jorio, A. *Physics Reports-Review Section of Physics Letters* **2005**, *409*, 47.

(8) Odom, T. W.; Huang, J. L.; Kim, P.; Lieber, C. M. *Nature* **1998**, *391*, 62.

(9) *http://www.personal.rdg.ac.uk/~scsharip/tubes.htm*. (20-07-09)

(10) Wildoer, J. W. G.; Venema, L. C.; Rinzler, A. G.; Smalley, R. E.; Dekker, C. *Nature* **1998**, *391*, 59.

(11) Dresselhaus, M. S.; Dresselahaus.G; Eklund, P.C; *Academic Press, New York* **1996**.

(12) Hamada, T.; Furuyama, M.; Tomioka, T.; Endo, M. *Journal of Materials Research* **1992**, *7*, 1178.

(13) Mintmire, J. W.; Dunlap, B. I.; White, C. T. *Physical Review Letters* **1992**, *68*, 631.

(14) Saito, R.; Fujita, M.; Dresselhaus, G.; Dresselhaus, M. S. *Physical Review B* **1992**, *46*, 1804.

(15) Dresselhaus, M. S.; Dressalhaus, G.; Avouris, P.; *Springer- verlag, Berlin* **2001**.

(16) http://nanotube.korea.ac.kr/study_eng_2.html. (20-07-09)

(17) Joselevich, E. *Chemphyschem* **2004**, *5*, 619.

(18) Yu, Z. H.; Brus, L. *Journal of Physical Chemistry B* **2001**, *105*, 1123.

(19) Kataura, H.; Kumazawa, Y.; Maniwa, Y.; Umezu, I.; Suzuki, S.; Ohtsuka, Y.; Achiba, Y. *Synthetic Metals* **1999**, *103*, 2555.

(20) Chattopadhyay, D.; Galeska, L.; Papadimitrakopoulos, F. *Journal of the American Chemical Society* **2003**, *125*, 3370.

(21) Maeda, Y.; Kimura, S.; Kanda, M.; Hirashima, Y.; Hasegawa, T.; Wakahara, T.; Lian, Y.; Nakahodo, T.; Tsuchiya, T.; Akasaka, T.; Lu, J.; Zhang, X.; Gao, Z.; Yu, Y.; Nagase, S.; Kazaoui, S.; Minami, N.; Shimizu, T.; Tokumoto, H.; Saito, R. *J Am Chem Soc* **2005**, *127*, 10287.

(22) Zheng, M.; Jagota, A.; Semke, E. D.; Diner, B. A.; Mclean, R. S.; Lustig, S. R.; Richardson, R. E.; Tassi, N. G. *Nature Materials* **2003**, *2*, 338.

(23) Zheng, M.; Jagota, A.; Strano, M. S.; Santos, A. P.; Barone, P.; Chou, S. G.; Diner, B. A.; Dresselhaus, M. S.; McLean, R. S.; Onoa, G. B.; Samsonidze, G. G.; Semke, E. D.; Usrey, M.; Walls, D. J. *Science* **2003**, *302*, 1545.

(24) Huang, H. J.; Kajiura, H.; Maruyama, R.; Kadono, K.; Noda, K. *Journal of Physical Chemistry B* **2006**, *110*, 4686.

(25) Ryabenko, A. G.; Dorofeeva, T. V.; Zvereva, G. I. *Carbon* **2004**, *42*, 1523.

(26) Giordani, S.; Bergin, S. D.; Nicolosi, V.; Lebedkin, S.; Kappes, M. M.; Blau, W. J.; Coleman, J. N. *Journal of Physical Chemistry B* **2006**, *110*, 15708.

(27) Dresselhaus, M. S.; Dresselhaus, G.; Saito, R.; A. Jorio *Physics Reports* **2005**, *409*, 47.

(28) Jorio, A.; Saito, R.; Hafner, J. H.; Lieber, C. M.; Hunter, M.; McClure, T.; Dresselhaus, G.; Dresselhaus, M. S. *Physical Review Letters* **2001**, *86*, 1118.

(29) Strano, M. S.; Doorn, S. K.; Haroz, E. H.; Kittrell, C.; Hauge, R. H.; Smalley, R. E. *Nano Letters* **2003**, *3*, 1091.

(30) Bachilo, S. M.; Strano, M. S.; Kittrell, C.; Hauge, R. H.; Smalley, R. E.; Weisman, R. B. *Science* **2002**, *298*, 2361.

(31) Strano, M. S. *Journal of the American Chemical Society* **2003**, *125*, 16148.

(32) Paillet, M.; Poncharal, P.; Zahab, A.; Sauvajol, J. L.; Meyer, J. C.; Roth, S. *Phys Rev Lett* **2005**, *94*, 237401.

(33) Jiang, C.; Kempa. K.; Zhao, J.; Schlecht, U.; Kolb, U.; Basche, T.; Burghard, M.; and Mews, A.; *Phys. Rev. B 66, 161404, (2002).* **2002**, *66, 161404, (2002).*

(34) Heller, D. A.; Barone, P. W.; Swanson, J. P.; Mayrhofer, R. M.; Strano, M. S. *Journal of Physical Chemistry B* **2004**, *108*, 6905.

(35) Chen, Z. H.; Du, X.; Du, M. H.; Rancken, C. D.; Cheng, H. P.; Rinzler, A. G. *Nano Letters* **2003**, *3*, 1245.

(36) Chattopadhyay, D.; Galeska, I. E.; Kim, S. N.; Papadimitrakopoulos, F. *Abstracts of Papers of the American Chemical Society* **2003**, *226*, U479.

(37) Karachevtseva, V. A.; Glamazda, A. Y.; Dettlaff-Weglikowska, U.; Kurnosov, V. S.; Obraztsova, E. D.; Peschanskii, A. V.; Eremenko, V. V.; Roth, S. *Carbon* **2003**, *41*, 1567.

(38) Fantini, C.; Jorio, A.; Santos, A. P.; Peressinotto, V. S. T.; Pimenta, M. A. *Chemical Physics Letters* **2007**, *439*, 138.

(39) O'Connell, M. J.; Bachilo, S. M.; Huffman, C. B.; Moore, V. C.; Strano, M. S.; Haroz, E. H.; Rialon, K. L.; Boul, P. J.; Noon, W. H.; Kittrell, C.; Ma, J. P.; Hauge, R. H.; Weisman, R. B.; Smalley, R. E. *Science* **2002**, *297*, 593.

(40) Islam, M. F.; Rojas, E.; Bergey, D. M.; Johnson, A. T.; Yodh, A. G. *Nano Letters* **2003**, *3*, 269.

(41) Moore, V. C.; Strano, M. S.; Haroz, E. H.; Hauge, R. H.; Smalley, R. E.; Schmidt, J.; Talmon, Y. *Nano Letters* **2003**, *3*, 1379.

(42) Matarredona, O.; Rhoads, H.; Li, Z. R.; Harwell, J. H.; Balzano, L.; Resasco, D. E. *Journal of Physical Chemistry B* **2003**, *107*, 13357.

(43) Yurekli, K.; Mitchell, C. A.; Krishnamoorti, R. *Journal of the American Chemical Society* **2004**, *126*, 9902.

(44) Dukovic, G.; Balaz, M.; Doak, P.; Berova, N. D.; Zheng, M.; Mclean, R. S.; Brus, L. E. *Journal of the American Chemical Society* **2006**, *128*, 9004.

(45) Huang, X. Y.; McLean, R. S.; Zheng, M. *Analytical Chemistry* **2005**, *77*, 6225.

(46) Landi, B. J.; Ruf, H. J.; Worman, J. J.; Raffaelle, R. P. *Journal of Physical Chemistry B* **2004**, *108*, 17089.

(47) Maeda, Y.; Kimura, S.; Hirashima, Y.; Kanda, M.; Lian, Y. F.; Wakahara, T.; Akasaka, T.; Hasegawa, T.; Tokumoto, H.; Shimizu, T.; Kataura, H.; Miyauchi, Y.; Maruyama, S.; Kobayashi, K.; Nagase, S. *Journal of Physical Chemistry B* **2004**, *108*, 18395.

(48) Ausman, K. D.; Piner, R.; Lourie, O.; Ruoff, R. S.; Korobov, M. *Journal of Physical Chemistry B* **2000**, *104*, 8911.

(49) Cheng, Q. H.; Debnath, S.; Gregan, E.; Byrne, H. J. *Journal of Physical Chemistry C* **2008**, *112*, 20154.

(50) Hedderman, T. G.; Keogh, S. M.; Chambers, G.; Byrne, H. J. *Journal of Physical Chemistry B* **2006**, *110*, 3895.

CHAPTER 3

Experimental Techniques

3.1 Electronic Spectroscopy

3.1.1. Basic Principle

The electronic states in a molecule or atom are quantised into different energy levels as indicated in figure 3.1 for the case of a diatomic molecule. The number of energy levels or states available for electrons depends on the chemical nature of the material. Usually the electrons at a low energy state (E_0) can be excited in to a higher energy state (E_1) by ***absorption*** of a photon ($E_p = \hbar\omega_a$) as indicated in figure 3.2. This can be achieved when electromagnetic radiation is incident on the material and the energy of the incident radiation is equal to the energy difference between the two available electronic states that is $E_p= E_1-E_0$. The absorption spectrum of a material reflects the distribution of energy levels in the absorbing species. ***Emission*** of a photon $E_p = \hbar\omega_f$ can also take place when electrons from a higher energy state fall back into their lower energy ground state. Before emission, the system takes time to release some of the extra vibration energy as heat to the surroundings and relaxes into a lower vibration state of the excited energy level. The energy of the emitted photon is less than that of the incident photon and the emission spectrum of a molecule tends to be shifted to longer wavelengths (a red or Stokes shift) relative to the absorption spectrum. Emission can be of two types, fluorescence and phosphorescence. The former re-radiates the absorbed energy immediately while phosphorescence (not shown) involves a spin flip in the excited state and an emission from long lived metastable state.

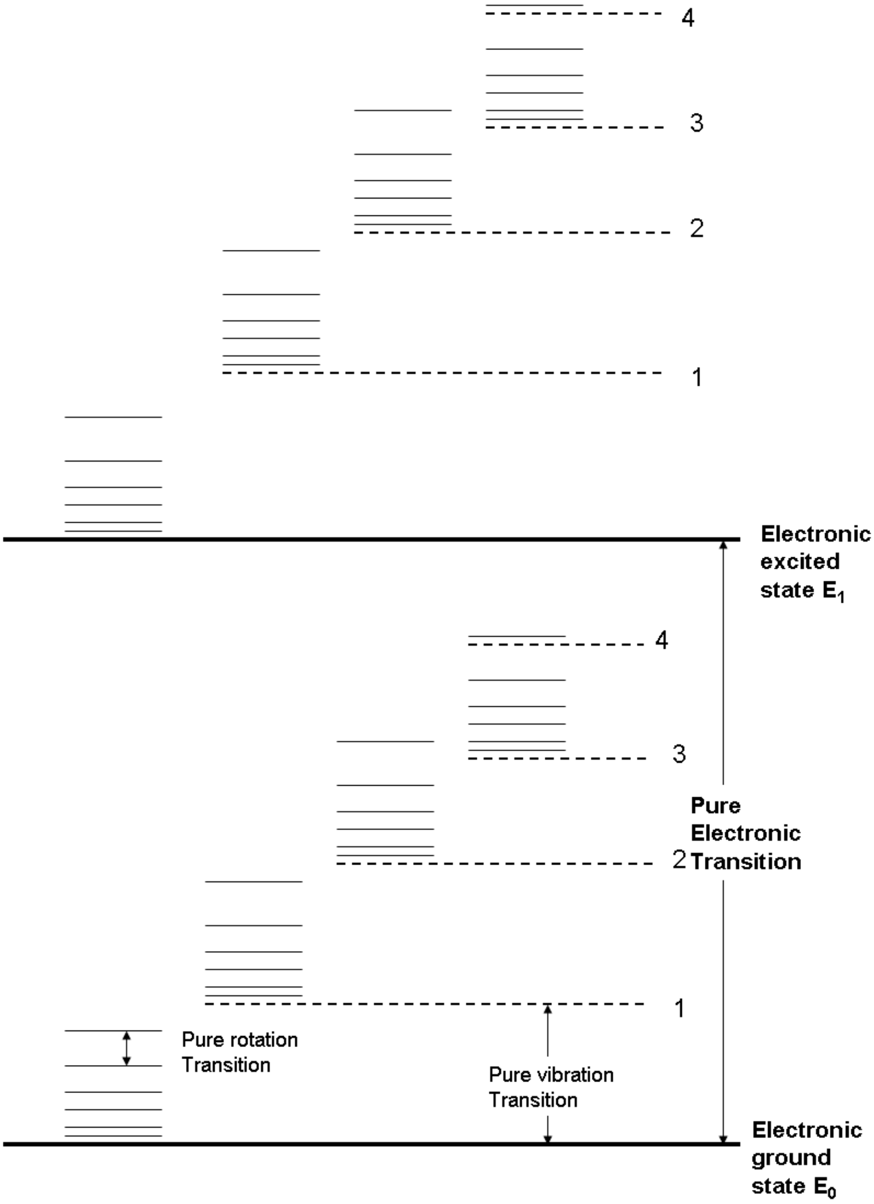

Figure 3.1: Different Sates in a di-atomic molecule[1]

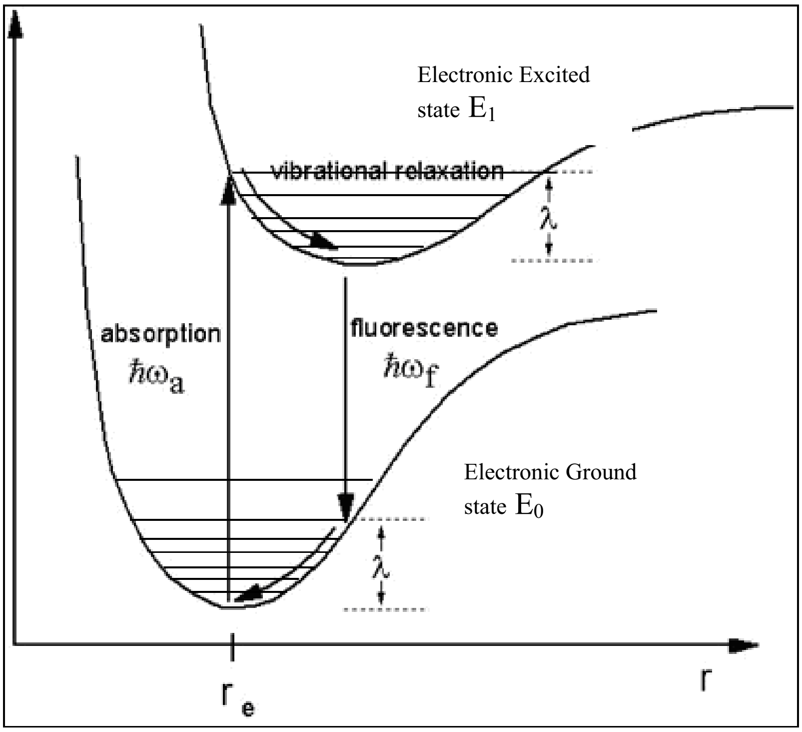

Figure 3.2: Energy levels showing absorption and emission (Fluorescence)

Both these processes (Absorption and Emission) can be used to probe the electronic transitions in a given system by absorption spectroscopy or emission spectroscopy. In this thesis, only UV/Vis/NIR Absorption spectroscopy has been detailed as it is the only electronic spectroscopy that has been used.

3.1.2. Absorbance and Scattering

When an electromagnetic wave of intensity I_{in} passes through a sample, exponential attenuation of the light intensity as a function of the path length *l* of the sample takes place and the intensity of the light that is transmitted I_t is given by the following equations

$$I_t(l) = I_{in}\exp(-\alpha_{ext}\, l) \qquad \text{Equation 3.1}$$

$$T = I_t/I_{in} = \exp(-\alpha_{ext}\, l) \qquad \text{Equation 3.2}^2$$

$$\alpha_{ext} = N\sigma_{ext} \qquad \text{Equation 3.3}$$

where T is the transmittance, is the path length of the given sample, α_{ext} is the extinction co- efficient, σ_{ext} is the extinction cross section per species and N is the number of species per unit volume.

Usually a conventional spectrometer displays absorbance as given by the Lambert - Beer law[3]

$$A = \varepsilon cl = -\log_{10}T \qquad \text{Equation 3.4}$$

where ε is the molar extinction co-efficient, c is the molar concentration. The spectrum of the sample yields information of the electronic properties of the material and any changes to them as a result of physical or chemical interactions.

When light is incident on a sample both absorption and scattering can take place. Depending on the particle size, elastic scattering can be mainly of two types, Rayleigh and Mie scattering. Rayleigh scattering occurs when the diameter of the particle is less than one tenth of the wavelength of the incident beam and the scattered intensity is inversely proportional to the fourth power of the wavelength of the incident beam[3]. On the other hand, Mie scattering occurs when the particle size is equal to or greater than the incident wavelength. As the particle size increases, forward scattering dominates over back scattering and a forward lobe is formed, unlike Rayleigh scattering which occurs in all directions forming forward and backward lobes around the particle as shown in figure 3.3[3].

Increasing the particle size leads to increased Mie scattering and further results in interference of the scattered lobes.

In a suspension of absorbing species, depending upon the refractive index, size, shape and homogeneity of the particles in suspension, extinction can be caused by either absorption or scattering or both. Therefore the extinction coefficient can be described by

$$\alpha_{ext} = \alpha_{abs} + \alpha_{sca} \qquad \text{Equation 3.5}$$

$$\alpha_{ext} = N(\sigma_{abs} + \sigma_{sca}) \qquad \text{Equation 3.6}$$

where σ_{abs} and σ_{sca} are the absorption and scattering cross section. Thus the measured spectrum contains information about the energy levels of the absorbing species and also the particle size distribution in the suspension.

In chapter 4, the absorption and scattering of SWNT suspensions will be differentiated to characterise the debundled process and the characteristics of the two states.

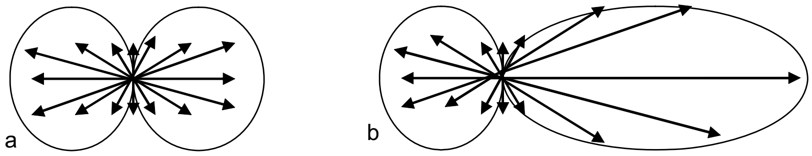

Fig 3.3: a) Rayleigh scattering from particles much smaller than the wavelength of the incident light b) Formation of forward lobe as the particle size approaches the wavelength[3].

3.1.3. Schematic set up of UV/Vis/NIR Absorbance Spectrometer

The absorbance spectrometer used in this study is a Perkin Elmer Lambda 900 UV/Vis/NIR Spectrometer. UV/Vis/NIR quartz cells were used as the sample containers for observing the SWNT-water-surfactant system in UV/Vis/NIR spectroscopy. Figure 3.4 is a schematic set-up of the UV/Vis/NIR Spectrometer showing the section for the integrating sphere (explained in section 3 .1. 4) and “normal” sample chamber. Continuous electromagnetic waves from a halogen lamp for the near infra red to visible region and a deuterium lamp for the ultra violet region are directed towards the sample using the mirror set up as shown. Diffraction gratings followed by variable slits are used as the monochromator to select a narrow band of the wavelength from the spectral range before passing through the samples. The Perkin Elmer Lambda 900 uses two double grating arrangements, one for the UV/Vis region and the other for NIR region in order to reduce the background or stray radiation giving a higher absorbance range. The filter spindle acts to further reduce stray light in the spectrometer. The rotating half mirror acts as a chopper which splits the single beam into two, one for the reference and the other for the sample that is to be measured. The sample absorbs light of a resonant wavelength and the transmitted energy is detected by the photomultiplier in the (UV-Vis range) or a lead sulphide detector (NIR range).

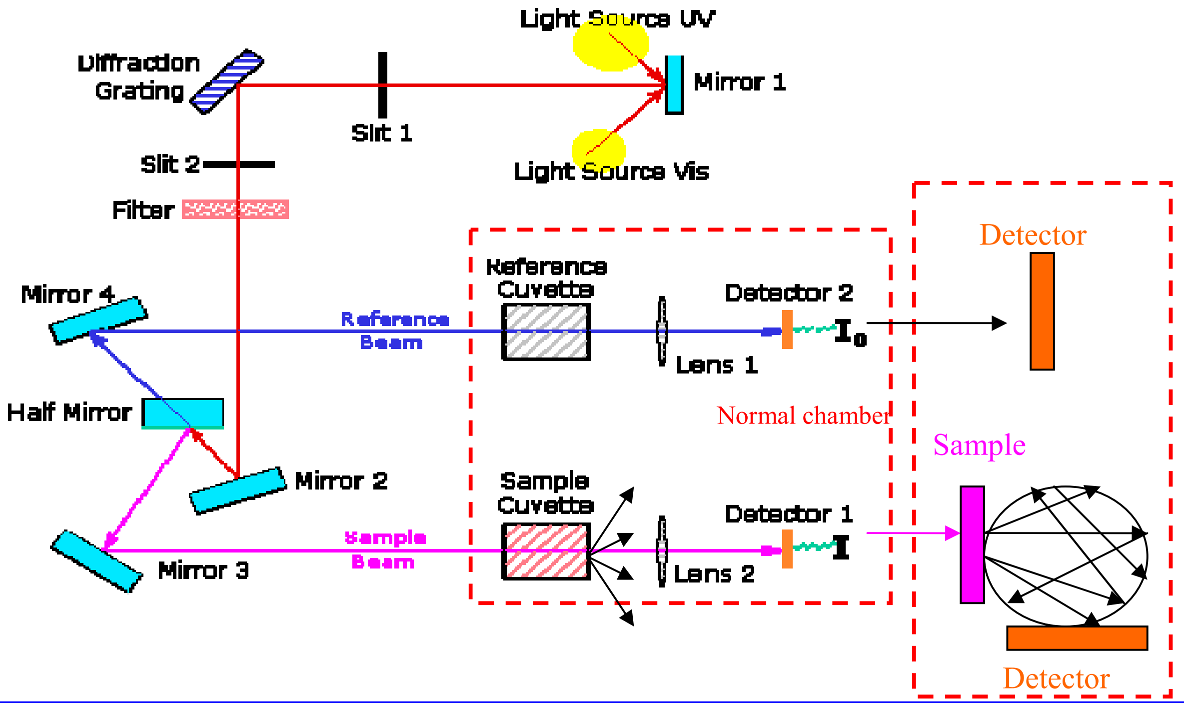

Figure 3.4: Schematic set-up of UV/Vis/NIR[4]

3.1.4. Integrating Sphere

An integrating sphere functions as a light collector and it can be used to determine the scattering of a sample. Figure 3.5 is a schematic representation of an integrating sphere. The inside of the sphere is coated with a high reflectance material, usually Spectralon (Reflectance - 95%), which is useful for UV/Vis/NIR applications in the spectral region 200nm-2500nm.

Light that is collected through the collection port in the integrating sphere undergoes multiple reflections until it finally reaches the detector through the detection port. Thus scattered light which is often lost before it reaches the detector in a conventional UV/Vis/NIR spectrometer geometry is collected by the integrating sphere and the registered loss of light can be attributed to absorption alone. A comparison of the two spectrometer setups can thus be employed to distinguish between absorption and scattering.

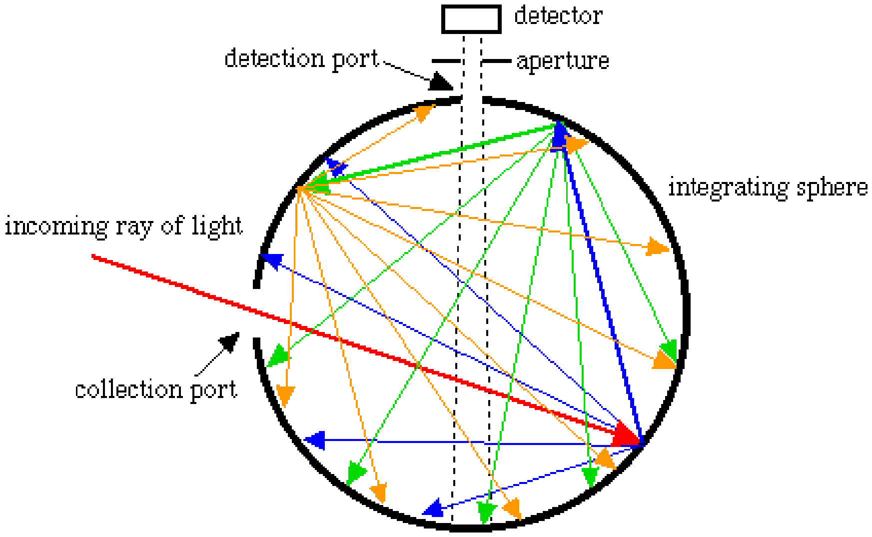

Figure 3.5: Schematic representation of the integrating sphere[5]

3.2. Vibrational Spectroscopy

3.2.1. Basic Principles

In addition to electronic transitions, there are rotational and vibrational transitions associated with molecules (figure 3.1). Vibrations of molecular bonds have different frequencies depending on the elements and the type of bonds. The atoms in a diatomic molecule with the chemical bonds which are involved in the vibrations can be imagined as two masses at the end of a flexible spring. The frequency with which it vibrates can be explained by Hooke's law[9],

$$\nu = \left(\frac{1}{2\pi}\right)\sqrt{\frac{K}{\mu}} \qquad \text{Equation 3.7}$$

where ν is the frequency of the vibration, K[10] is the spring constant and μ is the reduced mass of the atoms.

If a diatomic molecule with atoms A and B can be considered as two masses (M_A and M_B) and then μ is given by equation 3.8

$$\mu = (M_A M_B)/\,(M_A+M_B) \qquad \text{Equation 3.8}$$

The greater the strength of the bond the higher the frequency of the fundamental vibration. Similarly, the higher the masses of the atoms attached to the bond, the lower the frequency of the fundamental vibration.

In a real molecular system the vibrational energy states are quantised such that

$$E_v = h\nu(n+1/2) \qquad \text{Equation 3.9}$$

where E is the Vibrational Energy, h is Planck's constant, ν is the frequency of vibration and n is the quantum number. Transitions between vibrational states can be induced by frequencies between 4000 cm^{-1} to 400 cm^{-1} which belong to the mid infra red (IR) region of the electromagnetic spectrum. Thus vibrations in this spectral range can be used as a finger print to characterise and identify the molecules using "Vibrational" spectroscopy. Both Raman and infra red spectroscopies are the two methods that are routinely used to probe the vibrational states of a molecule.

3.2.4. Fourier Transform Infra Red Spectroscopy- Basic Principle

When infrared Light is passed through a sample, absorption at this wavelength takes places in molecules with strong dipole moment leading to vibrational transitions. The transmitted light is a fingerprint of the molecular vibrational states. The vibrations in a molecule can be of different types namely symmetrical and asymmetrical stretching, scissoring, rocking, wagging and twisting. Depending on the different types of stretching observed in molecules, the vibrating patterns can serve as finger prints for various functional groups to be identified by the IR spectroscopy. Briefly for IR absorption to occur there must be a nonzero dipole moment change during the vibration. The term Fourier Transform Infra Red Spectroscopy (FTIR) refers to a fairly recent development in the manner in which the data is collected and converted from an interference pattern to a spectrum. FTIR is also preferred over dispersive or filter methods as all frequencies are measured simultaneously.

3.2.5. Instrument Set up

Figure 3.6 a shows a schematic representation of the Perkin Elmer FTIR Spotlight 400 and figures 3.6 b a and 3.6 c show the light path set up for visual and IR imaging in Transmittance mode respectively. The Perkin Elmer FTIR Spotlight 400 is a Michelson interferometer based, automated dual beam splitter spectrometer and can be used to measure from mid IR to near IR range. The interferogram produced by the interfometer is converted into the spectra using the Fourier Transformation and hence the name. The set up uses a Cassegrain system for focussing the light beam, Z fold design and apertures. Dual Linear Array and MCT detectors (Mercury Cadmium Telluride) are used for image mode and the point mode respectively. Z-fold design in the instrument permits pixel size down to 6.25 µm and also permits larger scanning areas in limited time. Apart from Transmittance mode the instrument can be set up for both Reflectance and ATR (Attenuated Total Reflectance). As can be seen from the figure 3.6a the IR light beam from the source enters the Spotlight System and is focussed towards the first Cassegrain, the light beam passes through the sample, is collected by the second Cassegrain and the signal enters the detectors and the transmittance or the absorbance of the IR signal can be obtained. For the Z fold design, pair of concave and plane mirrors is provided and automated apertures are provided to block stray light or to select the area of interest.

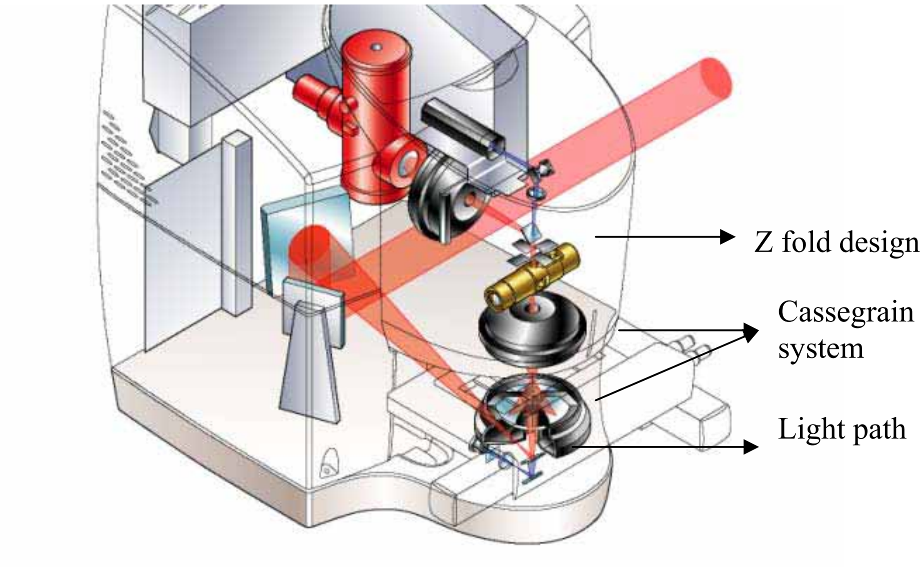

Figure 3.6 a: Schematic Setup of FTIR Imaging System. (From Perkin Elmer Spotlight FT-IR/NIR Imaging Presentation)

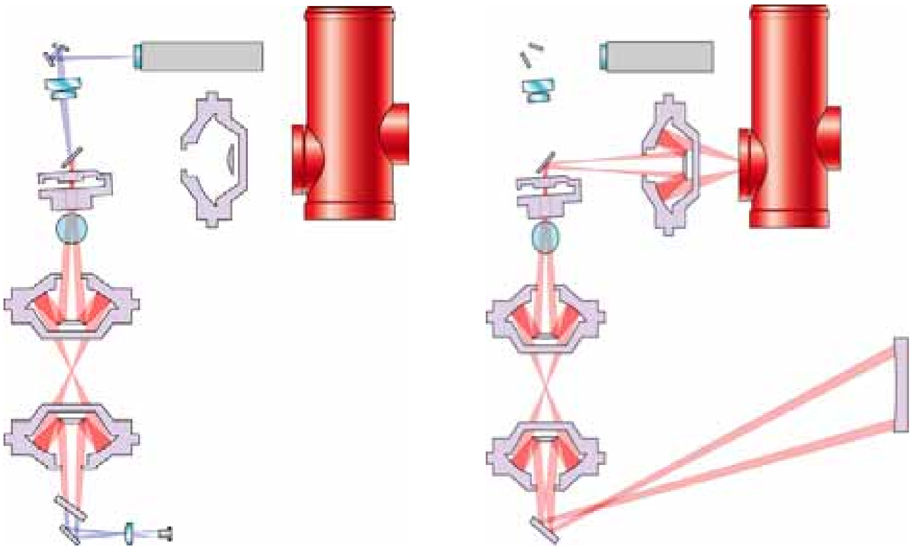

Figure 3.6 b: Visual Image /Transmittance c) IR/Transmittance (From Perkin Elmer Spotlight FT-IR/NIR Imaging Presentation)

3.2.2. Raman Spectroscopy - Raman Scattering

When light is incident on matter, the photons may be absorbed or scattered. Scattering can be of two types, namely elastic scattering and inelastic scattering. The former, which can be termed as Rayleigh or Mie scattering as described in section 3.2.1, occurs when the energy of the incident light is same as the energy of the scattered light. The latter case occurs when there is a shift in the energy of the scattered light with respect to the incident energy. The most commonly explored form of inelastic scattering of optical photons is Raman Scattering which was discovered by C.V Raman[6].

In Raman scattering, light interacts with the molecules and distorts or polarizes the cloud of electrons. This polarisation can be considered as the formation of a short lived state called the virtual state from which the photons are quickly reradiated. The induced polarisation depends on the polariazability of the molecules which in turn can be influenced by the vibrational state of the molecule. Thus, the reradiated or scattered light is mixed with the vibrational frequencies and contains information on the vibrational states of the molecule and thus the spectrum of inelastically scattered light is a vibrational fingerprint of the material. Raman scattering is a weak process, only 1 in $\sim 10^7$ photons undergo inelastic scattering and so Raman spectroscopy, although discovered in 1928, really only came of age since the advent of the laser.

Figure 3.8 a (same as 3.1) shows the relationship between the rotation, vibration and electronic transitions that occur in a diatomic molecule and figure 3.8 b shows the transitions that can be visualized in normal Raman spectroscopy and resonance Raman spectroscopy. Raman scattering can be of two types depending on the occupancy of the

Figure 3.7 a **Figure 3.7 b**

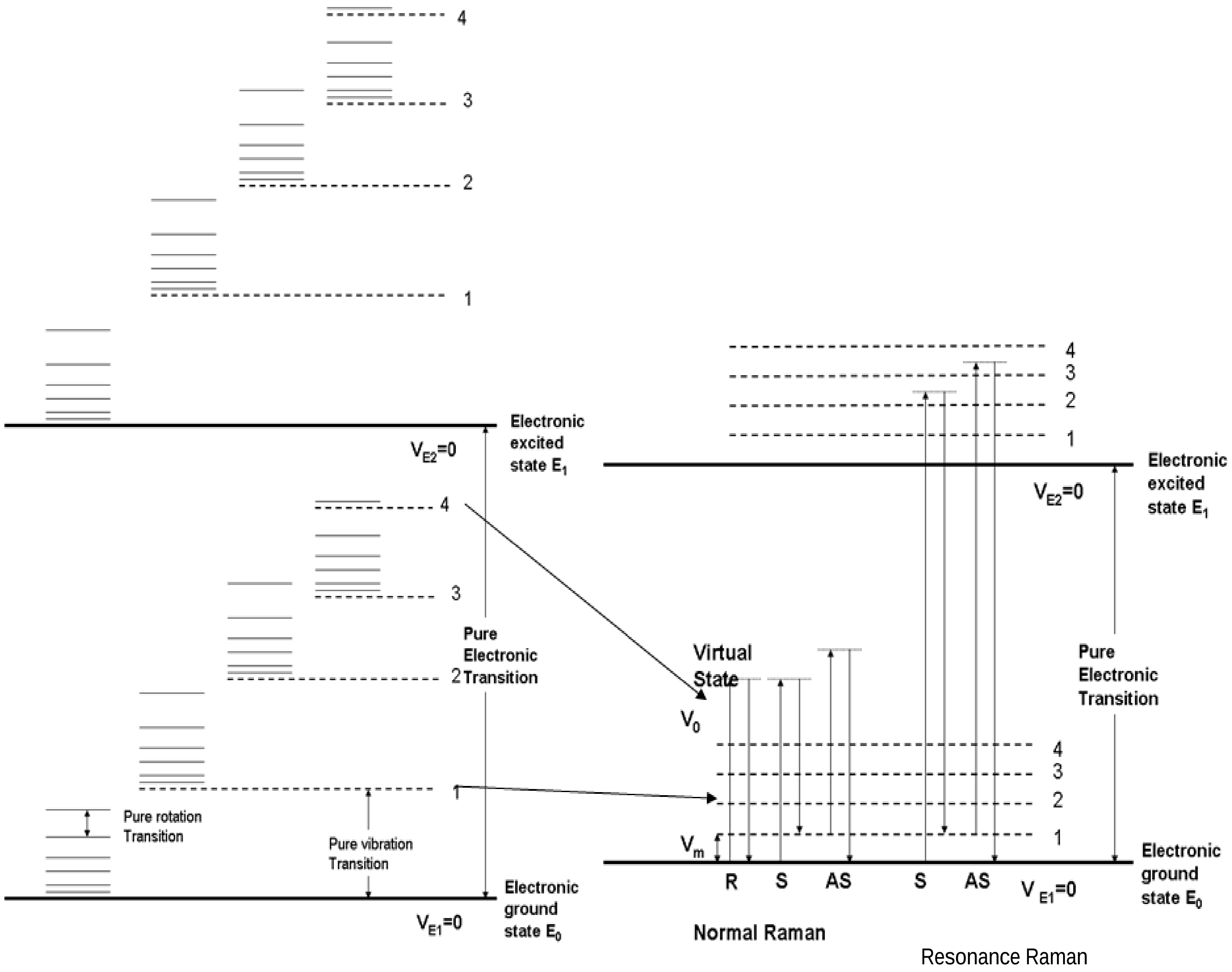

Figure 3.7 a) Schematic representation of the energy levels of a diatomic molecule b) Shows the Stokes and the anti Stokes shift in the normal Raman and the resonance Raman R- Rayleigh scattering, S-Stokes Raman scattering, AS-Anti stokes Raman Scattering[1].

vibrational levels. These are Stokes Raman scattering and anti Stokes Raman scattering. Stokes scattering arises when the molecule is excited from the ground vibrational state ($V_{E1=0}$) to a virtual state and the resulting scattered energy is less than the incident energy.

The difference in energy corresponds to that of the vibrational state and the process generates a vibration in the material. However due to thermal energy some electrons may be present in an excited vibrational state $V_{E1}=1$. Scattering from these states to the ground state $V_{E1}=0$ results in transfer of energy to the scattered photon. The energy difference corresponds to a vibrational quantum and the process annihilates a vibration in the material.

The relative intensities of these two processes depends on the number of molecules in the excited state and the ground state. According to the Maxwell-Boltzmann distribution the population of the molecules at the ground state $V_{E1}=0$ should be greater than the excited state $V_{E1}=1$, depending on the temperature and the energy spacing. At room temperature the Stokes shifted Raman signal is normally stronger than the anti-Stokes.

Raman scattering can alternatively be explained in a polarisation model as follows.
The incident electric field E can be expressed as

$$E= E_0 \cos 2\pi V_0 t \qquad \text{Equation 3.9}$$

where E_0 is the amplitude, V_0 is the frequency of the incident light and t is the time.
If a diatomic molecule is irradiated by this energy, the induced polarisation is given by

$$P=\alpha E=\alpha\, E_0 \cos 2\pi V_0 t \qquad \text{Equation 3.10}$$

where α is the polarizability of the molecule.

If a molecule is vibrating with a frequency V_m then the displacement q(t) is can be written as

$$q(t)= q_0 \cos 2\pi V_m t \qquad \text{Equation 3.11}$$

where q_0 is the equilibrium position. The polarizability is a linear function of q at smaller amplitude of vibration and can be related as follows

$$\alpha=\alpha_0 + (d\alpha/dq)_0\, q + \ldots\ldots\ldots \qquad \text{Equation 3.12}$$

Combining the above three equations the polariazability can be written as

$$P= \alpha_0 E_0 \cos 2\pi V_0 t + (d\alpha/dq)_0\, q_0 E_0 \cos 2\pi V_0 t \cos 2\pi V_m t \qquad \text{Equation 3.13}$$

$$= \alpha_0 E_0 \cos 2\pi V_0 t +1/2\, (d\alpha/dq)_0\, q_0 E_0 \{\cos(2\pi t(V_0+V_m))+\cos(2\pi t(V_0-V_m)\}$$

Equation 3.14

The induced polarisation represents an accelerated charge and so will reradiate at the oscillation frequency. The first term in the equation represents the Rayleigh scattering that radiates light which is equal to the incoming frequency V_0. The second term corresponds to the Raman anti Stokes scattering of frequency V_0+V_m and the Stokes scattering of frequency V_0-V_m. So from the above equation it is evident that if $d\alpha/dq$ is zero then there is no Raman scattering and the so the vibration is not Raman active. Raman active modes are normally symmetric modes which have highly delocalised electrons.

Thus Raman scattering is a result of the mixture of the vibrational energy with the incident photon energy resulting in an energy shift. In general, there will be a number of molecular vibrations of differing energies and the spectrum of scattered frequencies is a fingerprint of the material.

The Raman process differs from absorption and emission in many ways. Firstly the incident energy does not promote an electron to any of the excited electronic states of the static molecule. A virtual state is evoked for graphical representation, but the energy of this state is dependent on the energy of the laser used and the amount of distortion of the molecule depends on the electronic properties of the molecule. The lifetime of this virtual state is infinitely short. The radiation is not lost due the energy transfer within the molecule or emitted at a lower energy. Resonant Raman scattering occurs when the excitation frequency is selected in such a way that it matches energy the electronic transition energy of a particular state as shown in figure 3.7b. The instrument used for non resonant and resonant Raman scattering is the same. Being resonant or non resonant depends on the sample being used. For instance if the sample is said to be resonant at an excitation wavelength of 633 nm and non resonant at other excitation wavelengths, it means that the material absorbs at 633nm and the result that the intensity of the Raman signal at the resonant wavelength (633nm) is very high (known as Resonance enhancement) when compared to the non resonant signal at other wavelengths.

3.2.3. Raman- Instrument Set Up

Raman Measurements were taken using an Instruments S. A. Labram 1B Raman microscope shown in figure 3.8. The system consists of a confocal Raman imaging microscope system. Two types of lasers, namely the Helium- Neon laser (632.8nm) and an external Argon ion laser (514.5nm) were used as sources. The laser light is focused on to the sample via the objective of the Olympus BX40 microscope and the scattered light is collected by the objective in a backscattering, confocal geometry and is directed to a Peltier cooled CCD array via any one of the interchangeable gratings 1800 lines/mm or 600 lines/ mm. For all the Raman experiment carried out, the 1800 lines/ mm grating was used. A dispersion of 1cm^{-1} per pixel can be achieved. The Raman scattering of all the samples were measured in solution. Horiba Jobion-Yvon LabRam HR800 UV was also used with 532nm and 660nm excitation wavelength

Fig 3.8: Instruments S. A. Labram 1B

3.2.6. Raman and FTIR spectroscopy – Comparison and selection Rules

Infrared (IR) and Raman spectroscopy both measure the vibrational energies of molecules but the methods rely on different selection rules and they can be considered as complementary techniques. For a molecule to be Raman active it should have a high polariazability and so weak dipole moment and for IR active it should be vice versa. Sometimes both spectroscopes can be used on a same system to acquire different datas. For example, carbon nanotubes, are strongly Raman active and show only weak signatures in the IR, but functionalizing ligands are manifest strongly in the IR. They can also be used to study different vibrational modes in the same material. CO_2 can have three kinds of stretching vibrations, as shown in figure 3.9. The symmetric stretch is Raman active as it has high polariazability and the other two asymmetric stretches are IR active.

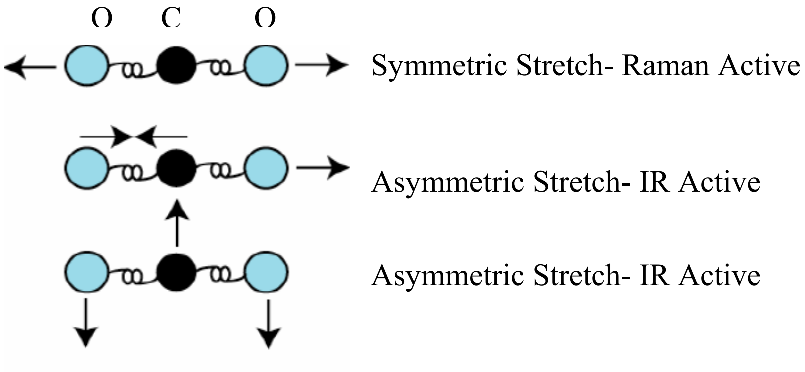

Figure 3.9: Different types of stretches in a carbon dioxide molecule (http://www.geo.lsa.umich.edu/~stixrude/GS232/Problems/PS1/Problems1_files/image017.jpg)

In the case of carbon nanotubes, the vibrational modes are predominantly highly polarisable, symmetric Raman active modes, and thus Raman spectroscopy has been an invaluable tool for the characterisation of SWNTs, and as such will be used extensively in this study. Infra red spectroscopy is employed in chapter 7 to explore the chemical functionalisation of nanotubes with asymmetric side groups.

3.3 Microscopy Techniques

3.3.1. Atomic Force Microscope - Working Principles and Instrument set up

Atomic Force Microscopy (fig. 3.10) comes under the general heading of scanning probe microscopy and is used to obtain three dimensional images of surfaces at nano meter resolution. The technique uses a tip with an atomically defined point to scan the surface. A laser beam is incident on the top surface of a tip-cantilever set up and is reflected into a photo detector. The vertical position is recorded and controlled via a feedback loop. As a first step the so called “deflection point” (a default value) is set to maintain a constant distance between the tip and the surface.

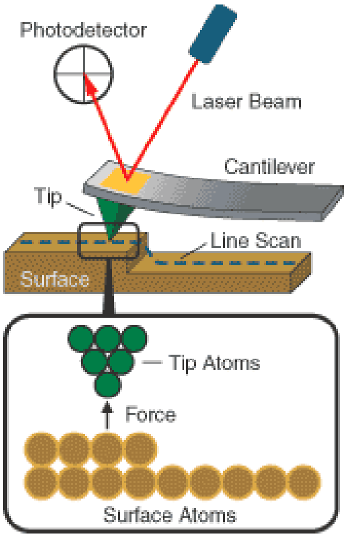

Figure 3.10: Shows the working principle of Atomic Force Microscope[7]

When the tip is made to scan the surface, it is deflected due to the force acting between the tip and the sample surface and as a result, the laser beam which is reflected in to the photo detector is deflected. The photodetector array is divided in four quadrants and measures the difference in light intensities between the upper and lower section of the deflected laser light, and then converts the deflection to voltage. This “difference signal” is sent into the piezo electric feedback (from the photodiode through software control from the computer) which compares the signal obtained with the default value of the deflection point that was set at the beginning of the scan. Depending upon the value obtained, the tip is positioned to produce the same deflection maintaining a constant force between the sample and the tip. The final image is the topography mapped along the xyz direction of the piezo elements.

AFM can be operated in three modes, namely contact mode, non contact mode and tapping mode, depending on the force that is acting between the tip and the sample, as shown in figure 3.11.

In contact mode, the tip is positioned in the repulsive region (figure 3.11) with a mean force of ~10^{-9} N and the tip is physically made to touch the surface. As soon as the cantilever is pushed towards the surface it enters in to the repulsive region. Once it enters this region the cantilever is deflected. This deflection is measured by the photo detector laser set up and the signal is sent to the feed back loop which aims to have a constant force between the tip and the sample by adjusting the deflection.

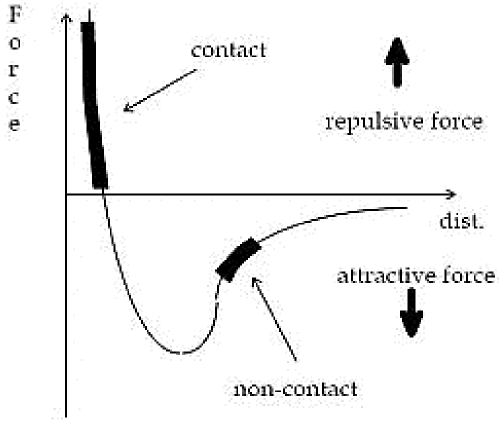

Figure 3.11: The region where the contact and non contact mode can be operated[8].

In tapping mode the cantilever is made to oscillate near to its resonance frequency between 50 kHz to 50,000 kHz. The oscillating cantilever is made to tap the sample and again come back to its original height and this is the process that occurs when the tip scans across the surface. During this tapping mode operation, the cantilever oscillation amplitude is maintained constant by the feedback loop. When the tip passes over a bump in the surface, the cantilever has less room to oscillate and the amplitude of oscillation decreases. Conversely, when the tip passes over a depression, the cantilever has more room to oscillate and the amplitude increases (approaching the maximum free air amplitude). The oscillation amplitude of the tip is measured by the detector and input to the controller electronics. The digital feedback loop piezo elements then adjust the tip-sample separation to maintain constant amplitude and force on the sample.

The radius of the tip is approximately 50 nm leading to lateral tip size effects. Because of this effect, vertical measurements are taken into account instead of horizontal measurements.

Non contact mode works in the attractive force regime, whereby a constant height is maintained between the sample and the tip. The tip is made to hover above the sample from a distance of 50 to 150Å and the imaging is done by the same principle as the tapping mode, using the photo detector, feed back loop and the piezo elements.

AFM is used in this work to characterise the aggregation state of the dispersed SWNTs from solution and is discussed Chapter 4. The Atomic Force Microscope (AFM) used in this work was a Veeco Multimode Nanoscope 3a shown in figure 3.12.

Figure 3.12 Veeco Multimode Nanoscope 3a

The Multimode Nanoscope 3a AFM is primarily used to study the topography of varios types of micro and nanostructured materials. It can operate in contact mode (where the tip is in continuous physical contact with the probed surface) or in tapping mode. TappingMode AFM, the most commonly used of all AFM modes, is a patented technique (Veeco Instruments) that maps topography by lightly tapping the surface with an oscillating probe tip as mentioned before. The Multimode system features multiple scanners that permit the user to tailor the system for individual research. Scanners with large scan ranges up to 15 µm in the X-Y plain, and a Z range up to 5 µm. The AFM can measure down to 1nm resolution. The Multimode's image analysis and presentation software contains provision for cross sectional analysis, roughness measurement, grain size analysis, depth analysis, power spectral density, histogram analysis, bearing measurement and fractal analysis.

3.4 Summary

The basic principles of UV/Vis/NIR absorption, Infra Red and Raman spectroscopy have been briefly discussed and the respective instruments have been described. Scattering and the integrating sphere which is used to measure scattering has also been discussed very briefly (their relevance to this work will be explained further in chapter 4). AFM has also been detailed in terms of the basic principles and instrumentation. Employment of these spectroscopic and microscopic techniques with respect to this thesis is discussed in the following chapters.

References

(1) Smith, E.; Dent, G.; *Modern Raman Spectroscopy A Practical approach* **2005**, *Wiley*

(2) Bohren, C. F.; Huffman, D. R.; Absorption and Scattering of Light by Small Particles, Wiley, 1983.

(3) Richard ; Tilley *Colour and Optical Properties of Materials* **1999**, *Wiley*.

(4) Spectroscopyhttp://www.chemicool.com/definition/spectronic_20.html. (20-07-09)

(5) http://omlc.ogi.edu/classroom/ece532/class1/collect_intsphere.html. (20-07-09)

(6) Raman, C. V.; Krishnan, K. S. *Nature* **1928**, *121*, 501.

(7) http://nano.tm.agilent.com/index.cgi?CONTENT_ID=809&User:LANGUAGE=en-US (20-07-09)

(8) http://www.spmagic.com/afm_techniques.htm. (20-07-09)

CHAPTER 4

"SWNTs Dispersions"

Adapted from- "Investigation of Sodium Dodecyl Benzene Sulphonate Assisted Dispersion and Debundling of Single Wall Carbon Nanotubes"- **J. Phys. Chem. C 2008, 112, 332-337**

4.1 Introduction

The main issue with SWNT is that they are produced in bundles (chapter 1) and these SWNT bundles need to be processed in order to obtain individually dispersed tubes before they can be employed for many application purposes. One of the solutions to bundling is the dispersion of the tubes in appropriate solvents with or without the aid of external stimuli. Many groups have suspended nanotubes in organic[1], aqueous[2-4] and composite[5-7] media. The selection of solvents for the SWNTs suspensions becomes important depending upon the application. For instance, the sorting of carbon nanotubes by diameter and their electronic properties using density gradient ultra-centrifugation has been demonstrated by solubilisation of the SWNTs in Sodium Cholate[8]. Nanotubes suspended in surfactants can be spontaneously aligned by means of an aqueous liquid crystal host[9]. Recently it was reported that carbon nanotube networks provide a flexible backbone structure for electrochemically deposited polyanaline and such a device allowed the determination of pH ranging from 1 to 13[10]. Besides the selection of solvents, for high efficiency of all the applications mentioned above, the concentration at which the tubes are completely isolated is critical. To achieve this criterion the first step is to disperse the bundles and the next step is to establish the concentration at which the tubes become completely dispersed resulting in isolated tubes. The following paragraph gives a brief introduction to what has been done to achieve steps 1 and 2.

"Removing Bundles" - The stability of the SWNT suspensions mainly depends on the solvent being employed and the sonication and centrifugation time. Attempts to optimise the UV/Vis/NIR absorption measurement using an integrating sphere (discussed in chapter 3.1.4) were also performed. In this chapter, a well defined method to check the presence of bundles using light scattering techniques and to remove and/or disperse them using centrifugation are discussed. Scattering is an indication of the presence of bundles which affects the absorption spectra. Differentiating this from the standard transmission measurement enables an estimate of the scattering spectrum. Extinction due to scattering (α_{sca}), and absorption (α_{ext}) (discussed in chapter 3.1.2) of SWNT dispersions in surfactant solutions are thus determined quantitatively.

"Isolated tubes" - Concentration dependent absorption and Raman spectroscopic studies were used to analyse the SWNTs behaviour in water based solution, and AFM is employed to examine the aggregation state of the nanotubes over the concentration range. The concentration dependent studies of the SWNT dispersions from optical absorption measurements are correlated with those of concentration dependent SWNTS dispersions using Raman Spectroscopy. Moreover, both spectroscopic techniques demonstrate a clear concentration below which the nanotube bundles become significantly dispersed in the solution and this concentration, known as the dispersion limit, is found using the Lambert Beer Law.

4.2 Experimental

A stock solution (SS) containing 1% by weight of Sodium Dodecyl Benzene Sulphonate ((SDBS) from Sigma Aldrich) in de-ionized water was made up. This concentration was chosen such that it is below the critical micelle concentration which is 0.73mg/ml[11] as solutions with surfactants above this concentration become turbid and viscous. 25 mg of as-prepared HiPco Single Wall Carbon Nanotubes (from Carbon Nanotechnologies Inc) were added to 5 ml of the stock solution. The SWNT solution was tip sonicated (Ultrasonic processor VCX 750 W) for 1 minute at 26% of the power output. A separate study for establishing the optimal sonication time (section 4.3) was undertaken in which the sonication time was varied in steps of 10 s after an initial sonication period of 45 s. Finally, a time period of 1 minute was chosen for all subsequent studies in this chapter. The ultrasonicated sample was serially diluted with the stock solution by a factor of 2 down to 6 x 10^{-3} mg/5ml. Thus the surfactant concentration was kept constant while that of SWNT was serially reduced. The serial dilution was performed at each step by halving the sample of the previous concentration and diluting by a factor of two. One of the diluted samples was again tip sonicated for 20 seconds, while the other was used to generate the next concentration. As such each sample received the same sonication treatment. The whole set of samples produced by the dilution process was then bath sonicated for 3 hours. After sonication, all samples were centrifuged at 4000 rpm (1699 G – Eppendorf Centrifuge 5417C) for 1 hour. For each sample the well dispersed supernatant was taken for characterisation leaving behind the precipitate. For all studies the same batch (batch no PO289) of HiPco carbon nanotubes was used. For Raman characterisation, SWNT in deionised water was used and for the UV/Vis/NIR characterisation Deuterium Oxide (heavy water – Sigma Aldrich) was used as the solvent. Figure 4.1 shows the absorption spectra of both light water and the heavy water. The features in the NIR spectrum are higher order overtones of the H_2O IR absorptions, and are thus shifted to lower energy (frequency) by the addition of the heavier hydrogen isotopes (Chapter 3.2.1). Thus the heavy water has a broader transparency window in the NIR and is preferable. (The feature at 860 nm occurs due to the change in the detector.)

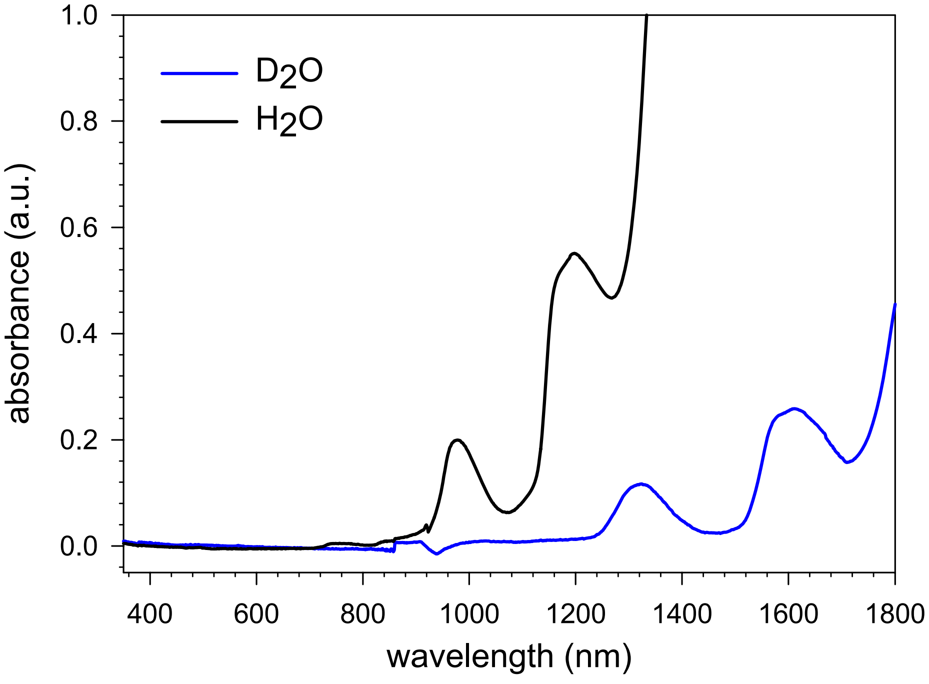

Figure 4.1: Shows the UV/VIS/NIR spectra of light water and heavy water.

The Perkin Elmer Lambda 900 UV/Vis/NIR spectrometer described in Chapter 3.1.3 was used to investigate the sample absorption in the wavelength range from 400 nm to 1800 nm. 10 mm quartz (UV/NIR optimised) cuvettes were used for all the measurements. The integrating sphere (chapter 3.1.4) was used to measure the scattering of the carbon nanotube bundles.

Raman measurements were taken using the Instruments S. A. (Jobin Yvon) Labram 1B with the Helium- Neon laser (632.8nm) as source (Chapter 3.2.3). The Raman scattering of all the samples were measured in solution using a x10 objective.

For AFM measurements the tubes were precipitated from the supernatant onto activated silicon surfaces. The activation was performed as follows: the silicon substrate (0.5 cm x 0.5 cm) was first cleaned. The cleaning procedure involved immersing the silicon substrates in boiling isopropanol for half an hour and then bath sonication in acetone. After cleaning, 1% v/v 1, 1, 1Tri-ethoxy Aminopropyl Silane (APTES) in deionised water was dropped on to the silicon substrates at room temperature. After 5 minutes the substrates were washed thoroughly using deionised water and left to air dry. Then the supernatant was dropped on the activated silicon surfaces and was left for 5-10 minutes, the surfaces were washed with deionised water and air dried. Depending upon the density of the tubes required on the substrate, the exposure time can be varied. The AFM used in this experiment was a Veeco Multimode Nanoscope 3A system (described in chapter 3 2.1). Point probe silicon cantilevers were used in all AFM studies and the tapping mode was employed to scan the surfaces.

4.3 Results and Discussion

As discussed in chapter 2.4, SDBS is believed to disperse SWNTs because of their benzene ring, smaller head group and slightly longer alkyl chain[2] and also the higher charge in the head groups strengthens the electrostatic repulsion among surface covered nanotubes which prohibits the aggregation of the tubes resulting in a more stable suspension[12].

As prepared HiPco SWNTs are always obtained in bundles[3] which can be visualised with the naked eye, as shown in figure 4.2. Sonication facilitates the initial dispersion of the tubes leaving both bundles and individual single tubes in the given solution and further sonication can affect improved dispersion of the nanotubes. Figure 4.3 shows the spectra of a sample (10mg of SWNT in 10ml of the stock solution containing SDBS) tip sonicated for increasing duration in steps of 10 seconds starting from 45 seconds. That is, the sample was sonicated for 45 seconds continuously and checked for the absorbance and after that, sonication was done in steps of 10 seconds and the spectra were measured. As the duration of the sonication is increased the absorbance increases monotonically, indicating increased solubilisation of the tubes. The initial solution, which was transparent, after vigorous sonication, turned in to a black solution which can be seen by the naked eye.

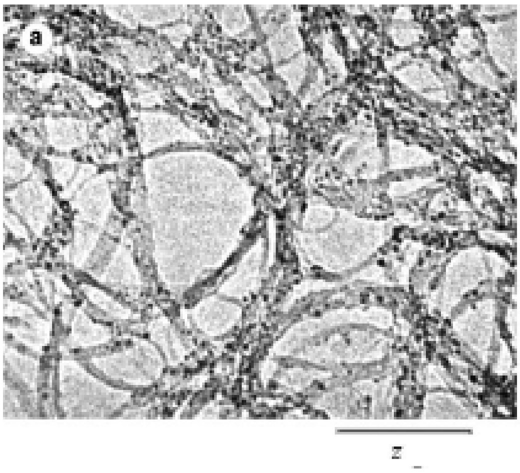

Fig 4.2: As prepared nanotube Carbon nanotube[13]

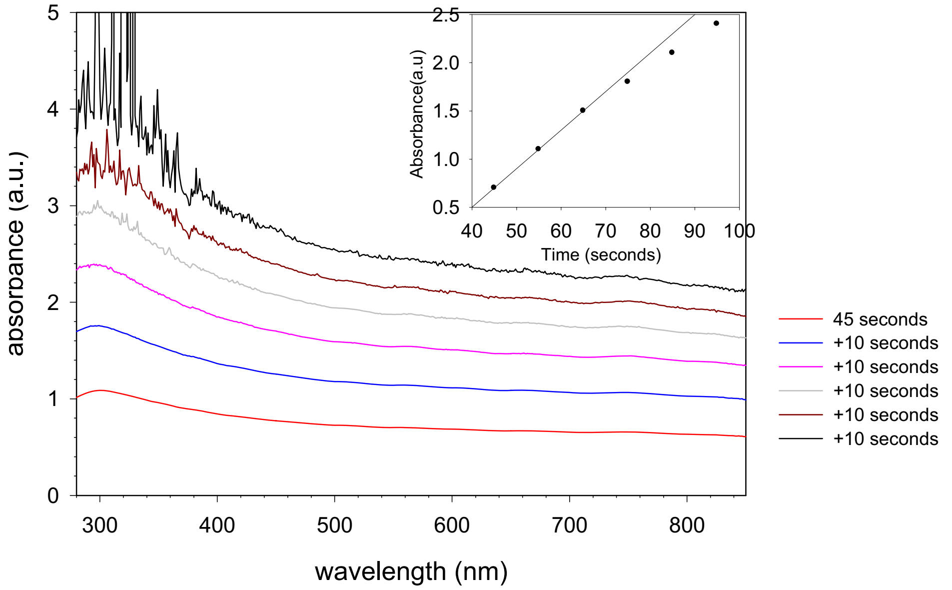

Figure 4.3: Shows the absorbance spectra after each sonication step. The inset shows the absorbance at 600 nm versus sonication time. (The concentration of the sample is 10 mg /10 ml)

However, excessive sonication has been shown to be detrimental to the tubes. Apart from debundling the tubes, sonication has a drastic effect on the pH of the nanotube-water surfactant system. Brian Benedict *et al.,*[14] reported that sonication-induced pH changes suppress the optical transitions of the first interband transition pair (S_{11}) in the density of states of the semi conducting SWNTs. It has also been reported that severe sonication can result in the cutting of tubes[3]. Such a suppression of the absorption of the suspension is indicated in the inset in figure 4.3 by the deviation from linearity of the behaviour above a sonication time of about 105 seconds. The inset of figure 4.3 is linear up until ~65 secs and therefore in order to avoid damage to the tubes but at the same time to have good dispersion of the tubes, tip sonication for the rest of the experiments was performed for not more than 1 minute continuously and was usually followed by milder bath sonication. Under these conditions, the ratio of the G-Band to D-Band of the Raman spectrum, which is an indication of the disorder of the tubes[15], was unchanged after sonication suggesting that the sonication had not induced any defects or cutting of tubes.

After sonication, to check the presence of bundles in the sample, the absorption spectrum was measured using both the integrating sphere and the standard measuring chamber. In the latter case, the sample is held approximately 30 cm - 33 cm from the detector and thus transmission losses due to both absorption and scattering are affected. Through the use of the integrating sphere, whereby the sample is placed at the entrance aperture, the scattered light is collected by the sphere and the contribution to the transmission losses is minimized enabling a more accurate measurement of the true absorption that is to be evaluated. Figure 4.4 shows the spectra of carbon nanotube dispersion in water surfactant solution (before centrifugation) obtained using the integrating sphere (solid line) and the standard chamber (dashed line) for a concentration of 0.156 mg/ml. The difference in the absorption observed by the two geometries is a measure of the extinction due to scattering losses indicating that there are a considerable number of large bundles present in the sample at this concentration, even after sonication.

The contribution of larger bundles can be removed by centrifugation[3]. It should be noted that the centrifugation conditions employed here are significantly lower than the ultra-centrifugation methods employed by others[3,12]. Nevertheless, a significant reduction in the scattering contribution and thus larger nanotube bundles can be achieved under these conditions.

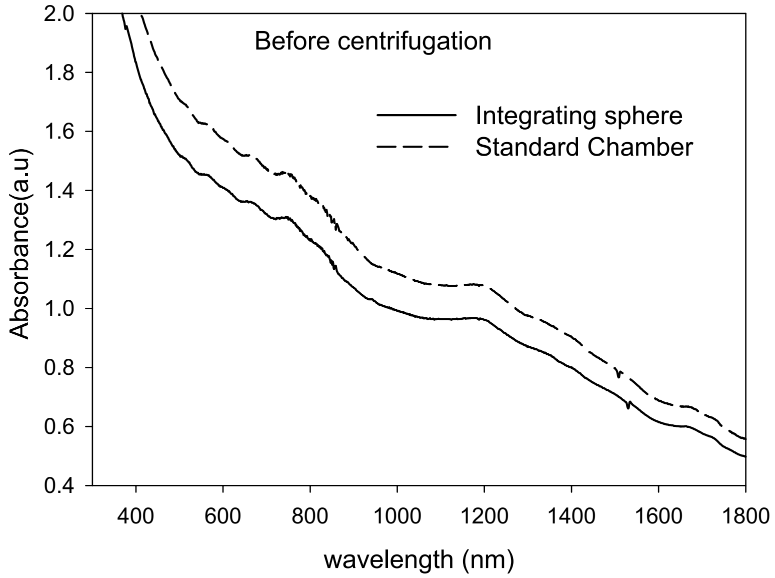

Figure 4.4: The absorption spectra of 0.156 mg/ml in 1% wt aqueous SDBS before centrifugation. The black line was taken placing the sample near the integrating sphere and the dashed lines in the standard chamber. The difference in the spectral absorbance is due to extinction caused by scattering.

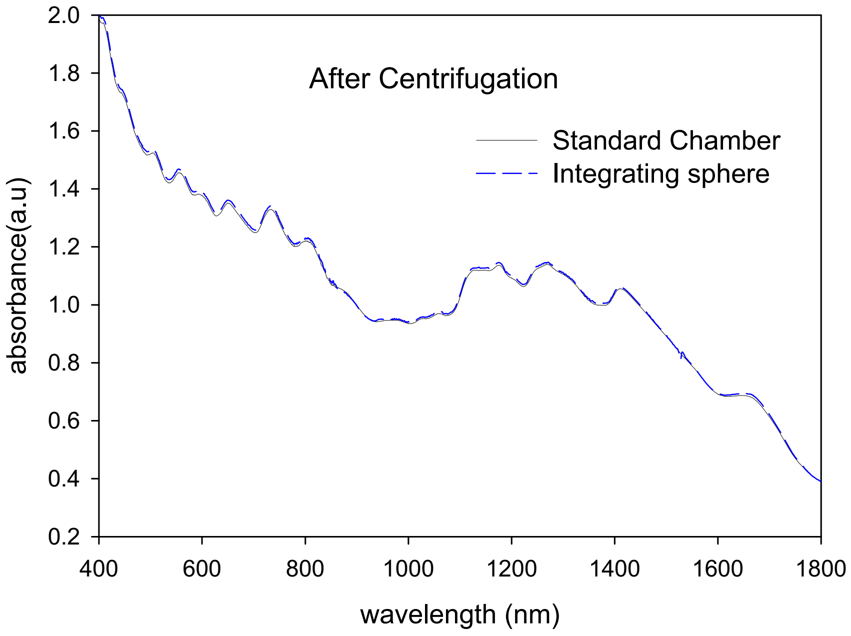

Figure 4.5: The solid line is a measure of absorbance in the standard chamber and the dotted one is the spectrum measured using integrating sphere. Both spectra are taken after centrifugation and the concentration is 0.156 mg/ml.

The absorption spectra, after centrifugation, of 0.156 mg/ml of HiPco SWNTs in 1%wt aqueous SDBS, as measured in the standard chamber geometry compared to the integrating sphere are shown in figure 4.5. It can be seen that there is negligible discernable difference in absorbance between the two spectra which indicates the aggregation state of the nanotubes has been significantly changed and that the extinction is mainly caused by the absorption of homogenously dispersed tubes or small bundles.

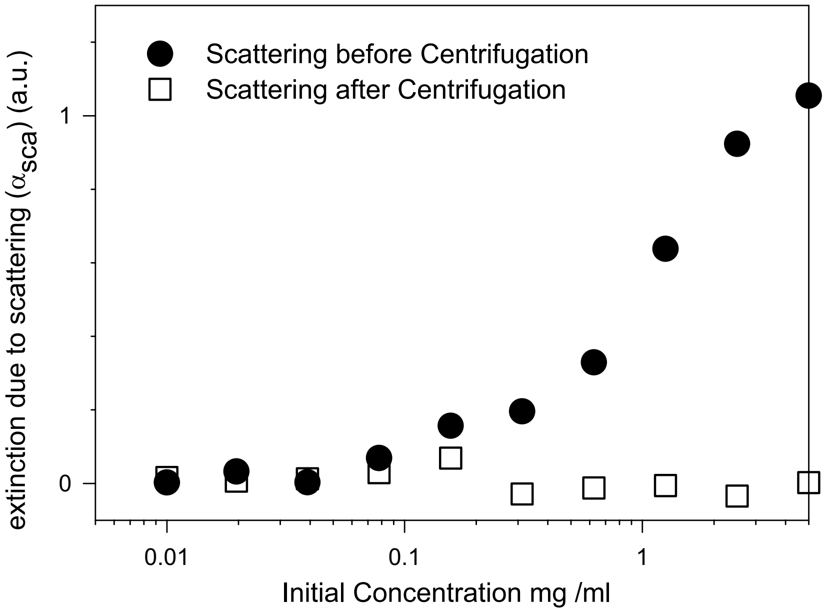

Figure 4.6: Extinction due to scattering measured before and after centrifugation at 600 nm for HiPco SWNT in 1% weight of aqueous SDBS.

The contribution due to scattering can be determined from the difference in absorbance as measured using the standard chamber and the integrating sphere (equation 3.4). Figure 4.6 shows the extinction due to scattering α_{sca} measured at 600 nm before (black filled) and after centrifugation (squares) for the series of concentrations measured. The behavior can be divided into two regions, the high concentration (>0.07 mg/ml) and the low concentration (<0.07 mg/ml) regions. In the high concentration region the scattering increases as the concentration is increased before centrifugation.

This scattering is due to the presence of bundles. After centrifugation (squares) the extinction due to scattering is minimal even in the high concentration region indicating that the large bundles which are the main scattering particles have been removed and/or the bundle size has been reduced. At lower concentrations it can be noticed that the α_{sca} remains approximately the same both before and after centrifugation suggesting that the tubes are in a significantly debundled state and therefore do not contribute to scattering.

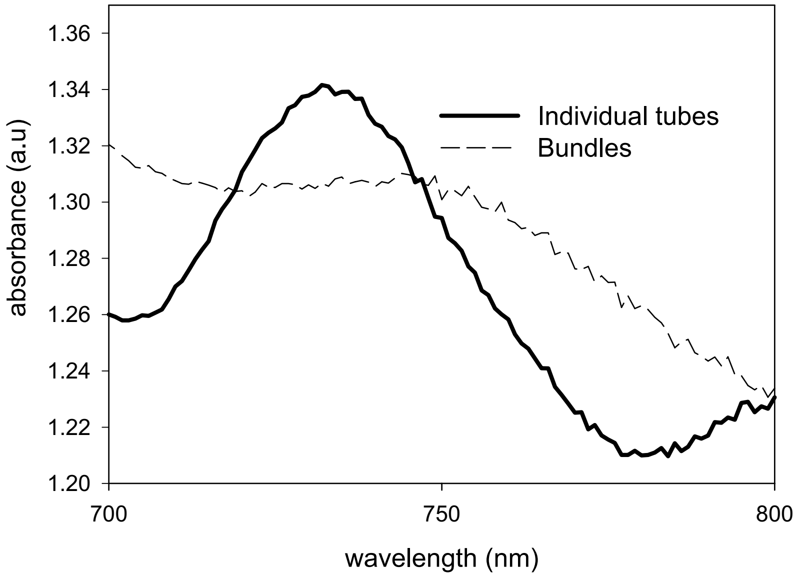

Figure 4.7: S_{22} region of the absorption spectrum showing a red shift at concentration 0.156mg/ml.

Figure 4.7 shows the red shift of the S_{22} region before (dashed line- bundles) and after (solid line- Individual tubes) centrifugation, reported to be characteristic of individually suspended tubes with respect to the bundles[16]. The spectra shown in figure 4.7 are the spectral extracts from figure 4.4 and figure 4.5, and were both measured using the integrating sphere. The other significant point is that the peak intensity has increased after centrifugation leading to sharp van Hove singularities[17] and also due to (more recently ascribed as) excitonic absorptions[18] .

Figure 4.6 indicates that significant debundling occurs as the concentration is decreased, in both as prepared and centrifuged samples. The next step is the determination of the exact concentration where the debundling commences. Figure 4.8 shows the absorbance of the serially diluted, sonicated and centrifuged HiPco carbon nanotubes in 1% weight aqueous SDBS solution at 600 nm, measured in integrating sphere. Above ~1 mg/ml, the absorbance becomes erratic, presumably because of the presence of large undispersed aggregations and is not shown.

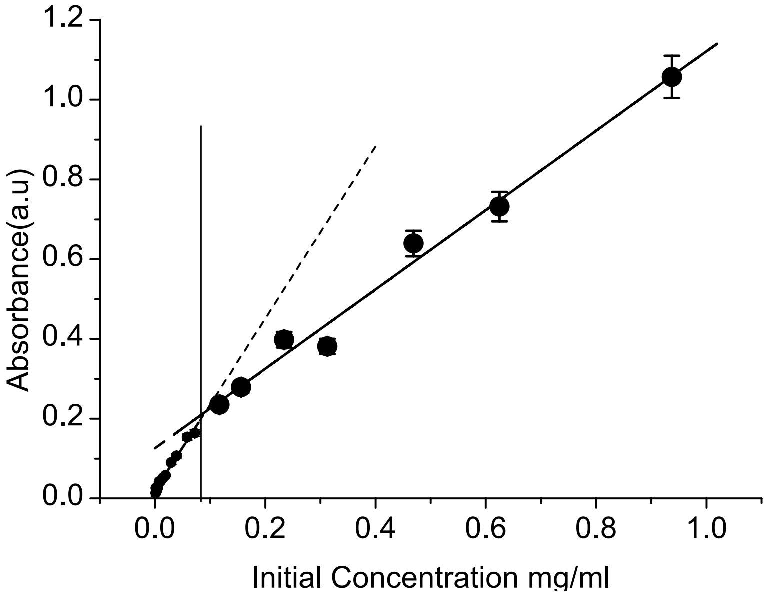

Figure 4.8: Absorbance vs. Initial Concentration at 600 nm of HiPco SWNT in 1% weight of aqueous SDBS.

The points shown in figure 4.8 can be divided into two sections, namely the high concentration region between 1.1 mg/ml to 0.07 mg/ml and the low concentration region from 0.07 mg/ml to1.2 x 10^{-3} mg/ml.

The black dotted lines represent a linear fit of the absorbance in both regions. In the low concentration range, between 1.2 x 10^{-3} mg/ml and 0.07 mg/ml, the absorbance increases linearly with respect to the concentration (in accordance with the Lambert Beer law, equation 3.6) and it is proposed to be the region consisting of significantly debundled SWNTs. The high concentration region is between 0.07 mg/ml to 1.1 mg/ml (From fig 4.8) is proposed to be the region of where decreasing concentration (from 1.1 mg/ml) decreases the number of bundles and individual tubes start to dominate. The vertical line is the representation of the Critical debundling point or the dispersion limit. The dispersion limit can be estimated from the plot by generating a smooth curve fit and observing the point at which the data deviates from the linear trend line[19,20] and is proposed to be 0.07 ± 0.03 mg/ml. This point is obtained from the intersection of the linear fits to the two regions. The extinction coefficient $\alpha_{ext=600}$ was found to be 215 mLmg^{-1}m^{-1} for low concentration and 99.5 mLmg^{-1}m^{-1} for higher concentration.

Figures 4.9 a and 4.10 a are AFM images taken at low concentration (0.0195 mg/ml) and high concentration respectively (0.156 mg/ml). Figure 4.9 b and figure 4.10 b are the sectional analyses of figure 4.9 a and figure 4.10a respectively. Figures 4.9 c and 4.10 c show histogram representations of the bundle size distribution for the concentrations mentioned.

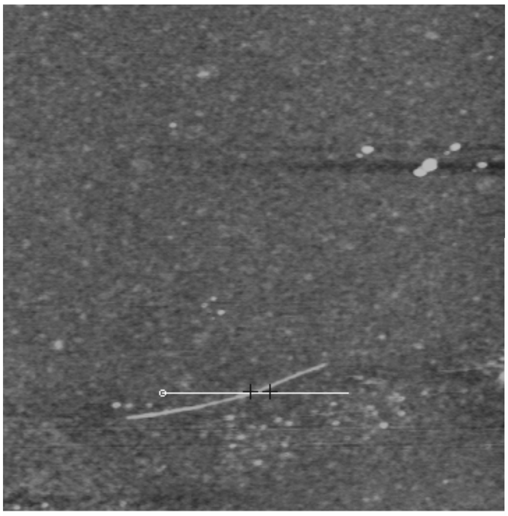

Figure 4.9 a

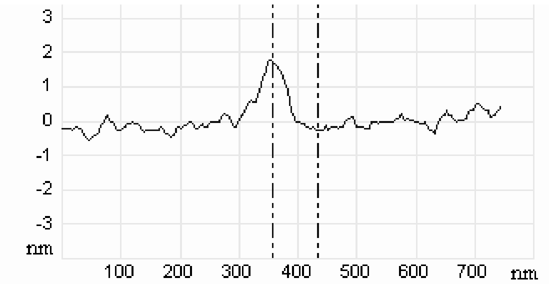

Figure 4.9 b

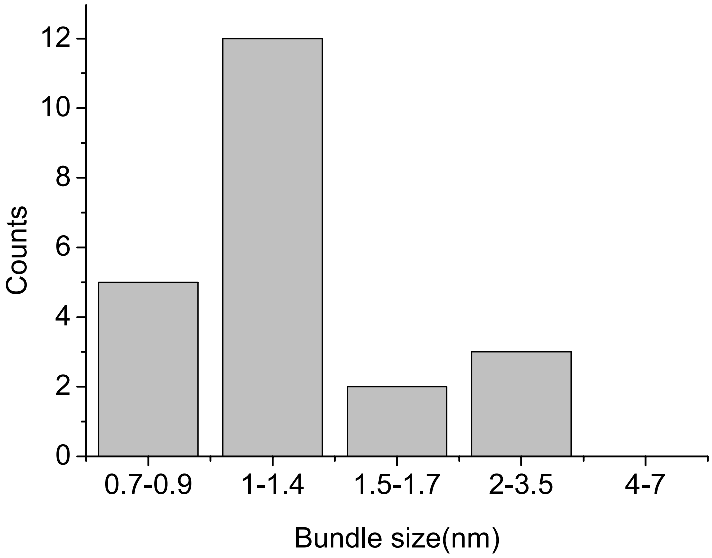

Figure 4.9 c

Figure 4.9: (a) AFM image of SWNT on activated silicon substrate. Concentration is 0.0195 mg/ml. (b) Shows the section analysis of SWNT shown in figure 4.9 a. The diameter was found to be 1.3 nm. (c) Shows the histogram of the bundle size distribution for the same concentration 0.0195 mg/ml.

Although the measurement cannot distinguish small bundles from isolated nanotubes in the lateral direction, the presence of features of vertical dimensions of ~1 nm is a strong indication of significantly dispersed nanotubes at low concentrations. For example, the feature identified in figure 4.9a with vertical dimensions of 1.3 nm is a strong candidate for an isolated nanotube. At higher concentrations, Figure 4.10 a, the AFM shows a higher distribution of bundles.

Figure 4.10a

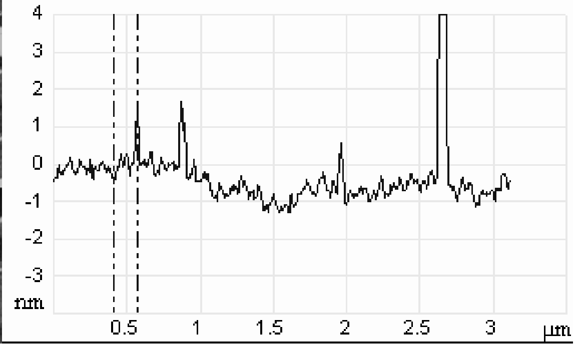

Figure 4.10 b

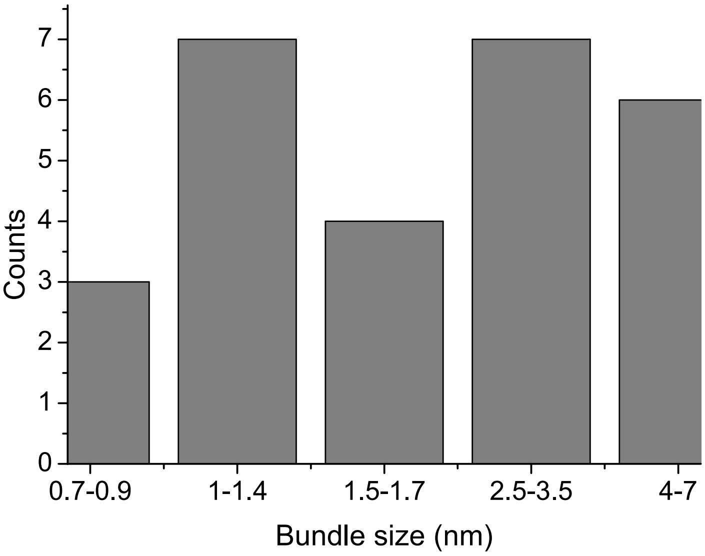

Figure 4.10 c

Figure 4.10: (a) AFM image of SWNT on activated silicon substrate. Concentration is 0.156 mg/ml. (b) is the section analysis of SWNT shown in figure 4.10 a. The diameter of the single tube is found to be 1.114 nm and that of the bundle is greater than 3nm. (c) Is the histogram of the bundle size distribution for the same concentration 0.156 mg/ml.

The observations from AFM agree very well with the results from UV/Vis/NIR absorption spectroscopy indicating that the identified transition concentration (CDP) region is where the tubes start to debundle. Above this concentration, predominantly bundles are present, whereas at approximately this concentration individually dispersed tubes begin to dominate although smaller nanotubes bundles still persist.

Thus, concentration dependent absorption spectroscopy can be used as an effective probe of the aggregation state of the nanotubes in suspension. Raman spectroscopy has also been used as a probe of surfactant suspension but no analysis of debundling state was performed[21,22].

Figures 4.11 a and 4.12 a show the Radial Breathing Modes (RBMs) and the Graphitic-Mode (G-Mode) of the Raman spectrum of a dispersion of concentration 5 mg/ml (with 632.8nm excitation wavelength) respectively. The background signal was measured for 1% wt of aqueous SDBS and found to be constant over the concentration range, eliminating the requirement for normalisation. All the spectra were SDBS and water subtracted. The spectra are fitted with a series of mixed Lorentzian/Gaussian for RBMs and a combination of Lorentzian and Breigt Wegner Fano (BWF) line shapes for G-Mode. Figures 4.11 b and 4.12 b show the Raman intensity versus initial concentration of the SWNT in water surfactant solution of the RBM Peak at 194.2 cm^{-1} and the BWF line shape (1545 cm^{-1}).

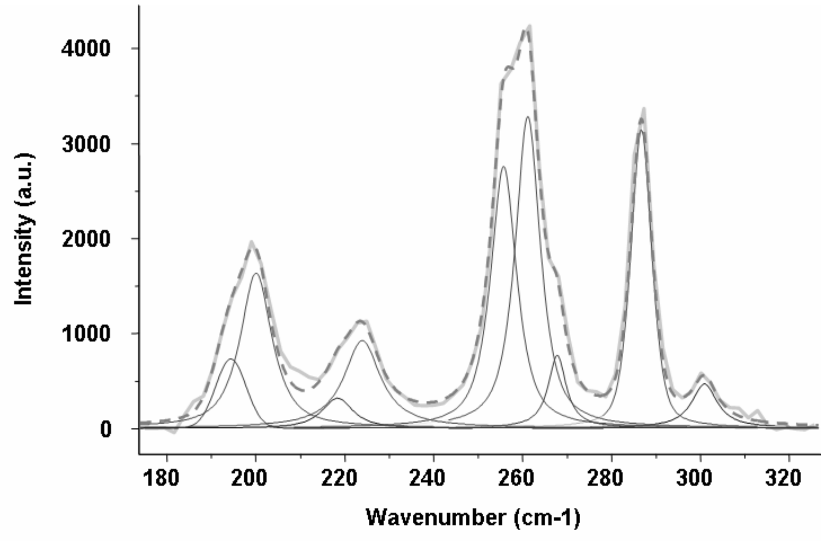

Figure 4.11 a

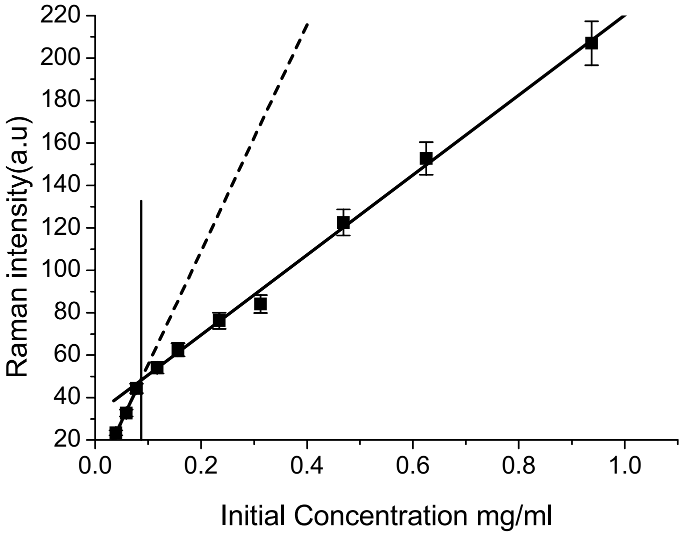

Figure 4.11 b

Figure 4.11: (a) Deconvoluted RBM spectra 5 mg/ml SWNT\SDBS. Excitation wavelength is 633 nm. (b) Raman intensity of RBM (194.2 cm^{-1}) vs. initial concentration.

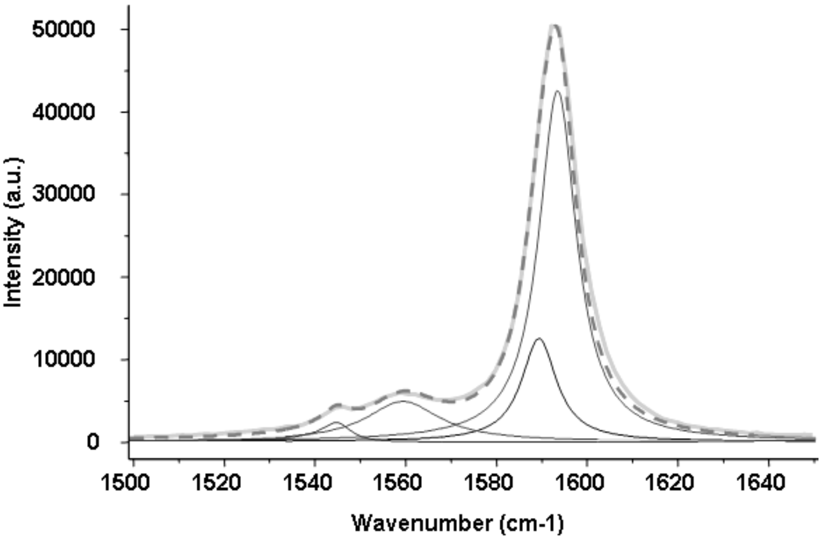

Figure 4.12 a

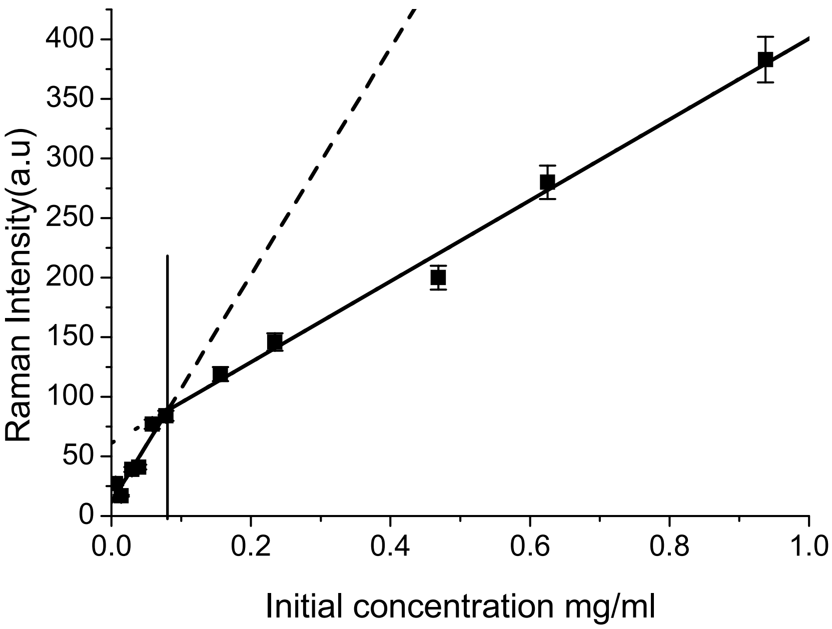

Figure 4.12 b

Figure 4.12: (a) Deconvoluted G band 5 mg\ml SWNT\SDBS. Excitation wavelength 633 nm. (b) Raman intensity of BWF (1545 cm^{-1}) vs. initial concentration.

As in the case of the concentration dependence of the UV/Vis/NIR absorbance, two distinct regions of linearity are observed and a similar plot is obtained with the Raman RBMs and the G- Modes. Only one of the nine RBM intensity versus initial concentration is shown here. Similar plots were obtained for all the RBMs and the G- Modes (not shown). The debundling point is found to be 0.07 mg/ml ± 0.03 mg/ml from all the measurements (vertical line) which agrees very well with the plot from the absorption spectroscopy. Similar to the case of the absorption and AFM measurements, Raman spectroscopy does not unequivocally illustrate the presence of individually dispersed nanotubes, but the measurements illustrate that at concentrations where a significant change in the aggregation state is inferred by scattering and AFM measurements, a significant change in the Raman scattering cross-section is observable and that Raman spectroscopy can also be considered as a potential method for studying the concentration dependent aggregation states of SWNT in surfactant water based solution.

The procedure undertaken in the sample preparation was a top down approach, which is breaking the bundles into single tubes by sonication and then separating them from the precipitate that contains aggregated tubes. Even after centrifugation the bundles are still present but the size is reduced. As the SWNT concentration is decreased, the bundle size is reduced and at a concentration of 0.07 mg/ml, called the dispersion limit [20], the debundling process begins resulting in a greater number of individual nanotubes along with a very small number of bundled tubes. Giordani et al reported that no aggregates were observed below 0.02 mg/ml of HiPco SWNT in NMP solution, suggesting that this can be considered the nanotube dispersion limit within the solvent[20] and their analysis indicated that almost

70% of all nanotubes existed in isolated form below this limit. This facile dilution effect allows nanotube bundles to be easily processed but could be enhanced by such process as density gradient ultracentrifugation[8,23,24].

A comparison of dispersion limits suggests that surfactant based media are significantly superior to organic solvents for nanotube dispersion. However, the extinction co-efficient measured is significantly lower than that measured in organic solvents. Table 4.1 compares the extinction co-efficient of various SWNT- solvent combinations. The substantially lower co-efficient in aqueous dispersions may be an indication that significantly lower amounts of bundles are initially suspended and retained after centrifugation, thereby resulting in a significantly lower number of tubes dispersed below the debundling concentration. It should be noted that Tan *et al*., have compared the dispersion of SWNT in various surfactants and, by examining the so called resonance ratio and normalized width of spectral features, reported that several surfactants were as good as or even better than SDBS[12]. Solvatochromic effects should also be considered, as should the reported effect of pH on the absorption characteristics[25].

Table 4.1: Measured parameters of HiPco dispersions

Groups	Extinction Coefficient solvent	Debundling Concentration
Giordani *et al.,*[20]	3264 mL mg^{-1}m^{-1}, NMP	0.02 mg/ml
Lindai *et a.,l*[19]	3000 to 3470 mLmg^{-1}m^{-1}, (various amide solvents)	DMF-1.56 µg/ml, DMA -6.25 µg/ml, DEA and DMP – 313 µg/ml
This study	215 mL mg^{-1}m^{-1}, SDBS	0.07 mg/ml

In addition to the observation of what appears to be the critical debundling concentration of the SWNT dispersions, it is also significant to note the differences of both absorption co-efficient and Raman scattering efficiency of individually dispersed tubes versus bundles. The aggregation of tubes is seen to reduce the absorption and scattering by over a factor of two. Such reductions in extinction are well known for organic aggregates. It is similarly not unexpected that the RBM and G-modes of the SWNT are inhibited within bundles. Indeed, previous Raman measurements of individual SWNTs have shown the RBM to dominate the spectrum[26]. Furthermore, that the behaviour above the critical concentration is approximately linear is an indication that the effect is independent of bundle size and is thus due to a nearest neighbour effect, as might be expected in a van der Waals aggregate.

4.4 Summary

Centrifugation has been shown to effectively remove bundles from the suspensions. With the aid of sonication and centrifugation bundles have been removed from the SWNT samples. This elimination of bundles has been quantitatively studied through the evaluation of scattering using the integrating sphere. After investigating the absorbance and the Raman intensity of a wide range of concentrations and using Lambert Beer law, homogenous dispersion of SWNT below the dispersion limit (0.07± 0.03 mg/ml) has been obtained. UV/Vis/NIR absorption and Raman spectroscopies have been shown to be capable of mapping the concentration dependent debundling of SWNTs in suspension. The observations from AFM studies also agreed well the spectroscopic studies. Further, debundling concentration/dispersion limit and the corresponding extinction coefficient for different solvents have been compared and finally water surfactant media has been verified/proved to be superior for nanotube dispersions. Having established a protocol for the dispersion of SWNTs and the concentration regimes in which they exist as isolated tubes, electronic assignment using UV/Vis/NIR absorption and the Raman spectroscopy techniques can now be performed, as described in the next chapter.

References

(1) Ausman, K. D.; Piner, R.; Lourie, O.; Ruoff, R. S.; Korobov, M. *Journal of Physical Chemistry B* **2000**, *104*, 8911.

(2) Islam, M. F.; Rojas, E.; Bergey, D. M.; Johnson, A. T.; Yodh, A. G. *Nano Letters* **2003**, *3*, 269.

(3) O'Connell, M. J.; Bachilo, S. M.; Huffman, C. B.; Moore, V. C.; Strano, M. S.; Haroz, E. H.; Rialon, K. L.; Boul, P. J.; Noon, W. H.; Kittrell, C.; Ma, J. P.; Hauge, R. H.; Weisman, R. B.; Smalley, R. E. *Science* **2002**, *297*, 593.

(4) O'Connell, M. J.; Boul, P.; Ericson, L. M.; Huffman, C.; Wang, Y. H.; Haroz, E.; Kuper, C.; Tour, J.; Ausman, K. D.; Smalley, R. E. *Chemical Physics Letters* **2001**, *342*, 265.

(5) Keogh, S. M.; Hedderman, T. G.; Lynch, P.; Farrell, G. F.; Byrne, H. J. *Journal of Physical Chemistry B* **2006**, *110*, 19369.

(6) Hedderman, T. G.; Keogh, S. M.; Chambers, G.; Byrne, H. J. *Journal of Physical Chemistry B* **2006**, *110*, 3895.

(7) Hedderman, T. G.; Keogh, S. M.; Chambers, G.; Byrne, H. J. *Journal of Physical Chemistry B* **2004**, *108*, 18860.

(8) Arnold, M. S.; Green, A. A.; Hulvat, J. F.; Stupp, S. I.; Hersam, M. C. *Nature Nanotechnology* **2006**, *1*, 60.

(9) Lagerwall, J. P. F.; Scalia, G.; Haluska, M.; Dettlaff-Weglikowska, U.; Giesselmann, F.; Roth, S. *Physica Status Solidi B-Basic Solid State Physics* **2006**, *243*, 3046.

(10) Kaempgen, M.; Roth, S. *Journal of Electroanalytical Chemistry* **2006**, *586*, 72.

(11) Bergin, S. D.; Nicolosi, V.; Cathcart, H.; Lotya, M.; Rickard, D.; Sun, Z. Y.; Blau, W. J.; Coleman, J. N. *Journal of Physical Chemistry C* **2008**, *112*, 972.

(12) Tan, Y. Q.; Resasco, D. E. *Journal of Physical Chemistry B* **2005**, *109*, 14454.

(13) Lafi, L.; Cossement, D.; Chahine, R. *Carbon* **2005**, *43*, 1347.

(14) Benedict, B.; Pehrsson, P. E.; Zhao, W. *J Phys Chem B* **2005**, *109*, 7778.

(15) Dresselhaus, M. S.; Dresselhaus, G.; Jorio, A.; Souza, A. G.; Saito, R. *Carbon* **2002**, *40*, 2043.

(16) Huang, H. J.; Kajiura, H.; Maruyama, R.; Kadono, K.; Noda, K. *Journal of Physical Chemistry B* **2006**, *110*, 4686.

(17) Saito, R.; Dresselhaus, G.; Dresselhaus, M. S. *Physical Review B* **2000**, *61*, 2981.

(18) Plentz, F.; Ribeiro, H. B.; Jorio, A.; Strano, M. S.; Pimenta, M. A. *Physical Review Letters* **2005**, *95*.

(19) Landi, B. J.; Ruf, H. J.; Worman, J. J.; Raffaelle, R. P. *Journal of Physical Chemistry B* **2004**, *108*, 17089.

(20) Giordani, S.; Bergin, S. D.; Nicolosi, V.; Lebedkin, S.; Kappes, M. M.; Blau, W. J.; Coleman, J. N. *Journal of Physical Chemistry B* **2006**, *110*, 15708.

(21) Strano, M. S. *Journal of the American Chemical Society* **2003**, *125*, 16148.

(22) Heller, D. A.; Barone, P. W.; Swanson, J. P.; Mayrhofer, R. M.; Strano, M. S. *Journal of Physical Chemistry B* **2004**, *108*, 6905.

(23) Crochet, J.; Clemens, M.; Hertel, T. *J. Am. Chem. Soc* **2007**, *129*, 8058.

(24) Arnold, M. S.; Stupp, S. I.; Hersam, M. C. *Nano Letters* **2005**, *5*, 713.

(25) Strano, M. S.; Huffman, C. B.; Moore, V. C.; O'Connell, M. J.; Haroz, E. H.; Hubbard, J.; Miller, M.; Rialon, K.; Kittrell, C.; Ramesh, S.; Hauge, R. H.; Smalley, R. E. *Journal of Physical Chemistry B* **2003**, *107*, 6979.

(26) Duesberg, G. S.; Blau, W. J.; Byrne, H. J.; Muster, J.; Burghard, M.; Roth, S. *Chemical Physics Letters* **1999**, *310*, 8.

CHAPTER 5

"Spectroscopic Assignment of Nanotubes"

5.1 Introduction

The diameter and the electronic structures of carbon nanotubes are uniquely related to the chiral integers m and n that describe their structure as a rolled up graphene sheet (Chapter 2). It is well accepted that if (n-m) is evenly divisible by 3, the nanotube exhibits a metallic or semi metallic behaviour whereas all other nanotubes show semiconducting behaviour[1]. The optical properties of SWNTs are dominated by electronic transitions between the van Hove singularities. Knowing the energies of these transitions for specific (n, m) structures is important not only for interpretation of absorption spectra but also for the widely used method of resonance Raman spectroscopy, in which resonance between the incident or scattered light frequencies and van Hove transitions of selected nanotubes enhances the scattering intensities and therefore their prominence in the spectrum.

Wildoer *et al.,* have directly observed the electronic density of states of individual SWNTs by scanning tunnelling microscopy and have shown good agreements with tight binding calculations[2]. Rao *et al.*, have shown Raman spectra of SWNTs for a wide source energy range[3]. Kataura *et al.,* for the first time, reported the optical absorption spectra and Raman spectra (for a wide range of excitation energy) of SWNTs with various diameter distributions[4]. They calculated the π bands of the SWNTs using a tight binding zone folding method for the assignment of the diameter. The resulting so-called Kataura plot (figure 5.3) has guided nanotube investigations based on optical measurements as it provides details about the transition energy and the corresponding nanotube diameter[4].

Structural assignment of SWNT based on UV/Vis/NIR absorption spectroscopy is based on this relationship between transition energy and diameter and is further discussed in 5.3.1. In terms of Raman spectroscopy, assignments can be made based on the RBM frequency and diameter as explained in 5.3.2. In terms of a fundamental understanding of these structure property relationships, it is imperative that these two techniques, based on differing theoretical bases, converge. In this chapter both techniques will be employed to assign the spectroscopic features of HiPco carbon nanotubes in an effort to demonstrate such convergence. In order to do so, it is important to minimise environmental contributions due to for example nanotube bundling and thus the sample processing techniques of the previous chapter serve as a basis.

5.2 Experimental

HiPco SWNTs were purchased from Carbon Nanotechnologies Inc. (USA). The samples were prepared as described in chapter 4 and a concentration of 0.07mg/ml, below the critical debundling point as determined in chapter 4, was chosen. The nanotubes were suspended in 1% SDBS aqueous solution, with the aid of tip sonication and bath sonication. Then the sample was centrifuged for one hour and 80% of the solution was decanted and taken for UV/Vis/NIR absorption and Raman spectroscopy using both 514 nm and 633 nm as source. In both cases, the measurements were performed in solution phase and the

UV/Vis/NIR absorption spectroscopy was performed to determine both absorption and scattering losses, as in chapter 3 and 4.

5.3 Results and Discussion

5.3.1 Absorption spectroscopy

The absorption spectrum of figure 4.5 (reproduced as figure 5.1) consists of a series of overlapping peaks, each corresponding to an interband transition of nanotubes of a given structure.

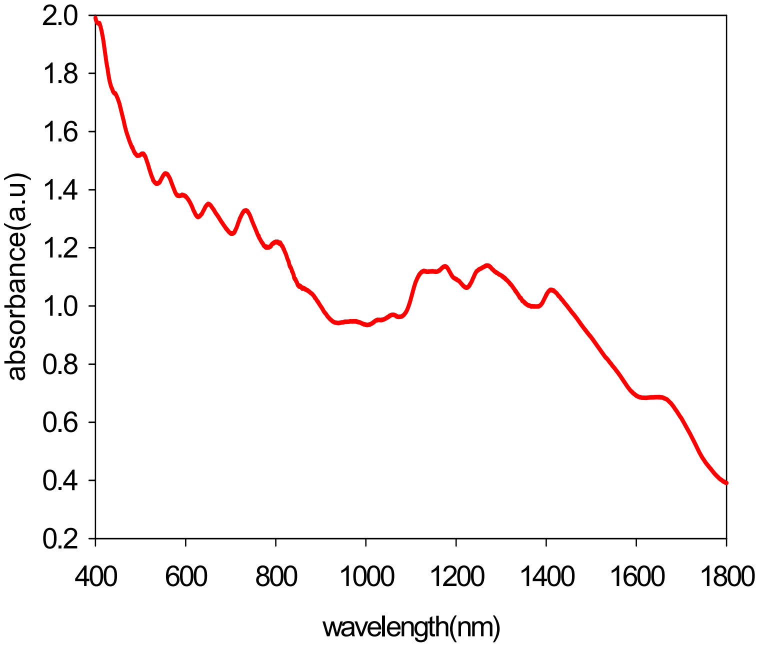

Figure 5.1: Is the absorption spectra of single walled carbon nanotubes dispersed in water SDBS surfactant solution (from chapter 4).

As described in chapter 2.3.1, three approximate spectral regions can be indentified for HiPco SWNT ~ 400 nm to 650 nm for metallic M_{11}, while those for semi conducting tubes lie between 550 nm to 900 nm for S_{22} and 800 nm to 1600 nm for S_{11} transitions.

Each curve in the spectrum corresponds to a tube of specific transition energy and in turn chirality. The transition energy can be related to the diameter of the tube as follows[5]

$${}^{M}E_{11} = 6\gamma\, a_{c\text{-}c}/d \qquad \text{Equation 5.2}$$

$${}^{S}E_{22} = 4\gamma\, a_{c\text{-}c}/d \qquad \text{Equation 5.3}$$

$${}^{S}E_{33} = 8\gamma\, a_{c\text{-}c}/d \qquad \text{Equation 5.4}$$

where E is the transition energy in the respective region, d is the diameter of the tube, γ is the over lap integral which is 2.75eV and $a_{c\text{-}c}$ is the C-C bond distance which is 0.142 nm. The superscript M or S represents metallic or semi conducting respectively. The subscript represents a transition between the energy level of the valence band to the conduction band. From these equations the diameter can be obtained for each absorption maximum and this in turn can be related to the chirality of the tubes using the expression[6]

$$d = \frac{a_{c-c}\sqrt{3\left(n^2 + m^2 + nm\right)}}{\pi} \qquad \text{Equation 5.5}$$

where n and m are the chiral indices of a given tube. Figure 5.2 is the Kataura plot[4] which relates the transition energy or the optical energy gap of the nanotube with the corresponding diameter (chapter 2). It has further been reported that the individual van Hove resonances sit on a background which has origin on the π Plasmon resonances which is maximum at ~ 350 nm[7-9]. These resonances are collective excitations of π electrons rather than single electron transitions.

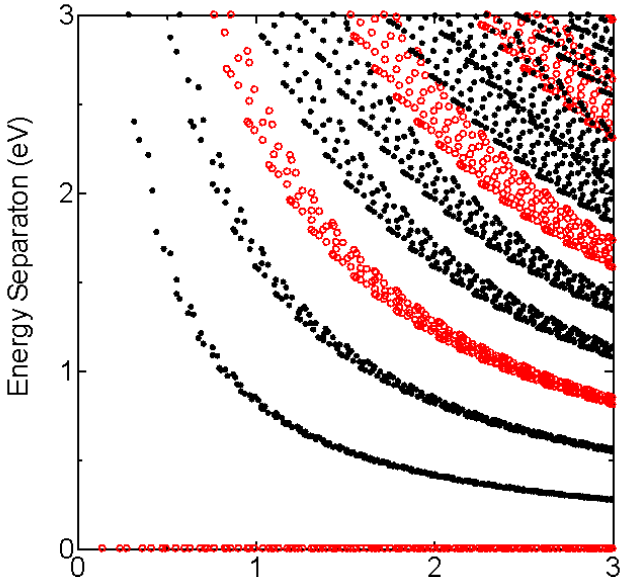

Figure 5.2: Kataura plot (chapter 2)

The chirality of the nanotubes can thus be determined from a UV/Vis/NIR absorption spectrum by the following steps.

1) Curve fitting each peak of the absorption spectra after background subtraction
2) Determining the energy position of each fitted curve
3) Calculating the diameter from the transition energy using equation 5.2, 5.3 or 5.4.
4) Calculating the chirality from the diameter using equation 5.5

The initial absorption spectrum of single walled carbon nanotubes dispersed in water SDBS surfactant solution is shown in figure 5.1. The first step is to remove the π plasmon background from the spectrum. The resonance profile can be approximated by simple exponential decay curve of the form

$$y = ae^{-bx} + ce^{-dx} + f \qquad \text{Equation 5.1}$$

which was generated and subtracted from the original spectrum in accordance with reference[10]

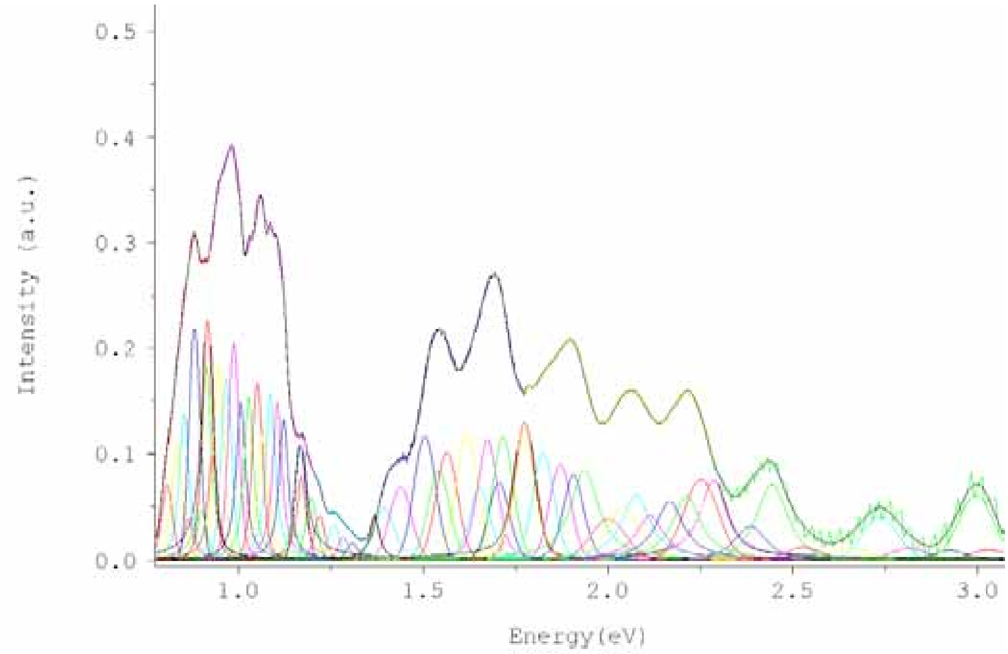

Figure 5.3: Curve fitting (mixed Lorentzian and Gaussian) of the background subtracted absorption spectrum.

Curve fitting was performed on the background subtracted spectrum using Labspec (Jobin-Yvon) software using mixed Lorentzian and Gaussian curves as shown in figure 5.3. The fitting procedure was guided by the report by Nitish Nair *et al.*,[10] describing the spectral dependence of the Full Width Half Maximum (FWHM) of the resonances associated with metallic and semi conducting carbon nanotubes. From the literature the FWHM for the best fits for each region of the spectrum were determined as metallic- M_{11}- 93.42 meV, semiconducting S_{22}- 57.96 meV, semi conducting S_{11}- 29.86 meV.

5.3.2 Raman Spectroscopy

Raman spectroscopy can also play an important role in characterising the structure and electronic properties of SWNTs. As described in chapter 2.3.2, the frequency of the RBMs can be related to the diameter of the tube as follows,

$$\omega_{RBM} = \frac{C}{d} + \Gamma \qquad \text{Equation 5.6}$$

where C is equal to 223.5 cm^{-1} and Γ is equal 12.5cm^{-1}(11-13). These parameters values were chosen for the work in this thesis because Strano *et al.,*[13] used these values for generating a revised Kataura plot[4] for the interpretation of SWNT dispersed in Sodium Dodecyl Sulphate surfactant. In this thesis all the experiments (unless specified) were carried out in solution phase using SDBS surfactant and water and so use of these values is more appropriate than those of Jorio *et al .,*[14] which were generated from analysis of SWNT on silicon substrates. From equation 5.6, diameters can be found from the Raman spectrum and in turn the chiral indexes and the transition energy can be calculated from equation 5.5.

Figures 5.4 and 5.5 show the RBM of the HiPco SWNTs obtained using 633 nm and 514 nm as source, respectively. The modes are fitted with mixed Gaussian and Lorentzian curves[15]. From these fits, the diameter, structural indices and associated transition energies can be determined.

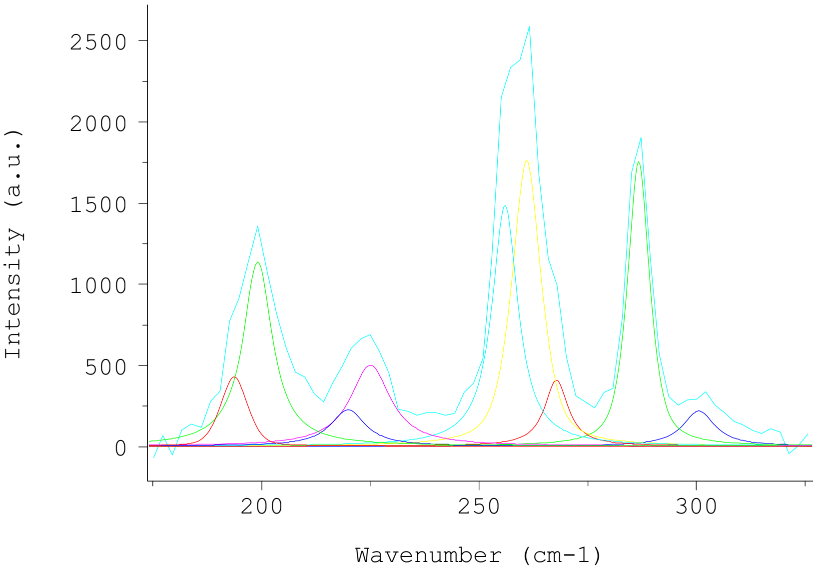

Figure 5.4: Curve fitted RBM of the HiPco SWNTs (in water surfactant solution) obtained at 633nm.

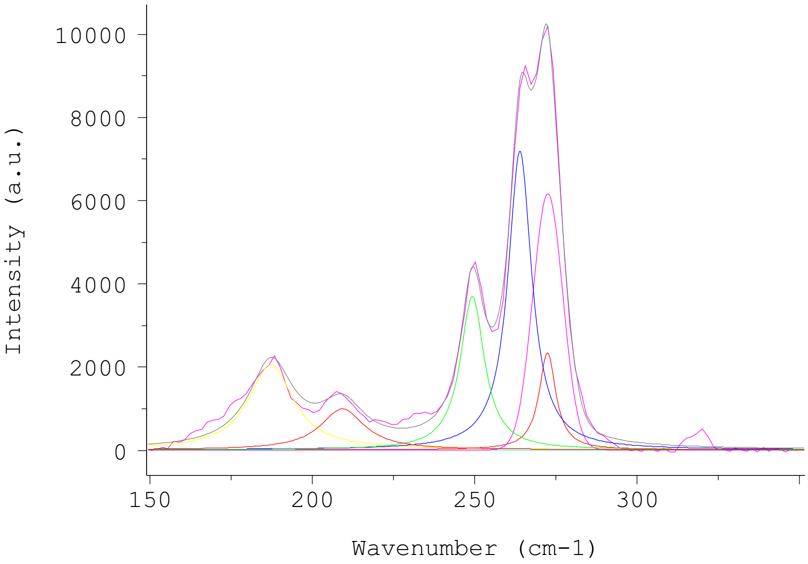

Figure 5.5 Curve fitted RBM of the HiPco SWNTs (in water surfactant solution) obtained at 514nm.

5.3.3 Assignment of Carbon Nanotubes

Table 5.1 lists the chiral indices of the range of nanotubes as assigned from the fitting of the absorption and the radial breathing modes of the Raman spectra. A so-called "Kataura plot[4]" is plotted in figure 5.6. Red, green and black filled circles represent the energies versus diameter of Metallic M_{11}, Semiconducting S_{22} and Semiconducting S_{11} transitions as determined from absorption spectroscopy and the yellow filled circles represent the energy vs diameter as determined from Raman spectroscopy using both 514 nm and 633 nm as sources. It can be seen that the values from both techniques match well indicating that Raman and UV/Vis/NIR absorption spectroscopy are compatible tools for the assignment of carbon nanotubes.

Table 5.1 Chiral index of HiPco SWNTS as calculated from the Absorption and Raman spectroscopy

Absorption spectroscopy Energy eV Metallic	(n,m)	**Absorption spectroscopy Energy (ev) Semi conducting 22**	(n,m)	**Absorption Spectroscopy Energy (ev) Semi conducting 11**	(n,m)	**Raman Spec RBM (633nm)**	(n,m)	**Raman Spec RBM (514nm)**	(n.m)
3.0389	(10,1) M	1.8702	(7,5) S2	1.2606	(7,2) S1	194.2	(13,4) M	185.6	(15,2) S
2.9960	(9,3) M	1.8336	(8,4) S2	1.233	(8,1) S2	199.8	(15,0) M	205.9	(14,1) S
2.9237	(11,0) S1	1.787	(11,0) S2	1.2071	(6,4) S1	218.2	(12,3) M	248.2	(12,0) M
2.8150	(8,5) M	1.7141	(8,5) M	1.1938	(7,3) S2	223.8	(10,5) S	261.9	(7,6) S
2.7363	(10,3) M	1.7031	(11,9) S1	1.1646	(9,0) M	255.7	(9,4) S	267.2	(11,0) S
2.6597	(11,2) M	1.6713	(10,3) S2	1.1429	(8,2) M	261.1	(7,65) M	272.6	(9,3) M
2.5285	(12,3) M	1.6505	(10,3) S2	1.1193	(6,1) S1	267.7	(11,0) S	318.7	(8,2) M
2.4438	(12,6) M	1.6157	(11,2)M	1.1015	(6,1) S1	286.7	(9,2) S		
2.3852	(11,5) M	1.5822	(9,5) S2	1.0831	(7,4) M	300.9	(10,0) S		
2.2864	(10,0) S1	1.5570	(11,3) S1	1.0632	(8,3) S1				
2.2514	(11,5)M	1.5163	(8,0) S2	1.0479	(10,0) S1				
2.2127	(14,1) S2	1.4437	(13,1) M	1.0243	(9,2) S2				
2.1665	(10,7) M	1.3965	(10,0) S1	1.0028	(7,5) S1				
2.1129	(12,5) S2	1.3657	(12,4) S1	0.9839	(8,4) S2				
2.0757	(13,4) M	1.3334	(13,8) S1	0.9640	(9,3) M				
2.0297	(12,6) M	1.3169	(11,7) S2	0.9424	(10,2) S1				
1.9997	(16,0) S1	1.2809	(13,4) S2	0.9267	(8,5) M				
1.9248	(12,3) M			0.9104	(9,1) S1				

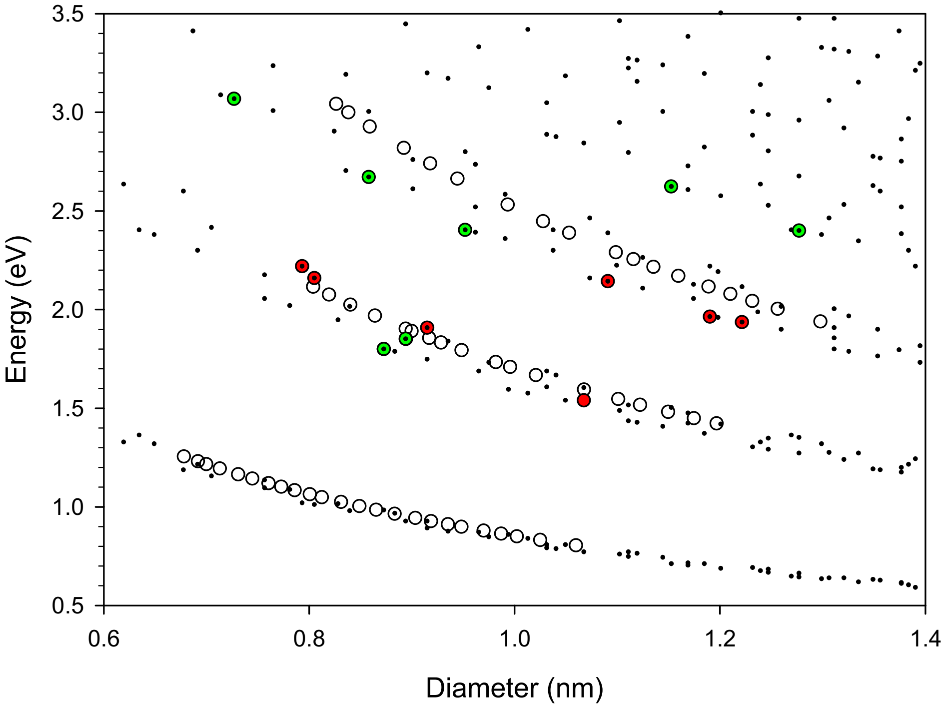

Figure 5.6: Kataura Plot[4] as calculated from the Absorption (open circles) and Raman spectroscopy (red filled – 633 nm excitation wavelength, green filled- 514 nm excitation wavelength), dots from original Kataura plot.

It is notable, however, that many more SWNTs have been identified in the UV/Vis/NIR absorption spectrum. This is due to the fact that, in the Raman spectrum of a sample of a broad range of diameters, the nanotubes which are resonant with the source laser energy dominate the spectrum. It is notable that the projection of the assigned nanotubes according to Raman spectroscopy is clustered around the source energies of 2.2 eV and 1.9 eV. Furthermore, in terms of equations (5.2 - 5.4) in comparison to 5.6, the rate of change of E with respect to (1/d) is much larger for the UV/Vis/NIR absorption, ~2.5 eV/nm compared with 235cm^{-1}/nm given that 1 cm^{-1} = 1.24 x 10^{-4} eV. Thus UV/Vis/NIR gives a greater dispersion of the SWNT features than Raman spectroscopy.

For the nanotubes identified using UV/Vis/NIR absorption spectroscopy, the assigned electronic character does not always fall within the windows identified as metallic or semi conducting according to the equations 5.2 - 5.4. In Table 5.1, the assignments that are pink coloured are those that match the electronic window and the ones that do not match are represented in black. It is stressed however that the assignments of the characteristics regions are approximate only, and indeed examination of the Kataura plot[4] reveals that, projected onto the energy axis, the different energy bands overlap considerably. Simple assignment of the different spectral regions to a given character and assignment of a FWHM bandwidth is estimation. The essential objective that lies behind the whole process of this curve fitting and in the determination of the chiral index is to find if the given tube carries metallic or semiconducting nature. Thus this process can be utilized as a best approximation to figure out the electronic character of a given sample. Therefore this technique is still useful for individual tubes in a bulk sample.

5.4 Summary

A method to elucidate the chiral index using absorption spectroscopy and Raman spectroscopy has been performed. Both techniques have proven to be straight forward methods to characterise the SWNTs quantitatively though uncertainty still exists to a certain degree. The most significant point is, though the assignment is based on different theories they have been shown to converge. Also the number of chiral indices assigned from UV/Vis/NIR is more when compared to Raman. Many excitation energies are required to assign more chiral indices which in turn is more expensive. On the other side unlike for microscopy (STM and AFM), the tube samples can still be used further when characterised using optical spectroscopes which is a major advantage when compared with the microscopical techniques. Also the UV/Vis/NIR and Raman are less labour intensive characterisation methods than AFM where in the former a wide range of tubes in water suspension can be measured and in the later each tube has to be measured individually. It is very important to mention here that chiral assignment is possible only when the tubes are in dispersed form rather than in bundles. At this juncture it is apparent that the concentration dependent dispersion studies described in the previous chapter are very important for further characterisations. The next step is to study the metallic and the semiconducting signatures in a given sample of pristine SWNT as detailed in chapter 6.

References

(1) Reich, S.; Thomsen, C.; Maultzsch, J. *Carbon Nanotubes- Basic concepts and physical properties* **2004** Wiley-VCH, Weinheim.

(2) Wildoer, J. W. G.; Venema, L. C.; Rinzler, A. G.; Smalley, R. E.; Dekker, C. *Nature* **1998**, *391*, 59.

(3) Rao, A. M.; Richter, E.; Bandow, S.; Chase, B.; Eklund, P. C.; Williams, K. A.; Fang, S.; Subbaswamy, K. R.; Menon, M.; Thess, A.; Smalley, R. E.; Dresselhaus, G.; Dresselhaus, M. S. *Science* **1997**, *275*, 187.

(4) Kataura, H.; Kumazawa, Y.; Maniwa, Y.; Umezu, I.; Suzuki, S.; Ohtsuka, Y.; Achiba, Y. *Synthetic Metals* **1999**, *103*, 2555.

(5) Mintmire, J. W.; White, C. T. *Physical Review Letters* **1998**, *81*, 2506.

(6) Odom, T. W.; Huang, J. L.; Kim, P.; Lieber, C. M. *Nature* **1998**, *391*, 62.

(7) Landi, B. J.; Ruf, H. J.; Evans, C. M.; Cress, C. D.; Raffaelle, R. P. *Journal of Physical Chemistry B* **2005**, *109*, 9952.

(8) Lin, M. F.; Shung, K. W. K. *Physical Review B* **1994**, *50*, 17744.

(9) Lin, M. F. *Physical Review B* **2000**, *62*, 13153.

(10) Nair, N.; Usrey, M. L.; Kim, W. J.; Braatz, R. D.; Strano, M. S. *Anal Chem* **2006**, *78*, 7689.

(11) Strano, M. S.; Doorn, S. K.; Haroz, E. H.; Kittrell, C.; Hauge, R. H.; Smalley, R. E. *Nano Letters* **2003**, *3*, 1091.

(12) Bachilo, S. M.; Strano, M. S.; Kittrell, C.; Hauge, R. H.; Smalley, R. E.; Weisman, R. B. *Science* **2002**, *298*, 2361.

(13) Strano, M. S. *Journal of the American Chemical Society* **2003**, *125*, 16148.

(14) Jorio, A.; Saito, R.; Hafner, J. H.; Lieber, C. M.; Hunter, M.; McClure, T.; Dresselhaus, G.; Dresselhaus, M. S. *Physical Review Letters* **2001**, *86*, 1118.

(15) Priya, B. R.; Byrne, H. J. *Journal of Physical Chemistry C* **2008**, *112*, 332.

CHAPTER 6

"DOPING OF SWNTS"

Adapted from - "*Quantitative Analysis of Dispersion and Doping of Individual Carbon Nanotubes in Water Based solutions using Absorption and Raman Spectroscopy*"-

Phys. stat. sol. (b) 245, No. 10 (2008)

6.1 Introduction

Different electronic entities in a given sample of carbon nanotubes can be analyzed for their distinct electronic behaviour by the process of adding impurities or doping. In this context, adding impurities is in the form of charges either by inserting extra electrons or holes into the singularities of the conduction band or the valence band respectively[1,2]. A simple technique of doping is to change the pH of the dispersed SWNT solution from neutral pH to both extremes (acidity and basicity). In this fashion, the Fermi level of different electronic species of SWNTs sample can be altered and this can act as a simple method to tailor the electronic properties in a given nanotube sample. The process can be monitored through absorption and Raman Spectroscopes. Apart from manipulation of the electronic properties, pH of carbon SWNT in solution becomes an important factor when it comes to applications such as the use of tubes as pH sensors[3], in biological studies[4], in the formation of homogenous dispersions and also when analyzing the tubes in solution using spectroscopy[5].

In this chapter, quantitative and qualitative analyses of the doping (by changing the pH of the SWNT solution) of metallic and semi conducting nanotube species in surfactant assisted water dispersion is reported. Semi conducting SWNT can be probed electronically by protonation and deprotontaion, and metallic tubes can be protonated near neutral pH[6]. The concentration dependence of the dispersion of carbon nanotubes in water surfactant solution was monitored using absorption and Raman spectroscopy revealing a debundling below ~0.07 mg/ml[7]. At this concentration, the pH of the dispersion was changed from 1 to 13 and quantitative analysis of the doping of individual carbon nanotubes was conducted and monitored using Raman spectroscopy. Mixed Gaussian and Lorentzian line shapes were fitted to the RBM and using a simple protonation model, an equilibrium constant K_p was obtained for each RBM. The protonation rate was related to the optical band gap of the tubes and the number of protons acting per entity was also calculated.

6.2 Experimental Procedures

A stock of 1% by weight SDBS in deionised water was made up and the initial dispersion was diluted serially with sonication and centrifugation and at a concentration of 0.07 mg/ml, individually dispersed tubes were obtained as described in chapter 4. At this concentration, the pH was varied from 1 to 13 by simply adding 1 M of NaCl and/or 1 M of NaOH solution drop wise to the carbon nanotube sample solution which was left for 2-4 minutes to attain equilibrium and then characterised using absorption (integrating sphere) and Raman spectroscopy. The acidic solution was not stable for more than 12 hours. Raman spectra at 633 nm excitation wavelength were measured in solution. For absorption measurements, SWNTs were dispersed in heavy water and for Raman measurement deionised light water was used as mentioned in chapter 3 and 4.

6.3 Results and Discussion

The concentration at the critical debundling point, 0.07 mg/ml, was chosen in order to examine the variability of the electronic properties of the carbon nanotubes with the change in pH. At this concentration, the solution is enriched with isolated tubes which are well suited for doping and also signatures from metallic and semi conducting species in the sample solution can be distinguished. Figure 6.1 a shows the relative spectral changes in the absorption spectrum of 0.07 mg / ml HiPco SWNT in water SDBS surfactant solution from pH 1.43 to 6.75 (by adding 1 M of HCl) and Figure 6.1 b shows the absorption spectrum with the changes in the peak intensities at 6.75(red line) and 1.43 (dark cyan) pH (taken from figure 6.1 a).

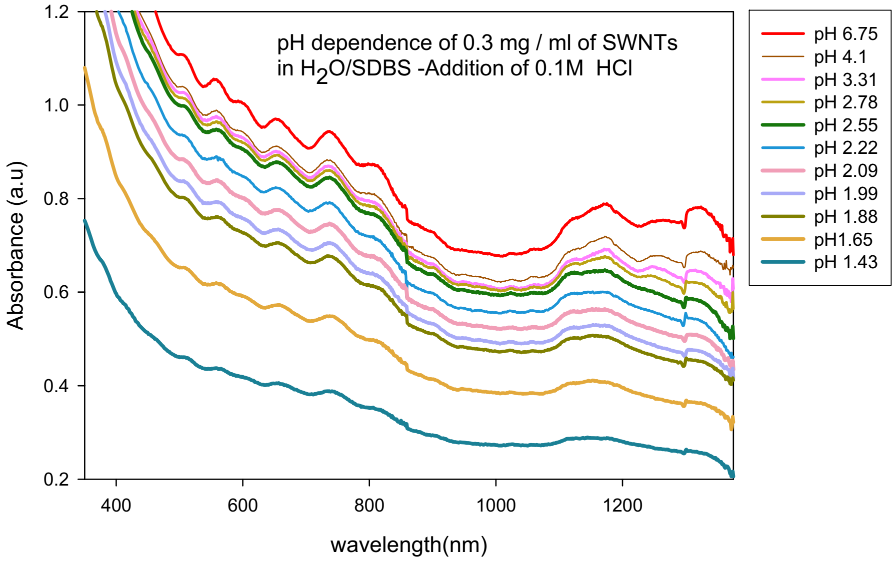

Figure 6.1 a: Absorption spectra of the 0.07mg /ml HiPco carbon nanotube dispersion at pH 1.43 to 6.75.

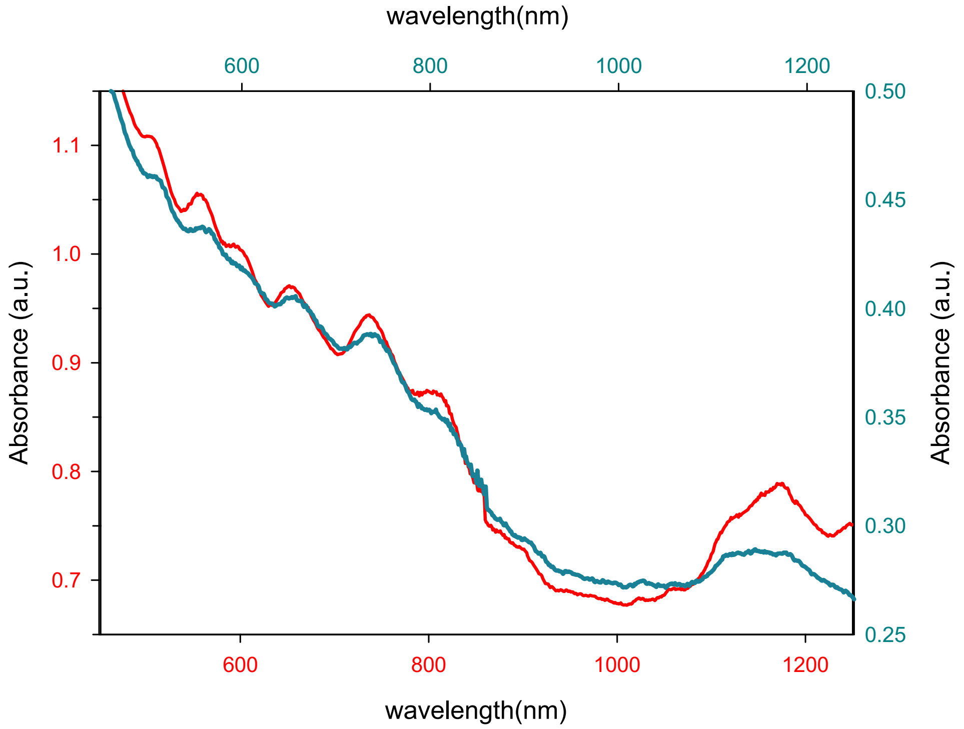

Figure 6.1 b: shows the absorption spectrum with the changes in the peak intensities at pH 6.75 (red line) and pH 1.43 (dark cyan).

One can clearly visualise from figure 6.1 b that, when the pH is changed from 6.75 to 1.43, the peak intensities have reduced significantly due to the change in the pH. As the pH is reduced, the reaction at the surface of the SWNT results in the localization of valence electrons diminishing the absorption at lower pH. It should be noted that the spectral changes that are observed here are due to the protonated state of the tube and not due to the aggregation state as reported by Strano *et al.,*[6] The aggregation state which can thus be visualised is achieved only after the sample is left for more than 12 hours to settle

Raman spectroscopy can also be used to check the reaction rates with respect to changing pH. Figures 6.2 and 6.3 are the Raman spectra (excitation wavelength 633 nm), showing the RBMs and the G-mode respectively, of the HiPco SWNT dispersion at 0.07 mg/ml taken at different pH. Also the process is completely reversible as the pH of the solution is changed from acidic to basic and again to acidic condition and can be checked with both UV/Vis/NIR and Raman spectroscopy.

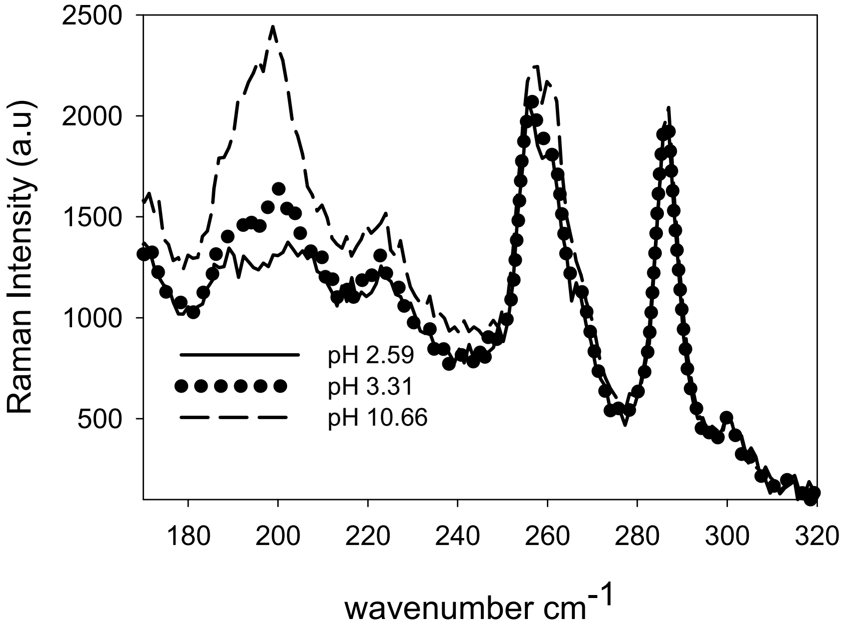

Figure 6.2: RBMat different pH measured using 633 nm as source.

The overall RBM intensity decreases when the pH is decreased (figure 6.2). Acidification of a solution of surfactant dispersed SWNT in water results in the reaction with H^+ at the side walls which localizes electrons. The changes in intensity of the RBM with respect to the change in pH thus represent the protonation and deprotontaion of the SWNTs. Unlike the peaks below 240 cm^{-1} (the majority of which are metallic tubes chapter 2.3.2)[8], the RBMs above 240 cm^{-1} (semi conducting tubes) do not show drastic changes in the peak intensity. This clearly shows that metallic tubes are more readily protonated than the semi conducting tubes, even at neutral pH.

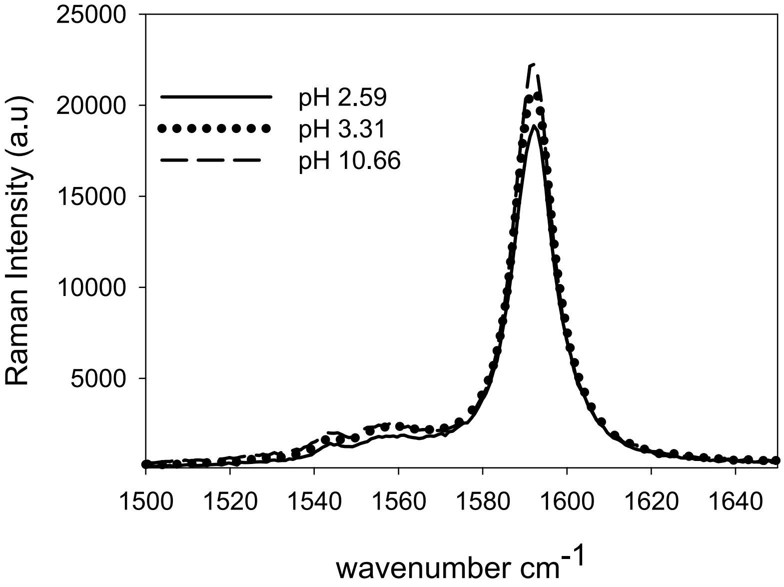

Figure 6.3: G-modes at different pH measured using 633 nm as source.

Figure 6.3 shows the G-mode as a function of pH. The G-mode does not show any drastic change in peak positioning or intensity (633 nm as source). The G-mode obtained at this wavelength is dominated by semi conducting tubes[9] which from the previous discussion do not undergo the same degree of protonation when compared with the metallic tubes.

Mixed Gaussian and Lorentzian line shapes were fitted to the RBM and, using a simple protonation model (Equation 6.1)[6],

$$\frac{RI(pH) - RI_p}{RI_d - RI_p} = \frac{K_p}{10^{-n(pH+\Delta pH)} + K_p} \quad \text{Equation 6.1}$$

an equilibrium constant K_p was obtained for each RBM. RI_p and RI_d are the Raman intensities of the protonated and the de-protonated states. n is the average number of protons reacting with a protonated entity and ΔpH is the interfacial change of pH induced by surfactant double layer.In figure 6.4 a and b, the Raman intensity of two example RBMs is plotted as a function of pH. The values for n and Kp were regressed using the protonation model[6] (Equation 6.1). The value of ΔpH for SDBS is equal to 1[6]. The average value of n was calculated to be 1.

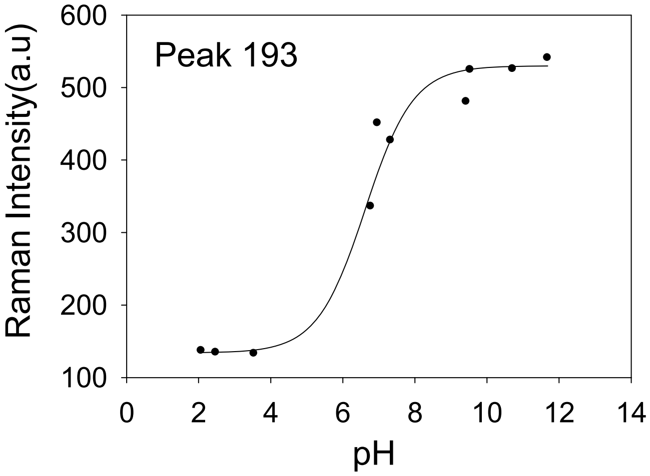

Figure 6.4 a: Raman Intensity is plotted against the pH for the peak 193 cm^{-1} (metallic peak) and regressed using equation 1.

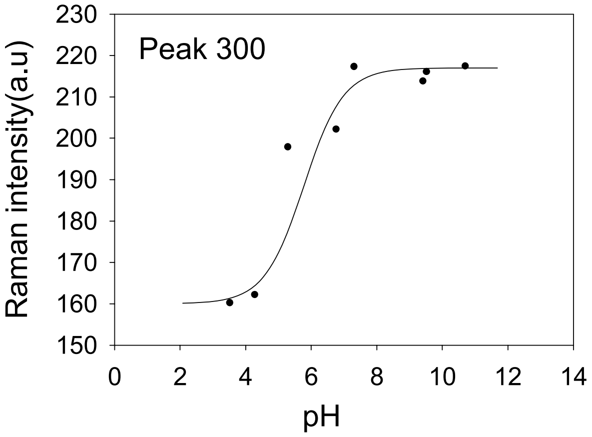

Figure 6.4 b: Raman Intensity is plotted against the pH for the peak 300 cm^{-1} (semiconducting peak) and regressed using equation 1.

Figure 6.5 is a plot of –ln K_p vs the band gap, as calculated from the dependence of the band gap on diameter derived from the RBM frequency [10]. The associated chiral index can be used to determine which tubes are metallic or semi conducting using equation 2.3.

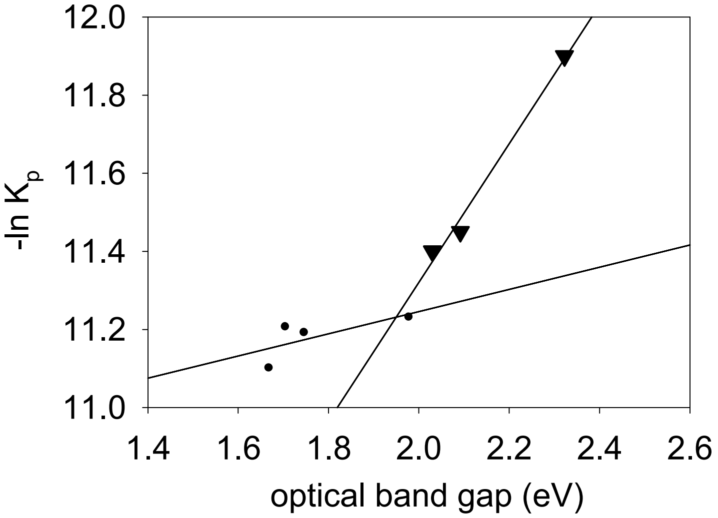

Figure 6.5: Is the plot of –ln K_p vs the band gap. Triangles represent the metallic tubes and filled circles represent the semiconducting tubes.

In figure 6.5, triangles represent metallic tubes and the circles are the semi conducting tubes. For metallic tubes, the band gap is that of the M_{11} transition of the first van Hove Singularities. The average -lnK_p value for metallic tubes is calculated to be -11.58 and that of semi conducting tubes is found to be -11.2.

Previous values obtained by Strano *et al.,*[6] for metallic tubes and semi conducting tubes are -37.7 and -33.97 respectively, as measured by the pH dependence of the UV/Vis/NIR absorption features. It should be noted that in the curve fitting regression, n and K_p are not independent parameters and therefore the absolute value of the rates may not be reliable. Also an electronic double layer is produced due to water at the surfactant nanotube interface which influences the protonation predominantly. The pH of the dispersion is also significantly affected by the nature of the surfactant being employed. In [6] a value of n=3 was extracted, resulting in the large values of K_p. Of physical relevance are the relative rates of the protonation process which clearly indicate that metallic SWNTs are more readily protonated than semi conducting.

6.4 Summary

It has been shown that, once dispersed, both metallic and semi conducting nanotubes can be doped by varying the pH of the dispersion and can be analyzed using Raman spectroscopy. The electronic states of the metallic tubes can be modified more easily than those of the semiconducting tubes. The K_p values have been obtained by regression of a first order protonation model and the values are different for different optical band gaps. Now that metallic and semiconducting signatures of pristine SWNTs have been demonstrated using the spectroscopic techniques, the next aim is to separate the tubes electronically in to metallic and semiconducting samples.

References

(1) Okazaki, K.; Nakato, Y.; Murakoshi, K. *Physical Review B* **2003**, *68*.

(2) Okazaki, K.; Nakato, Y.; Murakoshi, K. *Surface Science* **2004**, *566*, 436.

(3) Kaempgen, M.; Roth, S. *Journal of Electroanalytical Chemistry* **2006**, *586*, 72.

(4) Lin, Y.; Taylor, S.; Li, H. P.; Fernando, K. A. S.; Qu, L. W.; Wang, W.; Gu, L. R.; Zhou, B.; Sun, Y. P. *Journal of Materials Chemistry* **2004**, *14*, 527.

(5) O'Connell, M. J.; Bachilo, S. M.; Huffman, C. B.; Moore, V. C.; Strano, M. S.; Haroz, E. H.; Rialon, K. L.; Boul, P. J.; Noon, W. H.; Kittrell, C.; Ma, J. P.; Hauge, R. H.; Weisman, R. B.; Smalley, R. E. *Science* **2002**, *297*, 593.

(6) Strano, M. S.; Huffman, C. B.; Moore, V. C.; O'Connell, M. J.; Haroz, E. H.; Hubbard, J.; Miller, M.; Rialon, K.; Kittrell, C.; Ramesh, S.; Hauge, R. H.; Smalley, R. E. *Journal of Physical Chemistry B* **2003**, *107*, 6979.

(7) Priya, B. R.; Byrne, H. J. *Journal of Physical Chemistry C* **2008**, *112*, 332.

(8) Kataura, H.; Kumazawa, Y.; Maniwa, Y.; Umezu, I.; Suzuki, S.; Ohtsuka, Y.; Achiba, Y. *Synthetic Metals* **1999**, *103*, 2555.

(9) Kukovecz, A.; Kramberger, C.; Georgakilas, V.; Prato, M.; Kuzmany, H. *European Physical Journal B* **2002**, *28*, 223.

(10) Jorio, A.; Saito, R.; Hafner, J. H.; Lieber, C. M.; Hunter, M.; McClure, T.; Dresselhaus, G.; Dresselhaus, M. S. *Physical Review Letters* **2001**, *86*, 1118.

CHAPTER 7

“Separation based on Electronic properties- Chemical Functionalization”

7.1 Introduction

The dispersion of the raw samples to obtain isolated nanotubes and the determination of their chirality was discussed in the previous chapters. The next step is to attempt to separate the nanotubes by their electronic properties. As mentioned in chapter 1, SWNT exhibit both metallic and semiconducting properties depending upon the chirality of the nanotube structure[1]. Electronic separation of SWNT by their electronic properties, these entities becomes very important when it comes to electronic applications. There have been many techniques proposed for the separation of semi conducting and metallic SWNTs and they can be categorised under three methods: (1) chemical techniques which include covalent functionalization[2] and non-covalent functionalization[3] (2) physical technique such as dielectrophoresis[4], gradient centrifugation[5] and chromatography[6] (3) selective destruction of one type of tubes using hydrogen peroxide[7,8] or laser irradiation[9]. Each technique has its own limitations. For example it has been reported that the mass fraction of the end product is very low after dielectrophoresis[4]; electronic modification might occur when using diazonium reagents which instead of selecting metallic tubes modify them[10]; convolution of diameter or length during the separation process using ion exchange chromatography might occur[11].

The main objective of the experiments described in this chapter was to initially separate the tubes electronically and then disperse them in water surfactant solution and finally establish the critical debundling point for both electronic species of tubes. For this purpose, a separation technique using non covalent functionalization, reported by Chattopadhyay *et al.,*[3] has been used. This method was chosen as it was reported that both the metallic and the semi conducting tubes can be obtained from the same sample.

The technique involves functionalization of the carbon nanotubes with carboxylic groups –COOH through acid treatment and the again functionalization with amines through ODA treatment. Then finally dispersing the carboxylic-amine treated tubes in Tetra Hydro Furan (THF) to get metallic tubes in the deposit and semi conducting tubes suspended in the supernatant. A schematic representation is shown in figure 7.1 a.

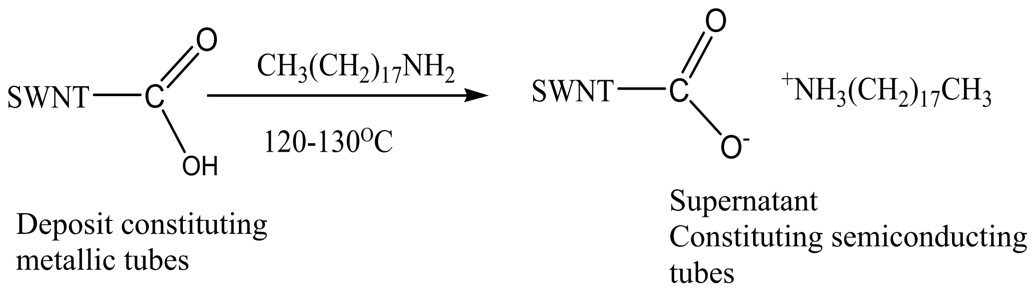

Figure 7.1 a: Schematic showing the reaction of the acid treated SWNT with ODA.

The method involves excellent physisorption between the amines and the side walls of the SWNT which has been well demonstrated both theoretically[12] and experimentally[13]. Chattopadhyay *et al.*,[3] reported an affinity of the amine groups for semi conducting SWNTS as opposed to their metallic counterparts and established a recipe for bulk separation of tubes electronically using amines. In this work the technique will be employed with a view to optimising the separation of metallic and semi conducting HiPco and Arc Discharge SWNTs and establishing their spectroscopic fingerprints independently. As will be outlined, Arc Discharge SWNTs were employed in addition to HiPco SWNTs as little success was achieved with the HiPco samples.

7.2 Experimental

60mg HiPco SWNT and Arc Discharge (from Carbon nanotechnologies Inc and Sigma Aldrich) taken separately, were first bath sonicated in a mixture of 3:1 ratio of 50 ml of concentrated sulphuric and nitric acid[14] for less than 2 hours (100 min). The SWNTs (which are then –COOH functionalised after acid treatment) were washed to remove excess acid by dispersing in 1 litre of deionised water and were left to stand for 24 hours. The excess water was removed by vacuum filtration and the tubes were dried. Nearly 40 mg of tubes were retrieved after the acid treatment. The functionalised dried tubes were then treated with 80 mg ODA(2:1 ODA to –COOH functionalised tubes - ratio by weight) for 24 hours at 120º C to 130º C, and washed with ethanol seven times. Finally these amine functionalised tubes were dispersed in THF at a concentration of 0.1mg/ml, coarse filtered to remove nanotube bundles and left to dry. The supernatant and the deposit of SWNTs were then analysed spectroscopically for their electronic enrichment using UV/Vis/NIR absorption and Raman spectroscopy.

Sample preparation for FTIR: SWNTs along with potassium bromide (which served as a matrix to hold the SWNTs) was ground to a fine powder. They were exposed to high pressure to form optically transparent pellets and were taken for FTIR measurements.

The Perkin-Elmer Lambda 900 UV/Vis/NIR spectrometer was used to measure the absorption spectrum of the SWNT suspensions in the spectral region 400 nm to 900 nm. The integrating sphere (section 3.1.4) was used for all the absorption measurements in the UV/Vis/NIR spectrometer. Raman measurements were taken using the Instruments S. A. (Jobin Yvon) Labram 1B using 660 nm and 532 nm as sources. The UV/Vis/NIR absorption of all samples was measured in solution phase using a x50 objective. 10 mm quartz (UV/NIR optimised) cuvettes were used for all the measurements in UV/Vis/NIR spectrometer, for Raman measurements tubes were dispersed and dried on quartz slides.

7.3 Results and Discussion

The steps undertaken leading to the electronic separation process can be summarised as follows

1) Purification by acid treatment (oxidation) leading to non covalent functionalization –COOH (carboxylic acid group)-
2) Washing with deionised water
3) Drying

4) Heat Treatment with Octa Decyl Amine (ODA)- 24 hours
5) Removal of excess amines by washing with ethanol
6) Suspension of ODA treated tubes in THF
7) Evaporation of THF
8) Supernatant- semiconducting tubes
9) Deposit – metallic tubes

Figure 7.1 b shows the FTIR spectrum of pristine HiPco SWNTs. According to the space group symmetry the translation mode along the cylindrical axis and perpendicular to the cylindrical axis modes are IR active[15] and these peaks are at 819 cm^{-1} and 1592 cm^{-1} respectively [14].

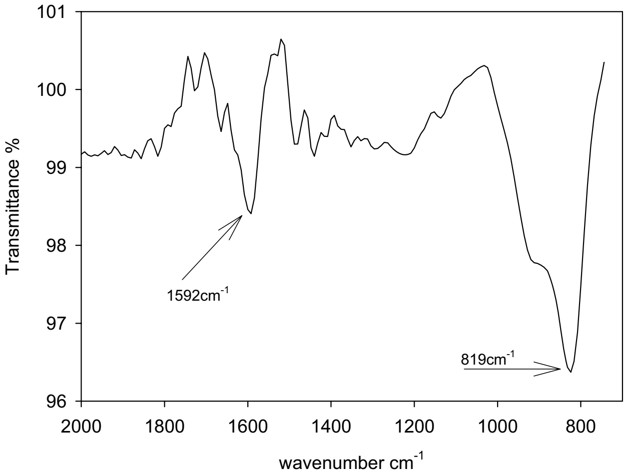

Figure 7.1b shows the FTIR spectrum of pristine HiPco

Figure 7.2 shows the spectra after acid treatment for 24 hours. The peaks at 1728 cm^{-1} and 1615cm^{-1} are the signatures of carboxylic and carboxylate groups respectively[14]. The efficiency of this step is very important as all the further steps depend on the amount –

COOH attached to the side walls of the carbon nanotubes. These tubes were further processed by amine treatment which was done by heating the –COOH functionalised tubes with ODA for 48 hours. The ratio of ODA to the –COOH functionalised tubes was 2:1 by weight as mentioned in the experimental section 7.2. The FTIR spectrum of pristine ODA is shown in figure 7.3. The peak at 1562 cm^{-1} comes from the vibrations from the amide bond.

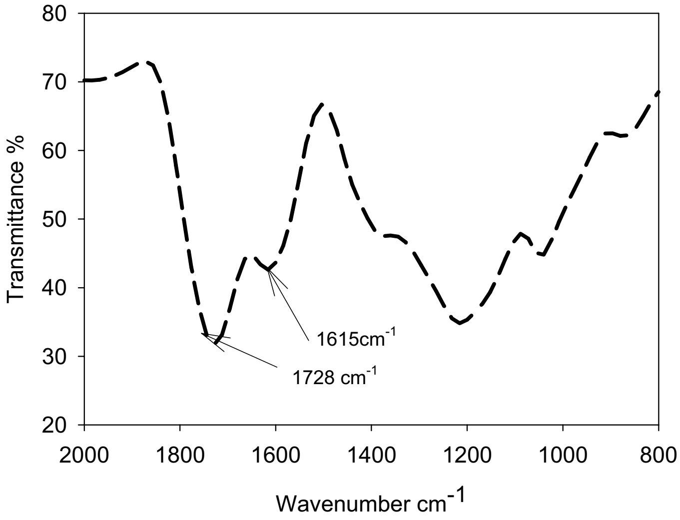

Figure 7.2: shows the spectra after acid treatment for 24 hours.

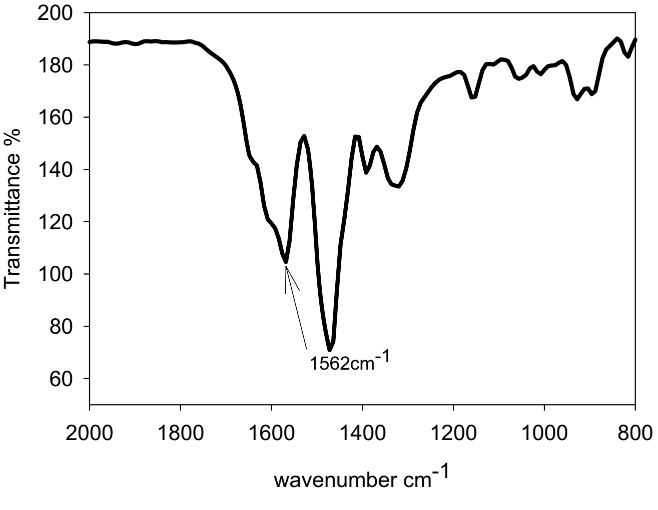

Figure 7.3: shows the FTIR spectrum of Pristine ODA.

After this amine treatment the tubes were washed with ethanol to remove excess ODA and then dispersed in THF and left for evaporation for more than 24 hours in order to obtain the supernatant and deposit of carbon nanotubes as Chattopadhyay[3] reported. Surprisingly, there was no signature of deposition of tubes which are supposed to be metallic tubes.

Thus it was deemed necessary to fine tune the reaction conditions in an attempt to optimise the process. In the literature, little or no detail was given on certain parameters which may be critical to the success of the process. These include 1) time for acid treatment 2) amount of ODA required for amine treatment. As there was no deposition of the carbon nanotubes observed, there is a suggestion that all the tubes have been amide functionalized and remained in suspension.

The peak at 1728 cm^{-1} shown in figure 7.2 is due to the –COOH group attached to the side wall of the carbon nanotubes after prolonged acid treatment. Zhang *et al.,*[14] made a systematic investigation of the positioning of the –COOH peak versus acid treatment time. They concluded that prolonged treatment time led to an increase in the number of –COOH attached to the side walls of the tube and the formation of hydrogen bonds among the –COOH groups. At high attachment densities, the COOH peak is seen to shift from 1737 cm^{-1} to 1728 cm^{-1}. From the FTIR spectrum (figure 7.2) it can be seen that the –COOH peak is at 1728 cm^{-1} indicating too much of functionalization as the acid treatment was done for 24 hours. So it was decided to reduce the treatment time to less than two hours. The FTIR spectrum for tubes treated under this condition is shown in figure 7.4, wherein the –COOH vibration is seen at 1737 cm^{-1} compared to 1728 cm^{-1} when treated for 24 hours. This indicates that the nanotubes have been less extensively functionalised.

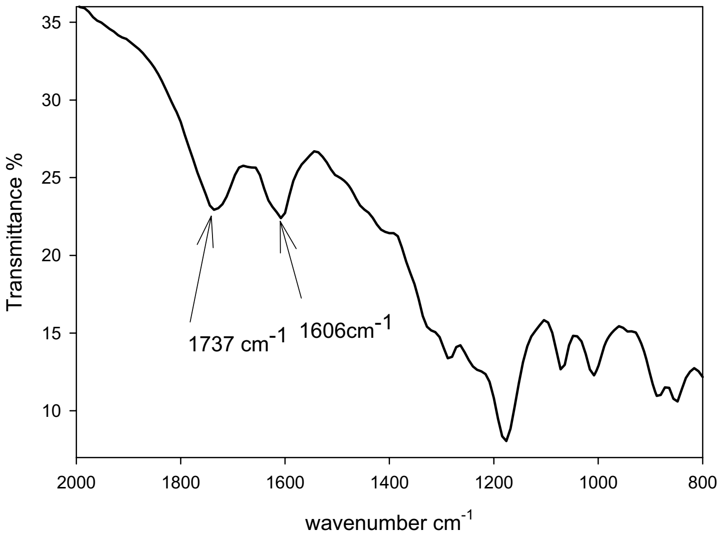

Figure 7.4: shows the FTIR spectra after acid treatment for 2 hours.

After this acid treatment, the –COOH functionalised SWNTs were subjected to the same ODA treatment. The amount was ODA to SWNT/-COOH was reduced to 1:1 by weight. After washing with ethanol to remove excess ODA the tubes were then dispersed in THF, left standing to dry and this time a deposit of nanotubes was seen. These tubes were checked for the FTIR spectrum. According to Chattopadhyay *et al.*,[3] the deposit should consist of metallic SWNT/ –COOH groups and the semi conducting SWNT/amine group should be in the supernatant. If that is the case the FTIR spectrum of the metallic deposit should carboxylic peaks, and the supernatant amide peaks. But the FTIR spectra of the deposit and supernatant, as shown in figure 7.5a and b respectively, show both amide and carboxylic groups in both of them.

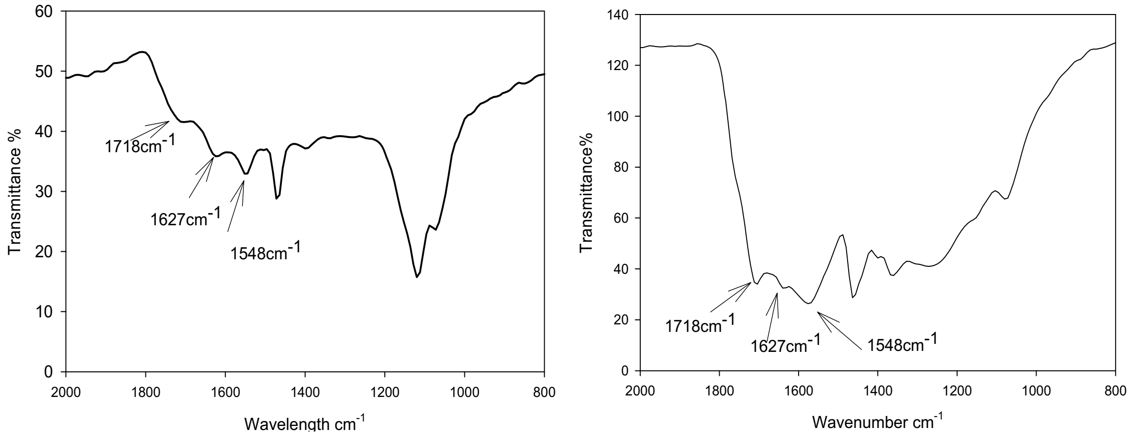

Figure 7.5 (a): The FTIR spectrum of deposit which is considered to be enriched with metallic (b) the FTIR spectrum of supernatant which is considered to be enriched with semiconducting tubes.

Further analysis of the deposit and the supernatant was performed using UV/Vis/NIR absorption and Raman spectroscopy. The absorption spectra of the supernatant and the deposit in THF are shown in figure 7.6. The same range of van Hove Singularities can be seen in both spectra leading to the conclusion that there was no electronic separation.

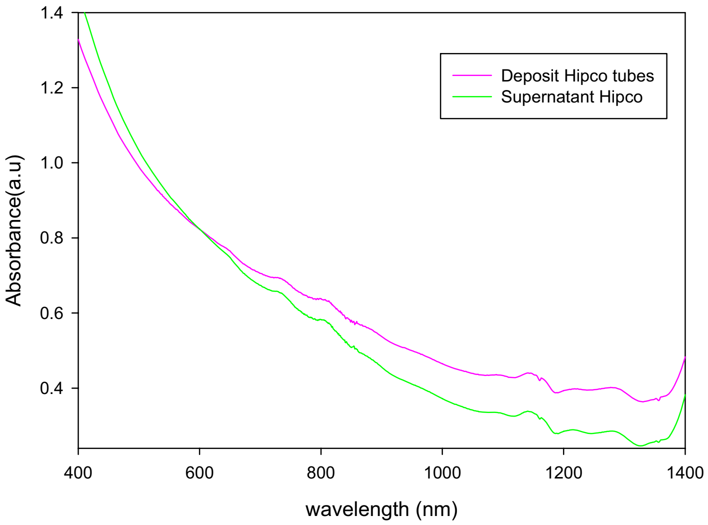

Figure 7.6: Absorption spectroscopy of deposit and supernatant.

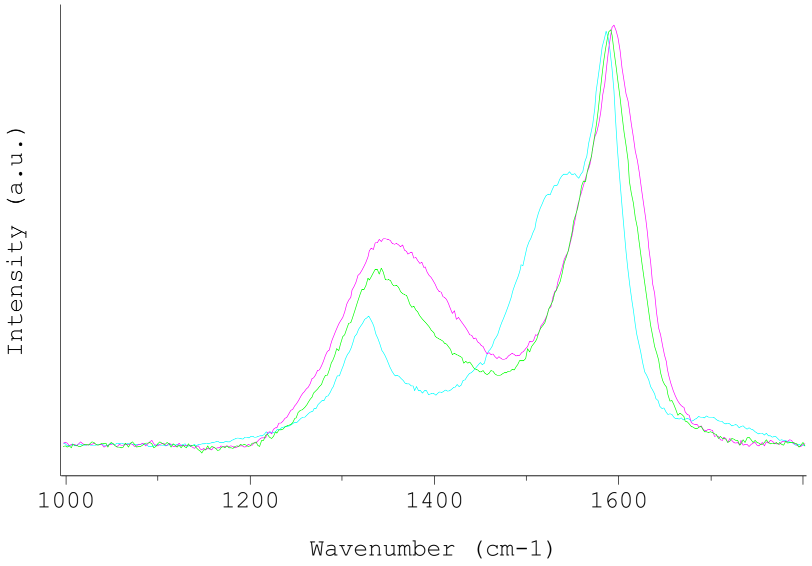

Figure 7.7: Raman spectra at 532 nm of HiPco SWNTs of the raw (cyan) supernatant (green) and deposit (pink).

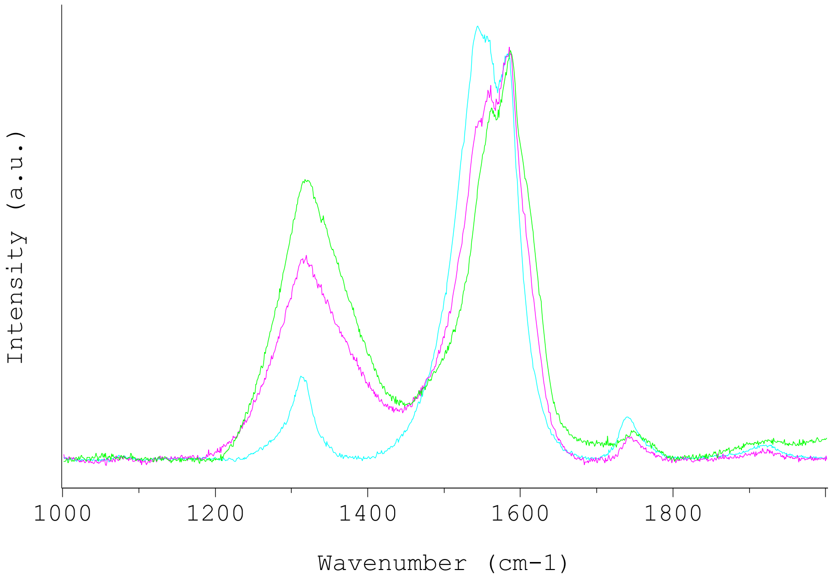

Figure 7.8: Raman spectra at 660nm of arc discharge SWNTs of the raw (cyan) supernatant (green) and deposit (pink) is shown.

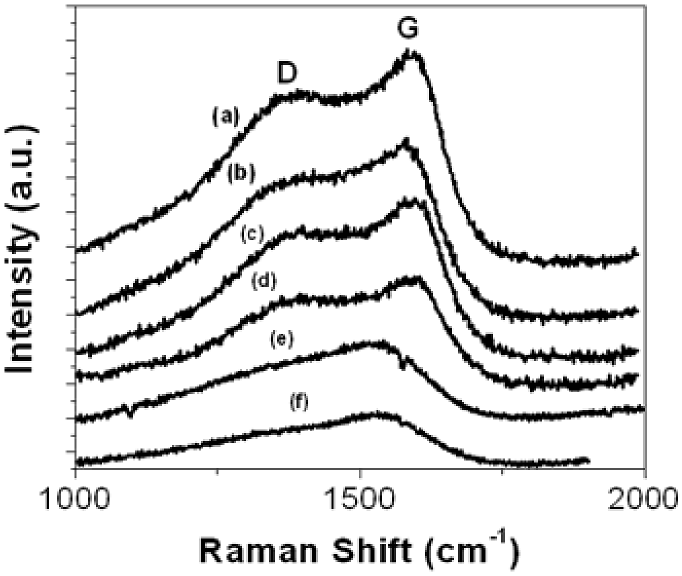

Figure 7.9: Raman spectra of amorphous carbon films[16].

The Raman spectra (532 nm for HiPco tubes and 660nm for Arc Discharge tubes) of the samples are shown in Figures 7.7 and 7.8. The G mode gives the finger print of the electronic character of the nanotubes in a given sample as mentioned in chapter 2 and 5. In figure 7.7 it can be seen that huge amount of metallic tubes have been destroyed and the defects have also increased as indicated by the relative increase of the D-line. The damage to the nanotubes is as extensive that the line shape of the Raman spectrum of –COOH functionalised – acid treated tubes is similar to that of amorphous carbon as shown in figure 7.9. The same experimental procedure was undertaken for arc discharge SWNTs and the G-mode (660 nm excitation wavelength) is seen to similarly lose its metallic character and a significant increase in the D band is observed, indicating extensive damage of the nanotubes. Although the process could be further optimised, several questions regarding the mechanism of functionalization should be established:

1) at the first stage of –COOH functionalization, should all the tubes be functionalised or only the semi conducting tubes
2) if all the tubes are functionalised, it is important to know how long the ODA treatment should be carried out for and also the amount of ODA that should be sufficient for the semiconducting tubes alone.
3) if only the semiconducting tubes should be functionalised then it is important to know how long the acid treatment should be carried out for.

That the mechanism is not fully understood is highlighted by the conflicting literature reports. While Chattopadhyay *et al.,* [3] the deposit should consist of metallic SWNT/ –COOH groups and the semi conducting SWNT/amine group should be in the supernatant, Yutaka Meada[17] indicated that the amines interact more preferably with as prepared metallic tubes rather than the semiconducting tubes. It was finally concluded that this method cannot be used for routine electronic separation and to explore alternative methods of separation.

7.4Summary

-COOH functionalised tubes were prepared using acid treatment. These functionalised tubes were further amine treated and dispersed in THF. The deposit as reportd by Chattopadhyay *et al.,*[3] contain metallic tubes and the supernatant contain semi conducting nanotubes. This happens because the semi conducting tubes have a higher affinity towards the amines than their metallic counter part. This concept was contradicted by Yutaka Meada[17] who claimed that the metallic tubes and the amines interact better than the semiconducting tubes. The experiments carried out here showed that optimisation was required at every stage of functionalization and unless that is performed this procedure of separating SWNTs electronically cannot be used for routine processing. Therefore, as a next step towards enriching the semi conducting nanotubes, selective destruction of nanotubes by microwave irradiated was investigated.

References

(1) M. S. Dresselhaus, G. D., P. Avouris. *Springer- verlag, Berlin* **2001**.

(2) Campidelli, S.; Meneghetti, M.; Prato, M. *Small* **2007**, *3*, 1672.

(3) Chattopadhyay, D.; Galeska, L.; Papadimitrakopoulos, F. *Journal of the American Chemical Society* **2003**, *125*, 3370.

(4) Krupke, R.; Hennrich, F.; von Lohneysen, H.; Kappes, M. M. *Science* **2003**, *301*, 344.

(5) Arnold, M. S.; Green, A. A.; Hulvat, J. F.; Stupp, S. I.; Hersam, M. C. *Nature Nanotechnology* **2006**, *1*, 60.

(6) Zheng, M.; Jagota, A.; Strano, M. S.; Santos, A. P.; Barone, P.; Chou, S. G.; Diner, B. A.; Dresselhaus, M. S.; McLean, R. S.; Onoa, G. B.; Samsonidze, G. G.; Semke, E. D.; Usrey, M.; Walls, D. J. *Science* **2003**, *302*, 1545.

(7) Miyata, S.; Takemura, G.; Kawase, Y.; Li, Y. W.; Okada, H.; Maruyama, R.; Ushikoshi, H.; Esaki, M.; Kanamori, H.; Li, L. H.; Misao, Y.; Tezuka, A.; Toyo-Oka, T.; Minatoguchi, S.; Fujiwara, T.; Fujiwara, H. *American Journal of Pathology* **2006**, *168*, 386.

(8) Banerjee, S.; Hemraj-Benny, T.; Wong, S. S. *J Nanosci Nanotechnol* **2005**, *5*, 841.

(9) Huang, H. J.; Maruyama, R.; Noda, K.; Kajiura, H.; Kadono, K. *Journal of Physical Chemistry B* **2006**, *110*, 7316.

(10) Balasubramanian, K.; Sordan, R.; Burghard, M.; Kern, K. *Nano Letters* **2004**, *4*, 827.

(11) Strano, M. S.; Zheng, M.; Jagota, A.; Onoa, G. B.; Heller, D. A.; Barone, P. W.; Usrey, M. L. *Nano Letters* **2004**, *4*, 543.

(12) Kong, J.; Dai, H. J. *Journal of Physical Chemistry B* **2001**, *105*, 2890.

(13) Basiuk, E. V.; Basiuk, V. A.; Banuelos, J. G.; Saniger-Blesa, J. M.; Pokrovskiy, V. A.; Gromovoy, T. Y.; Mischanchuk, A. V.; Mischanchuk, B. G. *Journal of Physical Chemistry B* **2002**, *106*, 1588.

(14) Zhang, J.; Zou, H. L.; Qing, Q.; Yang, Y. L.; Li, Q. W.; Liu, Z. F.; Guo, X. Y.; Du, Z. L. *Journal of Physical Chemistry B* **2003**, *107*, 3712.

(15) M. S. Dresselhaus, G. D., P. C. Eklund. *Academic Press, New York* **1996**.

(16) Marques, F. C.; Lacerda, R. G. *Brazilian Journal of Physics* **2000**, *30*, 527.

(17) Maeda, Y.; Kimura, S.; Kanda, M.; Hirashima, Y.; Hasegawa, T.; Wakahara, T.; Lian, Y.; Nakahodo, T.; Tsuchiya, T.; Akasaka, T.; Lu, J.; Zhang, X.; Gao, Z.; Yu, Y.; Nagase, S.; Kazaoui, S.; Minami, N.; Shimizu, T.; Tokumoto, H.; Saito, R. *J Am Chem Soc* **2005**, *127*, 10287.

CHAPTER 8

“Separation and Dispersion– Semiconducting Tubes”

Adapted from –“Quantitative Analyses of Microwave Treated HiPco Carbon nanotubes using Absorption and Raman Spectroscopy”- **J. Phys. Chem. C 2009, 112, 332-337**

8.1 Introduction

One of the most straight forward techniques to separate/enrich (one type) of tube is based on microwave treatment, which comes under the category (from chapter 7.1) of “selective destruction of one type of nanotube”, whereby exposing the tubes to high microwave powers preferentially destroys the metallic tubes[1]. The average microwave power absorbed per unit volume is directly proportional to the relative dielectric constant of the material. The dielectric constant of a material affects how electromagnetic signals (light, radio waves, millimeter-waves, etc.) move through the material. The availability of electrons at the Fermi level for the metallic tubes results in high dielectric constants and therefore metallic tubes absorb the microwave radiation more efficiently than the semi conducting tubes, resulting in selective destruction.

J. W. Song *et al.,*[2] have exposed the SWNTs for 10 seconds , 20 seconds, 30 seconds , 1 minutes and 5 minutes using microwave radiation and reported the observed changes in the corresponding RBMs of the Raman spectrum at 514 nm excitation wavelength. Although they predicted that excess irradiation would deteriorate the degree of separation by burning out the semi conducting tubes, there was no further demonstration or optimisation of the process. Furthermore, no analysis of the destruction of the metallic tubes was carried out to establish whether all metallic tubes are affected equally.

Thus the aim of this work is

1) To quantitatively and qualitatively assess the preferential destruction of metallic nanotubes using Raman and UV/Vis/NIR absorption spectroscopy,

2) To explore the rates of the reaction using Raman spectroscopy,

3) To disperse the microwave treated tubes produced under optimum conditions in water/surfactant suspension, and to investigate the dispersion limit[3]

4) To compare the dispersion limits and solubilities of the microwave processed tubes and the pristine samples.

8.2 Experimental

Pristine HiPco (High Pressure carbon monoxide disproportionation) tubes (Carbon Nanotechnologies Inc. batch no. PO289) were dispersed in chloroform (from Sigma Aldrich) through tip sonication (Ultrasonic processor VCX 750 W) at 32% power output. The as prepared concentration of carbon nanotubes in chloroform was 0.8 mg/ml. 1 ml of the suspension was uniformly drop cast onto clean small ceramic tiles and was air blown to evaporate the chloroform. Fifteen such ceramic tiles were prepared. All the ceramic plates with the HiPco tubes were exposed to microwave radiation (Sharp R879SL 26ltr 900W Combination Microwave) for different intervals of time from 0 seconds to 1800 seconds. Post irradiation, the exposed tubes were dispersed in 1% by weight aqueous Sodium Dodecyl Benzene Sulphonate (SDBS from Sigma Aldrich) by mild bath sonication for 30 minutes and the samples were centrifuged at 4000 rpm (1699g Eppendorf centrifuge 5417C) for one hour. The decanted SWNT solution was characterised using UV/Vis/NIR absorption and Raman spectroscopy at 633 nm excitation wavelength. As previous studies[12] of surfactant dispersed SWNTs have shown no evidence of selective dispersion, any change in the spectral profiles compared to raw SWNT samples are attributed to the microwave treatment.

The Perkin-Elmer Lambda 900 UV/Vis/NIR spectrometer was used to measure the absorption spectrum of the microwave exposed SWNT suspensions in the spectral region 400 nm to 900 nm. The integrating sphere (section 3.1.4) was used for all the absorption measurements in the UV/Vis/NIR spectrometer. Raman measurements were taken using the Instruments S. A. (Jobin Yvon) Labram 1B using 633 nm as source. The Raman scattering of all the microwave treated samples was measured in solution phase using a x50 objective. 10 mm quartz (UV/NIR optimised) cuvettes were used for all the measurements.

8.3 Results and Discussion

Figure 8.1 shows a Raman spectrum of HiPco Single wall carbon nanotubes suspended in water/SDBS solution at 633 nm excitation wavelength. It is worth giving a brief reminder about the Raman spectrum of carbon nanotubes again here (although explained in section 2.3.2) as this chapter mainly deals with the changes in the Raman spectrum and so further concepts introduced in this chapter can be well interpreted. The main resonant features[4] in the Raman spectrum of SWNTs are the Radial Breathing Modes (RBM) which can be seen from 180 cm^{-1} to 340 cm^{-1}, and the Graphitic mode (G mode) around 1560 cm^{-1}. RBMs and the G band are shown in the insets of figure 8.1. The RBMs arise due to the radial breathing of the nanotubes and the G-band is a multi component spectral feature which arises due to the tangential vibrations of C=C along the tube axis[5]. Due to the high curvature of the tubes, the G band is doubly split into the high frequency or G^+ band and the low frequency or G^- band.

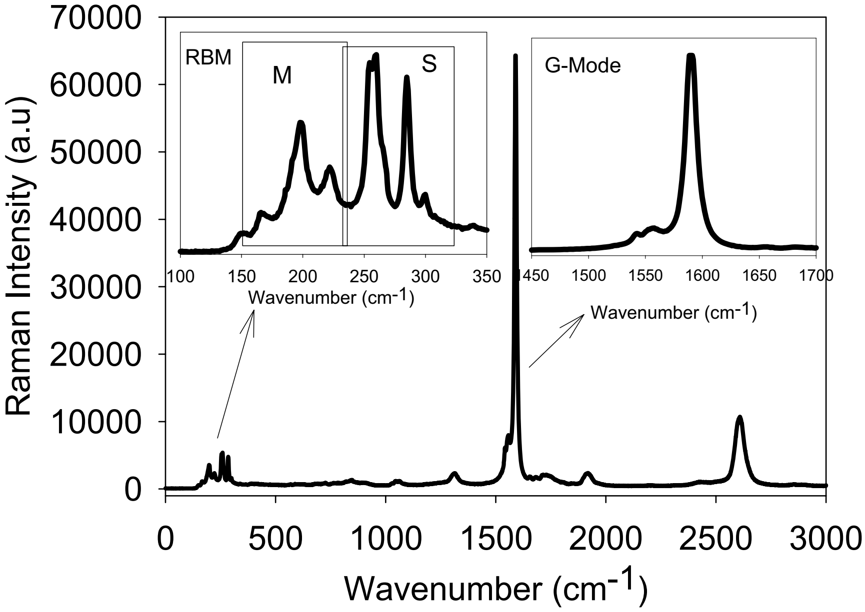

Figure 8.1: Raman Spectrum of SWNTs dispersed in water/SDBS solution at 633 nm excitation wavelength. The inset on the left hand side shows the RBMs with metallic region and the semiconducting region derived from the Kataura Plot [6,7]. The inset on the right hand side shows the G Band.

The G^+ band has a symmetric Lorentzian line shape and the line shape of the G^- band is sensitive to the electronic properties of the tubes. It exhibits an asymmetric Breit - Wigner - Fano (BWF) line shape if the tubes are metallic and a Lorentzian line shape if the tubes are semi conducting[8]. The RBM frequency can be directly related to the diameter d of the tubes

$$\omega_{RBM} = C/d + \Gamma \qquad \text{Equation 8.1}$$

where C = 248cm^{-1} for isolated SWNT on a SiO_2 substrate and Γ is a damping factor[9] (in the section 5.3.2 the values were used for surfactants instead of silicon substrate) In a sample of SWNTs of mixed diameter, the Raman spectrum has shown to be dominated by those which have an electronic absorption resonant with the excitation wavelength.[4]

In the absorption spectrum extending from UV to NIR region, interband transitions for metallic (M_{11}) occur between ~400 nm to 650 nm, while those for semiconducting tubes lie between 550 nm to 900 nm for S_{22} and 800 nm to 1600 nm for S_{11} transitions[10]. As already mentioned in chapter 2 and 5, the "Kataura plot"[6] is commonly used as a guide to relate the absorption features of SWNTs to their diameters. For an excitation wavelength of 633 nm the majority of the RBM peaks below 240cm^{-1} are metallic and above 240 cm^{-1} are semi conducting[6].

Figure 8.2 a compares the RBM spectrum of HiPco SWNTs exposed to microwave radiation for different time periods. The dotted line is the Raman spectrum of the tubes exposed for 5 seconds, the dashed line and the solid line are the Raman spectra obtained for tubes exposed at 240 seconds and 1800 seconds respectively. For the purpose of comparison, the spectra for both 5 seconds and 1800 seconds are normalised with respect to 240 seconds at the peak intensity of 255 cm^{-1}. The normalised spectra very well portray the depletion of metallic tubes when the exposure is increased from 5 s to 240 s and 1800 s. For instance, it can be seen from the Raman spectrum of the tubes exposed to 5 s that the intensity of the metallic peak at ~200 cm^{-1} is approximately the same as that of the semi conducting peak at 255 cm^{-1}. As the exposure time is increased to 240 s the intensity of the metallic peak at ~200 cm^{-1} has reduced significantly relative to that of the semi conducting peak at 255 cm^{-1}.

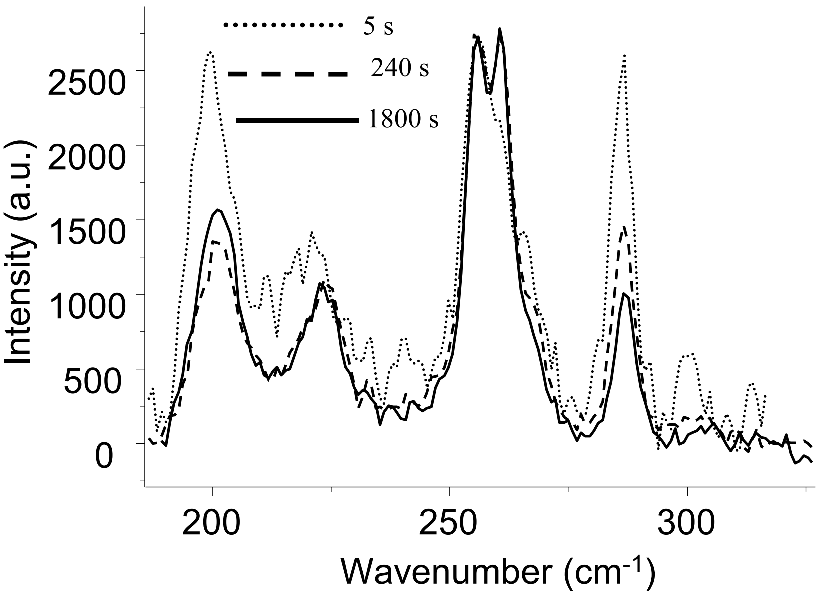

Figure 8.2a: RBMs of the SWNTs microwave treated at 5 seconds (dotted lines), 240 seconds (dashed lines) and 1800 s (solid line). It can be seen that as the time of exposure is increased the intensity of the metallic peak at 200 cm^{-1} has decreased (For the Raman measurement the microwave treated tubes were dispersed in water surfactant solution).

To visualise the process more clearly, the RBM peaks for 5 s and 240 s exposure have been deconvoluted by fitting Lorentzian line shapes, as shown in figure 8.2 b and 8.2 c respectively. The feature at ~200 cm^{-1} is deconvoluted into three Lorentzian line shapes at 199 cm^{-1}, 202 cm^{-1} and 208 cm^{-1}. From the deconvoluted spectra it can be seen that the metallic peak intensity at 199cm^{-1}, for example, has decreased relative to the semi conducting peaks at 255 cm^{-1}, 260 cm^{-1} and 266 cm^{-1} when the tubes were irradiated for 240 s. This is clear evidence that the metallic tubes are being preferentially destroyed when the pristine SWNTs are exposed to microwave radiation. A similar behaviour was reported by J. W. Song *et al.,* with 514 nm excitation wavelength.

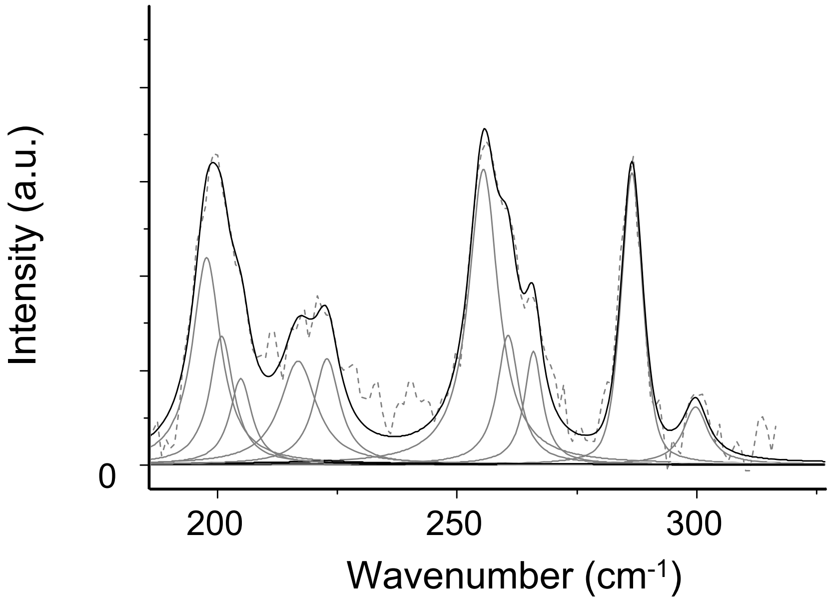

Figure 8.2 b: Deconvoluted RBMs of tubes treated at 5 seconds (from Figure 8.2 a).

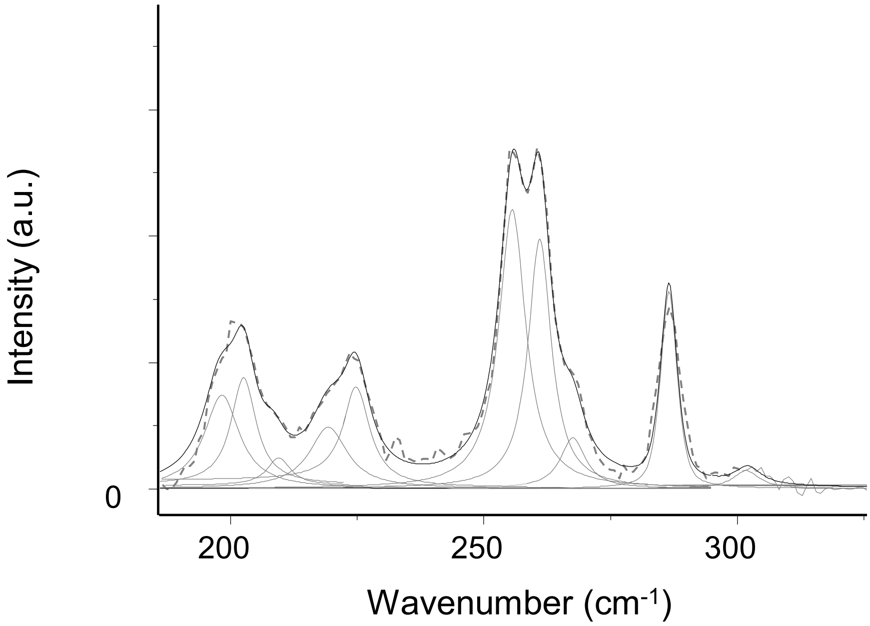

Figure 8.2 c: Deconvoluted RBMs of tubes treated at 240 seconds (from Figure 8.2 a).

Table 8.1: Peak contributions-633nm Excitation wavelength

Time of exposure (s)	Raman Intensity at $1545cm^{-1}$(BWF)	Raman Intensity at $1559cm^{-1}$	Raman Intensity at $1589cm^{-1}$	Raman Intensity at $1593cm^{-1}$
5	1296	2269	7064	25067
240	742	2492	9008	23468
1800	624	2301	8475	19427

The Raman G band for the solutions of nanotubes irradiated for 5 s, 240 s and 1800 s was similarly curve fitted with Lorentzian bands at 1559, 1589 and $1593cm^{-1}$and a BWF line shape at 1545 cm^{-1}. Table 8.1 presents the derived peak contributions. From the curve fittings it can be clearly seen that the Breit-Wegner-Fano (BWF) contribution at 1545 cm^{-1} has decreased at 240 seconds when compared to 5 seconds, which is additional evidence that the number of metallic tubes has decreased and the sample has been depleted of metallic tubes or effectively enriched with semi conducting tubes.

The absorption spectrum of solutions of SWNTs treated for 5 seconds, 120 seconds, 240 seconds and 1800 seconds are shown in figure 8.3 a. In this representation, no striking changes to the spectral profile are evident. All four spectra were therefore corrected for background according to the method reported by Nair *et al.,*[11] (as mentioned in chapter 5.3.1) and normalised to the integral area of absorption region from 700 nm to 900 nm. Figure 8.3 b shows a direct comparison of the background subtracted and normalised absorption spectra of tubes exposed to 5 seconds (grey area) and 1800 seconds (solid line). As the time of exposure is increased from 5 seconds to 1800 seconds it can be clearly seen that the metallic peaks have been reduced. In particular, the peak between 630 nm and 700 nm is seen to decrease by a factor of 5. It is worth noting, however, given that each feature in the UV/Vis/NIR spectrum represents a tube of different diameter and that those in the region 400 nm to 650 nm correspond to metallic tubes, that microwave treatment does not degrade all metallic nanotubes at equal rates. This is perhaps not surprising as metallic nanotubes of differing diameters have differing densities of states at the Fermi level and therefore dielectric constants. The maximally degraded nanotubes correspond to the lowest energy metallic feature at ~650 nm. From the relationship between the absorption features and the diameter [11] , and the diameter and the RBM frequency[9], the peak at ~ 650 nm in the absorption spectrum, at least partially resonant at 633 nm, corresponds to RBM frequencies of 199 cm^{-1} (646 nm), 202 cm^{-1} (636 nm) and 208 cm^{-1} (593.1 nm) which corresponds to the RBMs observed in the Raman spectrum of figures 8.1 and 8.2 a. It is also noted from figure 8.3 b that at prolonged exposures, the features associated with semiconducting tubes at e.g. 740 nm are also degraded.

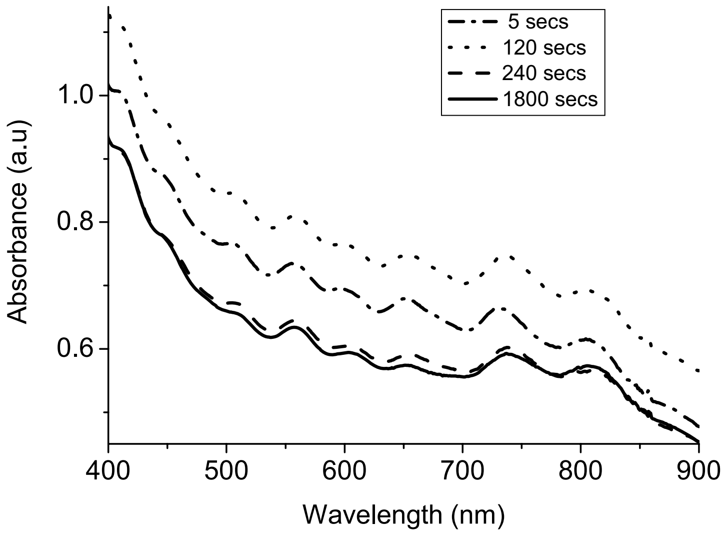

Figure 8.3 a: Absorption spectra of the SWNTs microwave treated at 5 seconds (dashed dotted lines), 120 seconds (dotted lines), 240 seconds (dashed lines) and 1800 seconds (solid line).

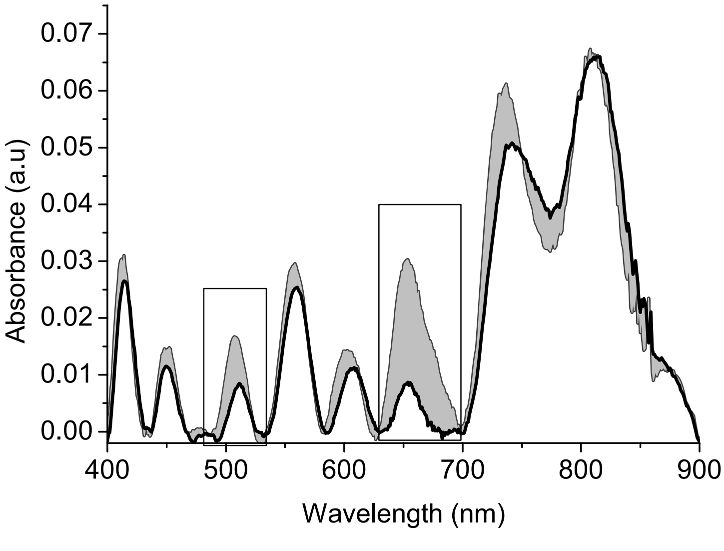

Figure 8.3 b: Background subtracted (from figure 7.3b) absorption spectra of the SWNTs microwave treated at 5 seconds and 1800 seconds. It can be clearly seen (from the area specified in the box) that higher exposure leads to degradation of metallic tubes, but not all the tubes degrade at the same rate.

It is clear therefore that although a preferential destruction of the metallic tubes is inferred by the Raman analysis, not all metallic nanotubes are destroyed at the same rates and that semiconducting tubes are also destroyed at prolonged exposures. It is therefore important to perform quantitative analyses in order to determine the optimised irradiation conditions for isolation of the semiconducting tubes. For this purpose, SWNTs deposited on the ceramic tiles were exposed to microwave radiation for different time periods starting from 5 seconds to 1800 seconds. In figure 8.4a the ratio of peak heights $RBM_{200cm^{-1}} / RBM_{255cm^{-1}}$ has been plotted as a function of microwave exposure. At times greater than ~600 seconds, the time dependence of the ratio becomes erratic and is not shown. It can be seen that the ratio decreases with increasing exposure time until an apparent saturation point after which it starts to increase. The initial decrease is as expected, indicating that the metallic tubes with RBMs at ~200 cm^{-1} are preferentially destroyed. The kinetic behaviour cannot be fitted with a simple ratio of two exponential decays,. The more complex behaviour can be fitted by recognising that in the initial stages, when there is a significant number of the more strongly absorbing metallic tubes, most of the radiation is absorbed by them and little penetrates to the semiconducting tubes. To a first order approximation, assuming a random distribution of all tubes, for constant input intensity, the decay of the metallic feature can be considered to be described by a simple exponential;

$$RBM_{200cm^{-1}}(t) = RBM_{200cm^{-1}}(0)\exp(-k_m t) \qquad \text{Equation 8.2}$$

where k_m describes the decay rate of the number of metallic tubes, N_m.

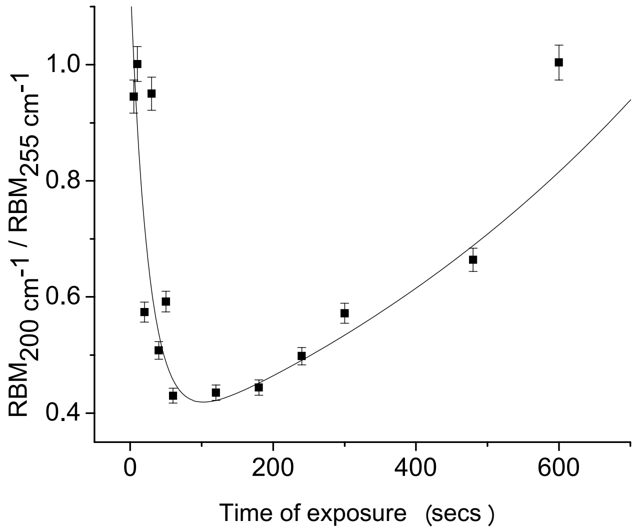

Figure 8.4 a: Decay Ratio of convoluted peak intensities of $RBM_{200cm^{-1}} / RBM_{255cm^{-1}}$ has been plotted as a function of microwave exposure and the rate constant has been established.

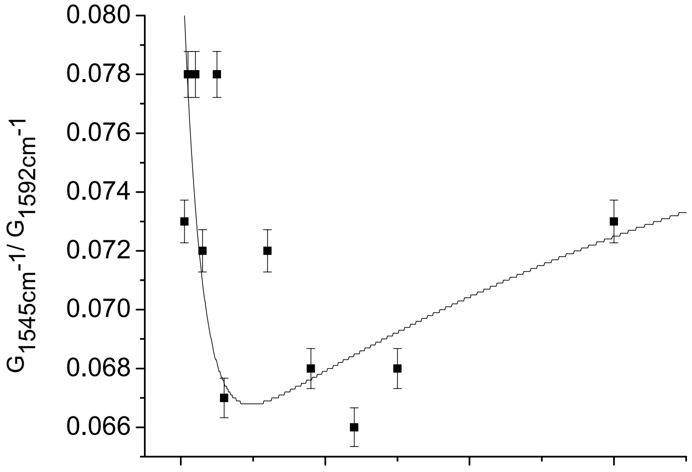

Figure 8.4 b: shows the decay of ratio of peak intensities of G^{-}(1545 cm^{-1}) to G^{+} (1592 cm^{-1}) versus the time of microwave exposure

Assuming the absorption is dominated by metallic nanotubes, the transmitted intensity distribution, seen by the semiconducting nanotubes is given by,

$$I(l) = I(0)\exp(-N_m\sigma_m l) \qquad \text{Equation 8.3}$$

where σ_m is the absorption cross-section of the metallic nanotubes.

The intensity experienced by the semi conducting tubes, and thus the decay rate k_s, is therefore dependent on the number of metallic nanotubes remaining.

$$k_s = K\exp(-N_m\sigma_m l) \qquad \text{Equation 8.4}$$

where K is a constant. N_m decays as a function of exposure time and thus, while k_s is initially small while there is a dominance of metallic nanotubes, it rapidly increases as the metallic nanotubes are destroyed and reaches an equilibrium constant.

The solid line of figure 8.4 a is a fit of a dependence of the form described by equation 8.4 to the temporal evolution of the RBM ratio.

$$\frac{RBM_{200cm^{-1}}(t)}{RBM_{255cm^{-1}}(t)} = \frac{RBM_{200cm^{-1}}(0)}{RBM_{255cm^{-1}}(0)}\exp(k_s-k_m)t \qquad \text{Equation 8.5}$$

Although the model is a very simplified approximation of the complex evolution of the radiation distribution experienced by the different tubes as the reaction proceeds, it successfully accounts for the observed behaviour. A more quantitative analysis is further complicated by the fact that the metallic catalytic residues present in the nanotubes samples will also contribute to the absorption. Any shortcomings of the simplicity of the model should be less manifest at the stages of the initial decay of the metallic tubes or the equilibrium decay of the semiconducting nanotubes at prolonged exposure. A decay constant for the metallic nanotubes, $k_m = 0.04$ sec^{-1} is obtained from the fit. By comparison an equilibrium value of $k_s = 1.4\text{x}10^{-3}$ sec^{-1} is obtained.

The same approach can be adapted to fit the evolution of the G-mode as a function of irradiation time, replacing $RBM_{200cm^{-1}} / RBM_{255cm^{-1}}$ by G^- (1545 cm^{-1})/G^+ (1592 cm^{-1}). Figure 8.4b shows the decay of the ratio of G^-(1545 cm^{-1}) to G^+ (1592 cm^{-1}) versus the time of microwave exposure. The model for the decay of the RBM ratios is similarly applied and is seen to fit well as illustrated by the solid line of figure 8.4 b. Most notably, the fit is for values of $k_{G+}=k_s$ and $k_{G-} = k_m$, lending further weight to the model. It is clear from the absorption spectroscopy data of figure 8.3 b that not all metallic nanotubes are degraded to the same extent and therefore at the same rate. The RBM modes chosen for analysis are the dominant ones for obvious reasons but the empirical analysis model should be applicable to the evolution of all peaks, albeit with different rate constants.

The next step was to do batch processing of the sample at the saturation level and to undertake concentration dependent studies to determine the critical debundling point. A 10 mg sample of HiPco SWNTs which had been microwave treated for 100 seconds was dispersed in 1% aqueous solution of SDBS surfactant. The sample preparation protocol [12] was undertaken as mentioned in chapter 4.2, but the batch processing was done at the starting concentration of 2 mg/ml. Serial dilution by a factor of 2 was performed until the concentration reached 4.8 x 10^{-4} mg/ml and then all the samples were tip sonicated at 26% percentage of output power (750 W) for 20 s and then bath sonicated for 1 hour. After the sonication process the samples were centrifuged for 1 hour at 4000 rpm. 80% of the solution was decanted for measurement after centrifugation.

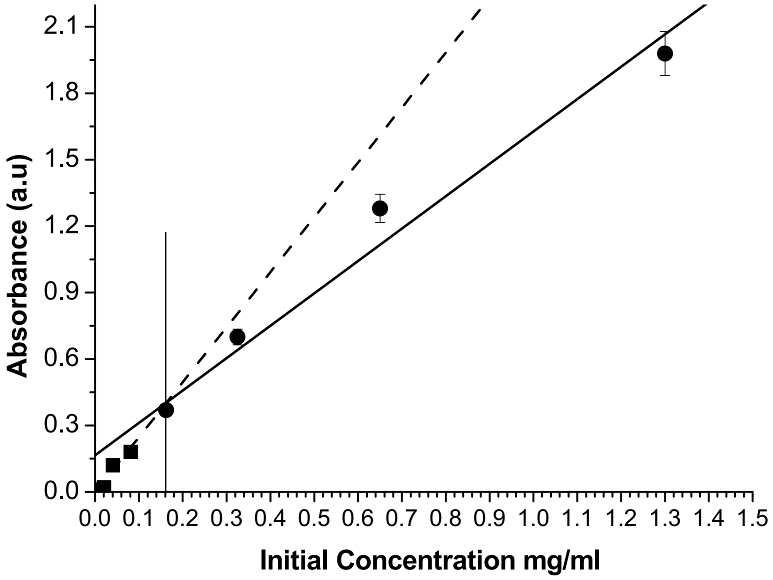

Figure 8.5: Plot of absorbance at 810 nm versus initial concentration

Figure 8.5 is a plot of absorbance at 810 nm, chosen as the minimally varying semiconducting feature in figure 8.3 b, versus initial concentration[12] showing a discontinuity in the absorption region of the lower concentration region. In both regions, the absorbance follows the Lambert Beer law which can be observed by the linear fits for the two concentration regions. A similar behaviour has been observed for the dispersion of pristine tubes in water/SDBS solution and it has been demonstrated that the two regions can be associated with the absorbance of bundles at higher concentrations and of mono disperse nanotubes at lower concentrations. The intersection of the two linear fits has been termed the critical debundling point or the dispersion limit[3] - the concentration where the debundling begins, resulting in a dispersion of individual tubes. The dispersion limit for this batch processed tubes is 0.16 ± 0.03 mg/ml. The dispersion limit for pristine HiPco tubes dispersed under identical conditions has been determined in chapter 4.3 to be 0.07 ±

0.03 mg/ml [12]. The extinction coefficient ($\alpha_{810\ nm}$) at higher concentration was found to be 146 ml mg^{-1} m^{-1} and that of lower concentration is 248 ml mg^{-1} m^{-1}. The corresponding values for unprocessed HiPco nanotubes were found to be 87 ml mg^{-1} m^{-1} and 203 ml mg^{-1} m^{-1} respectively at the same wavelength of 810 nm.

The dispersion limit of the microwave processed nanotubes is comparable to that of the pristine tubes although slightly higher, indicating that the processed nanotubes are more easily dispersed. Such a result is not unexpected as the nanotubes bundles may be partially de-aggregated due to the degradation process. The similarities of the absorption co-efficients for the semiconducting nanotubes below the dispersion limit indicate that the semiconducting tubes have been minimally degraded.

8.4 Summary

Microwave treatment of HiPco nanotubes has been confirmed to preferentially destroy metallic nanotubes leaving samples effectively enriched in semiconducting tubes. The preferential destruction is only partial however, and the degradation rates vary for metallic nanotubes of differing diameters. The samples prepared for irradiation are undoubtedly in bundled form and it is feasible that the process may be more selective if the nanotubes were debundled. Monitoring the decay as a function of time reveals that the optimal preferential degradation occurs at exposure times of ~100 seconds, under the conditions employed here, after which time significant degradation of the semiconducting nanotubes occurs. Concentration dependant dispersion measurements reveal that the microwave processed nanotube samples are dispersed more easily than the pristine samples.

References

(1) Song, J. W.; Seo, H. W.; Park, J. K.; Kim, J. E.; Choi, D. J.; Han, C. S. *Current Applied Physics* **2007**, *Article in Press*.

(2) J.W. Song, H. W. S., J.K. Park, J.E. Kim, D.G. Choi, C.S. Han *Current Applied Physics* **2007**, *Article in Press*.

(3) Landi, B. J.; Ruf, H. J.; Worman, J. J.; Raffaelle, R. P. *Journal of Physical Chemistry B* **2004**, *108*, 17089.

(4) Rao, A. M.; Richter, E.; Bandow, S.; Chase, B.; Eklund, P. C.; Williams, K. A.; Fang, S.; Subbaswamy, K. R.; Menon, M.; Thess, A.; Smalley, R. E.; Dresselhaus, G.; Dresselhaus, M. S. *Science* **1997**, *275*, 187.

(5) Dresselhaus, M. S.; Dresselhaus, G.; Saito, R.; Jorio, A. *Physics Reports-Review Section of Physics Letters* **2005**, *409*, 47.

(6) Kataura, H.; Kumazawa, Y.; Maniwa, Y.; Umezu, I.; Suzuki, S.; Ohtsuka, Y.; Achiba, Y. *Synthetic Metals* **1999**, *103*, 2555.

(7) Strano, M. S. *Journal of the American Chemical Society* **2003**, *125*, 16148.

(8) M.S. Dresselhaus, G. D., R. Saito, A. Jorio *Physics Reports* **2005**, *409*, 47.

(9) Jorio, A.; Saito, R.; Hafner, J. H.; Lieber, C. M.; Hunter, M.; McClure, T.; Dresselhaus, G.; Dresselhaus, M. S. *Physical Review Letters* **2001**, *86*, 1118.

(10) O'Connell, M. J.; Bachilo, S. M.; Huffman, C. B.; Moore, V. C.; Strano, M. S.; Haroz, E. H.; Rialon, K. L.; Boul, P. J.; Noon, W. H.; Kittrell, C.; Ma, J. P.; Hauge, R. H.; Weisman, R. B.; Smalley, R. E. *Science* **2002**, *297*, 593.

(11) Nair, N.; Usrey, M. L.; Kim, W. J.; Braatz, R. D.; Strano, M. S. *Anal Chem* **2006**, *78*, 7689.

(12) Priya, B. R.; Byrne, H. J. *Journal of Physical Chemistry C* **2008**, *112*, 332.

Chapter 9

Conclusions

9.1 Summary

The main objectives of this study were

1) Dispersion of SWNTs and establishment of a standard protocol for sample preparation

2) Doping studies of pristine SWNTs

3) Electronic separation of SWNTs

A protocol for the dispersion of HiPco SWNT in water based solutions was demonstrated in chapter 4. Centrifugation and sonication have been shown to effectively remove bundles from the suspensions and to disperse the tubes. This elimination of bundles has been quantitatively studied through the evaluation of scattering using an integrating sphere in a UV/Vis/NIR absorption spectrometer. Concentration dependent absorption measurements were demonstrated by finding the extinction coefficients for the bundle SWNTs and the isolated ones using Lambert Beer Law leading to critical debundling point (CDP 0.07±0.03 mg/ml). The CDP is the concentration below which individual tubes were obtained and these results were also confirmed using AFM studies. Further, CDP / dispersion limit and the corresponding extinction coefficient for different solvents have been compared and finally water surfactant media has been verified / proved to be superior for SWNT dispersions.

After validating a standard protocol to obtain isolated SWNTs in water based solution, a method to elucidate the chiral index using UV/Vis/NIR absorption spectroscopy and Raman spectroscopy was performed and this was discussed in the chapter 5. Although the use of both techniques is extensively reported in literature, a critical comparison is difficult to find. The objective was to show that although the structural assignment of the SWNTs for each technique is based on different theories, the results are comparable and the techniques converge. It has been concluded that both spectroscopies can be used to routinely characterise SWNTs quantitatively. The number of chiral indices assigned from UV/Vis/NIR was significantly higher, however, when compared to Raman and this fact is not only due to resonance conditions but also due to the fundamental difference in the structural dependence of the spectroscopic characteristics.

Chapter 6 discussed the doping studies which were carried out at the CDP concentration in order to establish the metallic and semi conducting nature of the tubes separately. It was concluded that the electronic states of the metallic tubes were modified more easily than those of the semi conducting tubes. The protonation rates obtained by regression of a first order protonation model were found to be dependent on the optical band gaps and thus on the electronic character of the nanotubes.

The third objective was to separate the tubes electronically which was initially attempted via chemical functionalization. SWNTs were -COOH functionalised using acid treatment. These functionalised tubes were further amine treated and dispersed in THF. After evaporation, according to literature reports, the deposit should contain metallic tubes and the supernatant nanotubes. This concept was contradicted by Yutaka Meada who claimed that the metallic tubes and the amines interact better than the semi conducting tubes. The experiments carried out here showed that optimisation was required at every stage of functionalization and unless that is performed this procedure of separating carbon nanotubes electronically cannot be used for routine processing. Notably the harsh chemical treatment degraded the nanotubes significantly.

As an alternative route to electronic separation, selective destruction of metallic nanotubes using microwave irradiation was explored (chapter 8). This process was found to destroy metallic tubes, partially enriching the semi conducting ones in the sample. It was confirmed that the degradation rate was different for different metallic tubes. The kinetics of the process was modeled and it was concluded that the semi conducting SWNTs were also susceptible to microwave degradation, albeit at a slower rate. Concentration dependant dispersion measurements revealed that the microwave processed SWNT samples were dispersed more easily than the pristine samples.

To conclude, a standard protocol for dispersion and doping of HiPco SWNTs was performed successfully. Electronic separation using chemical functionalization was unsuccessful and resulted in significant degradation of the SWNTs. Microwave treatment showed an enrichment of semi conducting SWNTs although the process is far from optimal as the degradation rates are not the same for all metallic nanotubes and significant degradation of semi conducting tubes was also observed.

9.2 Future Perspectives

Carbon nanotubes are remarkable materials but for many potential applications will be required in an electronically pure form. The work described in this thesis demonstrates that proposed post processing methods have significant deficiencies in that they are only weakly selective and degrade the nanotubes, such that complete separation cannot be achieved. Given the continuous nature of the variations of the electronic properties of as produced samples, the realization of an efficient bulk separation procedure is unlikely. Ultimately, mass production of nanotubes with either metallic or semiconducting character, or ideally with the same chirality is desirable although significant progress in synthetic methods is required. The growth of nanotubes of “specific chirality” on patterned substrates has also been proposed but again controlling the electronic properties requires a deep understanding and further extensive research has to be carried out. However, if the ultimate goal is integration of carbon nanotubes into CMOS technologies as wires and interconnects, growth of nanotubes of specific electronic character on chip will be a requirement.

Graphene nano ribbons have shown to have a promising future in electronics. Graphene based devices offer high mobility for ballistic transport, high carrier velocity for fast switching, monolayer thin body for optimum electrostatic scaling, and excellent thermal conductivity. However they potentially suffer from the same problems of agglomeration as the carbon nanotubes.

Irrespective of the likely success of the above approaches, this work has shed further light on the fundamental optical and spectroscopic characterization and the fundamental properties of carbon nanotubes.

Presentations at International Conferences

PUBLICATIONS

B. R. Priya, H. J. Byrne, **"Q*uantitative Analyses of Microwave Treated HiPco Carbon nanotubes using Absorption and Raman Spectroscopy*"**, J. Phys. Chem. C (2009) 113, 7134–7138.

B. R. Priya, H. J. Byrne, ***"Investigation of Sodium Dodecyl Benzene Sulphonate Assisted Dispersion and Debundling of SWNT"***, J. Phys. Chem. C (2008), 112, 332-337.

B. R. Priya, H. J. Byrne, ***"Quantitative Analysis of Dispersion and Doping of Individual Carbon Nanotubes in Water Based solutions using Absorption and Raman Spectroscopy"*** Phys. Stat. Sol. (b) 245, No. 10, 1964–1966 (2008).

ORAL PRSESENTATION

Intel European Research and Innovation Conference held in Leixlip, Dublin, **September 12th 2008.**

POSTER PRESENTATIONS

9th International Conference on Science and Application of Carbon Nanotubes Le Corum, Montpellier, France, **June 29 - July 4, 2008.**

International Winter School Euro Conference on Electronic Properties of Novel Materials held in Kirchberg-Tirol, Austria, March **1- 7th, 2008.**

4th Intel Research Conference held in Leixlip, Dublin, **September 2007.**

International Winter School Euro Conference on Electronic Properties of Novel Materials held in Kirchberg-Tirol, Austria, **March 10- 17th, 2007**.

3rd Intel Research Conference held in Leixlip, Dublin, **September 2006**.

International Conference on Science and Technology of Synthetic Metals held in Trinity College, Dublin, **July 2-7, 2006**.